TECHNISCHE UNIVERSITÄT WIEN
Vienna University of Technology

IAP

DIPLOMARBEIT

Surface analytics of bactericidal cicada wing nanopillars and development of a biomimetic nanoimprinting approach for functional replication

Zur Erlangung des akademischen Grades

Diplom-Ingenieur

Im Rahmen des Studiums

Biomedical Engineering – UE 066 453

eingereicht von

Alexander Michael Lukas Bürger

Matrikelnummer 01526882

Ausgeführt am Institut für Angewandte Physik
der Fakultät für Technische Physik der Technischen Universität Wien

Betreuung
Associate Prof. Dipl.-Ing. Dr.techn. Ille C. Gebeshuber

Wien, 30.03.2022 _____ _____

(Unterschrift Verfasser) (Unterschrift Betreuerin)

Kurzfassung

Neue Forschungsergebnisse über die vielfältigen Eigenschaften von Nanopillars auf Flügelmembranen von Zikaden beschreiben Superhydrophobie, Antireflexions- und Selbstreinigungseigenschaften. Weiters wurde sogar antibakterielle Wirkung entdeckt. Diese Beobachtungen eröffnen ein vielversprechendes Feld für weitere Untersuchungen. In der vorliegenden Arbeit werden die biologischen Vorlagen (Zikadenflügel) und daraus mittels einer an der TU Wien neu entwickelten Nano-Abdrucktechnik hergestellte Mikro- und Nanostrukturen mit oberflächenphysikalischen Mitteln hinsichtlich ihrer Topologie und Funktionalität untersucht. Dafür wurden die Nanostrukturen der Flügeloberflächen von drei verschiedenen Zikadenarten mit Rasterkraft- und Rasterelektronenmikroskopie miteinander verglichen. Zwei in Neuseeland endemische Zikadenarten (*Kikihia scutellaris* und *Amphipsalta cingulata*) wiesen im Vergleich zu einer amerikanischen Art (*Magicicada septendecim*) höhere Nanostrukturen auf. Trotz dieser Höhenunterschiede wurde festgestellt, dass alle drei Arten antibakterielle Wirkung aufweisen, sowohl gegen Gram-negative als auch gegen Gram-positive Bakterien (*Escherichia coli* und *Staphylococcus aureus*). Weiters wurde eine schnelle und kostengünstige Abformmethode entwickelt, mit der die Nanosäulchen von der biologischen Vorlage auf verschiedene Harze übertragen werden können, und zwar mit einer Genauigkeit auf der Nanoebene auf zentimetergroßen Flächen. Darüber hinaus konnte gezeigt werden, dass die derart hergestellten Replikate eine bakterizide Wirkung aufweisen. Die entwickelte Methode ist schnell und kosteneffizient und sie kann auf große Flächen übertragen werden. Dadurch wird ein weites Anwendungsgebiet eröffnet, von der bakteriziden Beschichtung von Krankenhausoberflächen, von Implantaten und auch von Smartphone-Displays. Dies könnte sich als erster Schritt zur erfolgreichen Bekämpfung der gefährlichen multiresistenten Bakterien erweisen.

Abstract

In recent years, various interesting properties have been reported for the pillar-like nanostructures found on the wing membrane of several cicada wings. Besides to superhydrophobicity, antireflection and self-cleaning, a bactericidal effect was discovered. This observation opened a promising field for further investigation. In this thesis, biological templates and related micro- and nanostructures produced via nanoimprint technologies from these templates are analyzed regarding their topology and functionality. The nanostructures of the wing membrane of three different cicada species were investigated with Atomic Force Microscopy and Scanning Electron Microscopy and compared with each other. The two cicada species endemic to New Zealand (*Kikihia scutellaris* and *Amphipsalta cingulata*) were found to have higher nanopillars compared to the American *Magicicada septendecim*. Despite these height differences it was observed that all three species show an antibacterial effect against the Gram-negative *Escherichia coli* and the Gram-positive *Staphylococcus* aureus. Moreover, a fast and low-cost imprinting method was developed which is capable to transfer the nanopillars from the biological template to various resins with nanoscale accuracy on large (cm^2) areas. In addition, it was shown that replicas produced in such a way show a bactericidal effect. As the method is straightforward it can be upscaled to large areas. This opens a vast field of applications from hospital surfaces over implants to smartphone displays and could be a big step to address the problem of multidrug resistance in bacteria.

Inhaltsverzeichnis

Terms described in the Glossary are marked with * at their first appearance in the main text.

Introduction

What is biomimetics?

Biomimetics* is a field that transfers functionalities of biological systems to technical applications. In 1993 the VDI (Verein Deutscher Ingenieure, Association of German Engineers) technology center defined biomimetics as a scientific discipline that systematically deals with the *„technical implementation and application of designs, processes and development principles of biological systems“* (Cerman et al., 2005). It must not be confused with the related term bioinspiration, which has a broader definition. An example of bioinspiration that is not biomimetic would be a simple copy of form without any functionality (Gebeshuber et al., 2020).

Over time, biomimetics has been categorized in different ways. Werner Nachtigall, a German pioneer in the field, divided it by functionality into 12 categories such as structure, construction, movement and evolution biomimetics (Nachtigall, 1992). In contrast, the approach of Guangtao Zan and Qingsheng Wu divided biomimetics by the underlying synthesis process. Categories include elementary biomimetic systems via biomass template or macromolecular inspired systems (Zan & Wu, 2016). Generally, there are two main approaches to biomimetics. The bottom-up (biomimetics by induction, solution-based) approach starts with basic research on biological samples. This way, specific functions and traits of morphologies and anatomies can be discovered. The next step is to investigate and understand the underlying principles. An abstraction of the biological model is used for technical implementation, leading to a biomimetic product. One prominent example of this solution-based approach (sometimes also called biology-push) is the famous Lotus-Effect®, which was utilized for the self-cleaning façade color Lotusan® (Barthlott & Neinhuis, 1997; Cerman et al., 2005). The top-down approach (biomimetics by analogies, problem-based) works in the opposite direction. It starts with the search for biological analogies to a technical problem. Once found, their underlying principles are studied and further abstracted for technical implementation. As a next step, the solution is tested with prototypes. If successful, a biomimetic product is developed. The development of Flectofin®, a hingeless flapping device inspired by the Bird-of-Paradise flower, would be an example of the problem-based approach

(also termed as technology-pull) (Knippers & Speck, 2012; Lienhard et al., 2011; Speck et al., 2017; Stachelberger et al., 2011).

Why learning from Nature?

Organisms have evolved over millions of years. Charles Darwin (1809 - 1882) first described the process of evolution in 1859 and coined the phrase „*survival of the fittest*“. Fitness can be described as quantitative and qualitative reproduction success (Darwin, 2009, reprint of the 6th edition (1872) of Darwin, 1859). The fitness depends on each individuum's total set of traits, which is defined by its genome. The genome can be recombined during sexual reproduction, resulting in different variants. Moreover, mutations can occur by chance in the form of deletions, insertions, inversions or translocations. These mutations can have a disadvantageous, neutral or beneficial effect on fitness (Graw, 2010).

Furthermore, a selection pressure acts on every organism. This selection pressure is determined by various factors such as competition, environment, partner attraction and predators. Over millions of years, selection led to an increase in the fitness of each species by optimizing the total composition of traits. Investing in one beneficial trait often means neglecting another. Consequently, no perfect organism can exist. A species is always a compromise but well-adapted to its living conditions. Organisms have developed to utilize limited resources and energy with outstanding efficiency, often resulting in multifunctional and complex solutions. If researchers study organisms, abstract functional principles and transfer them to technical applications, they learn from an optimization process that has been running over millions of years. It also gives the possibility to get closer to sustainable resource management because nearly everything is reused in Nature.

However, biomimetics is not necessarily connected with sustainability (as is often wrongly assumed). For example, a product can be biomimetic by copying the function solely but harming the environment by using materials such as fossil fuel-based plastics, toxic components and further consuming lots of energy for production. In addition, companies often try to improve the image of products by using terms such as inspired by Nature, biomimetic and bionic to make the products sound „greener“. This misleading and inflationary

usage of terms can lead to a decrease in trust in real and sustainable biomimetic development (Gebeshuber et al., 2009).

Selection pressure places particularly high demands on surfaces. This is because they represent the interface between organisms and their environment. Furthermore, they are the first protective layer to the outside world. Due to these high demands, biological surfaces have developed countless properties over millions of years, such as adhesion, superhydrophobicity*, structural colors and thermoregulation. These different properties are a result of the chemical composition of the surfaces and their (often hierarchical) macro- and nanostructures. Since versatile surfaces are of great use in technology, such surfaces have great potential for bionic inspiration because they combine several properties at the same time.

Famous examples of structural biomimetics

Biological surface structures have served as inspiration for engineering applications for many researchers. One of the best-known examples is probably the velcro* fastener, originally invented by the chemist Georges de Mestral. After a walk with his dog, some burrs of a burdock plant had become caught in the animal's fur. George de Mestral took a magnified look at one burr and discovered the many hooks. Shortly after the war, he learned that a synthetic fiber that could be deformed when heated and then retain that shape after cooling was developed. This allowed him to implement the principle of burrs by forming loops of the fiber and then cutting them open (Figure 1). His invention got patented in 1955. The rest is a success story. Almost everyone has had contact with velcro on shoes, bags, wristwatches, etc. (Budde, 1995; Mestral, 1955; Nachtigall & Wisser, 2013).

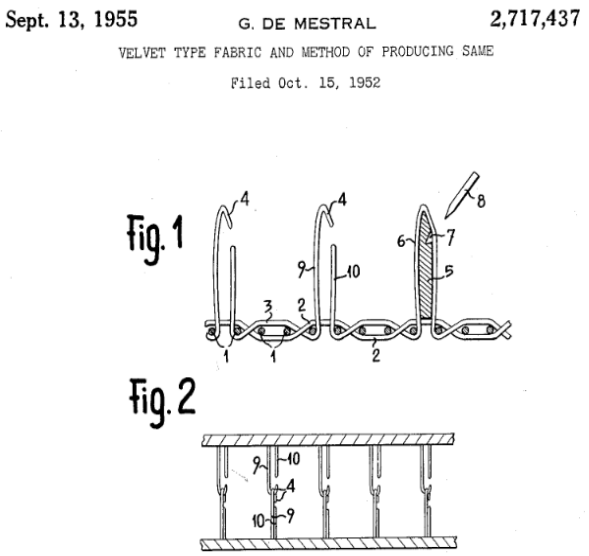

Figure 1. Illustration of the velcro fastener principle in the patent of Georges de Mestral. (Figure altered from Mestral, 1955) © Georges de Mestral

At the University of Bonn, the botanist Wilhelm Barthlott devoted himself to the study of epicuticular (see Glossary) growths. In the process, he discovered that some plants did not have to be cleaned first for the scanning electron microscope because they were already perfectly clean. More detailed examinations showed that the surface structures of these plants were not smooth but nubby (Cerman et al., 2005). Years later, Barthlott and his colleague Christoph Neinhuis conducted intensive research into the underlying mechanism. They discovered that the leaves of the sacred lotus (*Nelumbo nucifera*) had a particularly efficient self-cleaning surface. The epicuticular wax layer*, which is already chemically hydrophobic* when it is unstructured, is forming nubs, which extremely reduces the contact area with water droplets (Figure 2). This makes the surface superhydrophobic. Now, when water falls on the leaf surface, it simply rolls off, picking up any dirt particles on the leaf surface. In this way, the dirt is simply washed off. They described this principle as Lotus effect® (Barthlott & Neinhuis, 1997). In 1997, they patented the Lotus effect® and developed the first prototypes of artificial surfaces by copying the surface structure of the lotus plant. Gradually, companies began to take an interest and they received awards for their development. Nowadays, there are already many applications, such as the facade paint Lotusan® (Cerman et al., 2005).

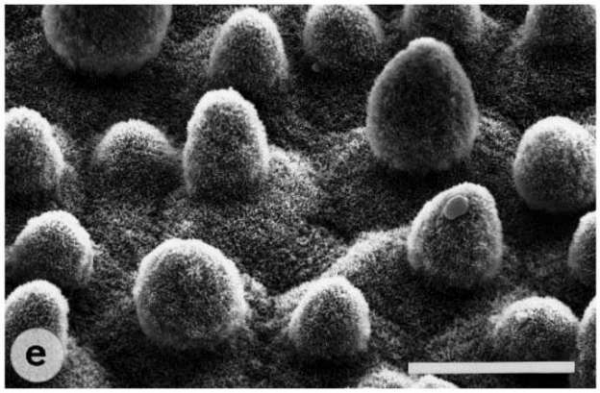

Figure 2. Scanning electron micrograph of the leaf surface structure of the sacred lotus *Nelumbo nucifera*. Scale bar is 20 µm long. (Figure altered after Barthlott & Neinhuis, 1997) © Springer-Verlag 1997

Insect wings

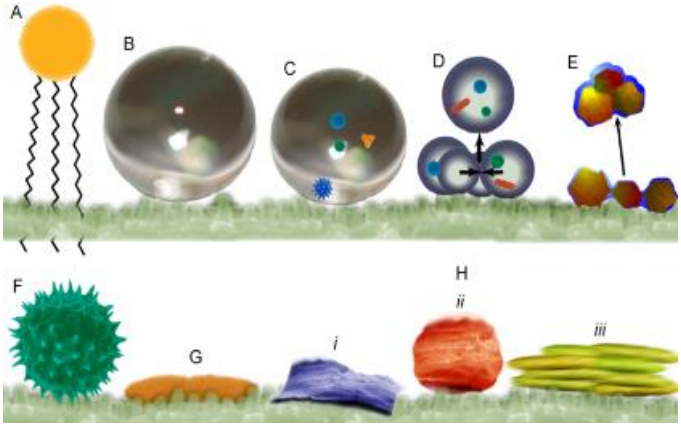

Figure 3. Reported properties of cicada wings. a) Transparency, antireflection and color, b) Xylemphobicity, c) Self-cleaning due to droplet rolling, d) Self-cleaning due to condensation droplet jumping, e) Self-cleaning due to aggregating particles, f) Low adhesion and friction of contaminants, g) Antibacterial, h) Control of eukaryotic cells: i) high adhesion, ii) low adhesion, iii) cell sheet promoting. (Figure taken from Watson et al., 2015) © 2015 Gregory S. Watson and Jolanta A. Watson, et al.

However, surfaces with amazing properties do not only occur in plants but also in the animal kingdom. The wings of various insects have proven to be particularly interesting and a suitable template for biomimetic projects. For example, it has already been possible to transfer the structural colors of butterflies to surfaces by nanoimprinting* techniques (Zobl, 2017; Zobl et al., 2016). In the case of cicada* wings, various remarkable properties were found (Figure 3). These range from anti-reflectivity over superhydrophobicity to self-cleaning* effects (Oh et al., 2017; Watson et al., 2015; Wisdom et al., 2013). Besides a similar effect to the lotus leaf, another one was discovered. This *„cicada effect“*, as the discoverers named it, occurs due to a special condensation phenomenon. Water droplets are self-propelled and jump off the superhydrophobic surfaces taking dirt particles with them (Watson et al., 2014). One of the most remarkable properties of cicada wings was found in 2012 by Ivanova et al. They showed that the wing surface of *Psaltoda claripennis* exhibits an antibacterial effect, which also occurred on wings covered with a gold layer (to exclude chemical interactions as a cause). This way, the group discovered that the underlying mechanism was a physical one (Ivanova et al., 2012). In addition, it was found out, that these nanopillar surfaces not only inhibit bacterial growth but show no cytotoxic effects to eukaryotic cells such as osteoblasts (Shahali et al., 2019). On the contrary, surfaces with nanopillar arrays showed even growth promoting effects for certain eukaryotic cells such as fibroblasts and the human retinal pigment epithelium (Pham et al., 2016; Watson et al., 2015). These findings led to various further studies and predestined cicada wings as biological templates with a high potential for biomimetic applications (Hasan et al., 2013; Kelleher et al., 2016; Nowlin et al., 2014; Pogodin, Hasan, Baulin, Webb, Truong, et al., 2013; Román-Kustas et al., 2020).

Related works

Antimicrobial properties in previous studies

Research on cicada wings revealed in the last few years amazing properties. For example, in 2012, Ivanova et al. showed for the first time, that the wings of the Australian cicada species *Psaltoda claripennis* were not only superhydrophobic but also capable of mechanically rupturing the cell walls of the Gram-negative* bacterium *Pseudomonas aeruginosa*. By coating the wing membranes with an inert gold layer, they excluded chemical interactions with the bacteria* by retaining the topography. A short time after this initial study, the group published further investigations, which revealed that only Gram-negative bacteria were susceptible to the bactericidal property of the *P. claripennis* wing nanostructures*. In contrast, the mechanism did not show an effect on Gram-positive* ones. It seems that the thicker peptidoglycan layer* of these bacteria prevents the cell wall from rupturing (Hasan et al., 2013). The same group also proposed a biophysical model of the underlying mechanism. They suggested that bacteria cells get adsorbed to the nanopillars, which induces tensions in the region lying in between. As a reaction to these tensions, the cell wall ruptures in the area hanging freely between the nanopillars (Figure 4). Moreover, they showed that the nanopillars had a similar effect on Gram-positive bacteria when treated with microwave radiation to decrease the turgor pressure (Pogodin et al., 2013).

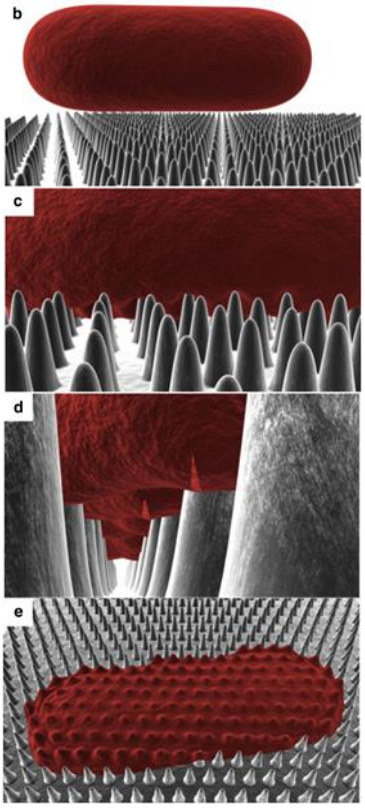

Figure 4. Biophysical model of bacteria cell wall rupturing on *Psaltoda claripennis* wings. Screenshots from animated model http://youtu.be/KSdMYX4gqp8 (Figure altered from Pogodin et al., 2013) © 2013 by the Biophysical Society

In 2014 Nowlin et al. investigated the effect of cicada wing surface on yeast cells. They did their experiments with two strains of *Saccharomyces cerevisiae* on the wings of two different species: an annual cicada *Neotibicen tibicen* (described under the former name *Tibicen tibicen*) and a periodical cicada *Magicicada septendecim* (which emerges in vast broods every 17 years). The high aspect ratio nanopillars of the morning cicada *N. tibicen* showed higher efficacy as fungicide compared to *M. septendecim* (Figure 5). To exclude the effects of different chemical compositions, both wings were coated with gold. The group explained the killing mechanism with the increased adhesion and cell-surface affinity caused by the nanostructures. They suppose that the higher the aspect ratio, the higher the efficacy of cell rupturing (Nowlin et al., 2014).

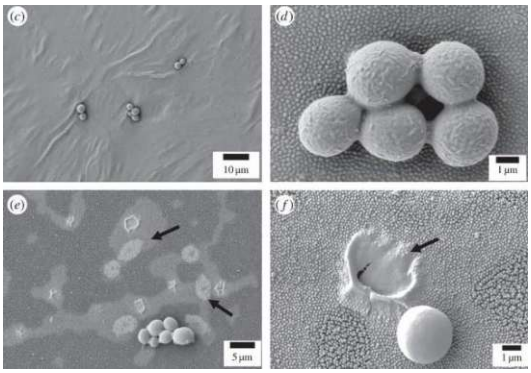

Figure 5. Scanning electron micrographs of the Brewer's yeast *Saccharomyces cerevisiae* on cicada wings (different magnifications): c) & d) Periodical cicada *Magicicada septendecim* wing, e) & f) Morning cicada *Neotibicen tibicen* (Figure altered from Nowlin et al., 2014*)* © 2014 Nowlin et al. Published by the Royal Society

In addition, Kelleher et al. suggested a correlation between the scaling of the nanostructures and the bactericidal capacity. They performed antibacterial tests on the wings of three different cicada species: *Megapomponia intermedia*, *Cryptotympana aguila* and *Ayuthia spectabile.* The nanopillars of these species differ in height and in spacing (Table 7). *M. intermedia* has the highest and most densely packed structures. Whereas *C. aguila* and *A. spectabile* have nanopillars about the same height, only differing in the distance between them (the latter has a larger distance). The findings showed that the efficacy in killing bacteria was highest in *M. intermedia*, followed by the less efficient *C. aguila. A. spectabile* showed the least effect and was not significantly different from the control surface. To sum up, the effectiveness of killing bacteria increases with pillar height and decreases with spacing distance (Kelleher et al., 2016).

All these studies mentioned focused on the physical effect underlying the bactericidal effect. In 2020 Román-Kustas et al. investigated the chemical compositions of the nanopillars and their importance for the antibacterial mechanism in two cicada species: *Neotibicen pruinosus* (higher aspect ratio, superhydrophobic) and *Magicicada cassinii* (lower aspect ratio, hydrophobic). They used a microwave-assisted extraction approach in combination with organic solvents to remove layers of the epicuticle surface. The extracted compounds were analyzed. Moreover, they tested after specific time frames if antibacterial and

superhydrophobic properties have changed. As a result, they showed that in the case of *N. pruinosus,* hydrophobic compounds such as fatty acids and saturated hydrocarbons were concentrated at the nanopillar surface and decreased within the structures. In contrast, the content of oxygen-containing molecules increased. Consequently, the contact angle* of water drops decreased, the surface structures did not show super- but only hydrophobic properties. Interestingly, the *M. cassinii* showed a different proportion of chemical compounds. Some saturated carbons increased with depth, while fatty acids showed the same distribution as in the other cicada species. All in all, the wing's hydrophobicity decreased with the extraction of chemical layers. Furthermore, the group observed in the high aspect ratio nanopillars of *N. pruinosus* an effect which they called „*kissing state*“: the tips of two or more pillars stick together due to van der Waals forces. As an explanation, they proposed the decrease in hydrophobic compounds with ongoing extraction. Moreover, they investigated the change of killing efficacy and bacterial attachment over the extraction duration (Figure 6). 70 percent of the bacteria found on the untreated wings were dead in both species. Except for the first two minutes in *N. pruinosus*, the bactericidal efficacy decreased with the chemical extraction. Especially in *M. cassinii,* the first layers, which have a high relative content of long-chain fatty acids, seem to be important for the bacteria interaction. To sum up, the group concluded that in the case of the high aspect ratio nanopillars of *N. pruinosus,* the topography and as well as chemical composition play important roles in killing bacteria. In contrast, the nanostructures of *M. cassinii* gain their antibacterial property mainly through their chemical composition (Román-Kustas et al., 2020). Their findings suggest that nanostructures comparable to *M. cassinii* seem not as relevant for biomimetic purposes, only transferring structure (rather than chemistry).

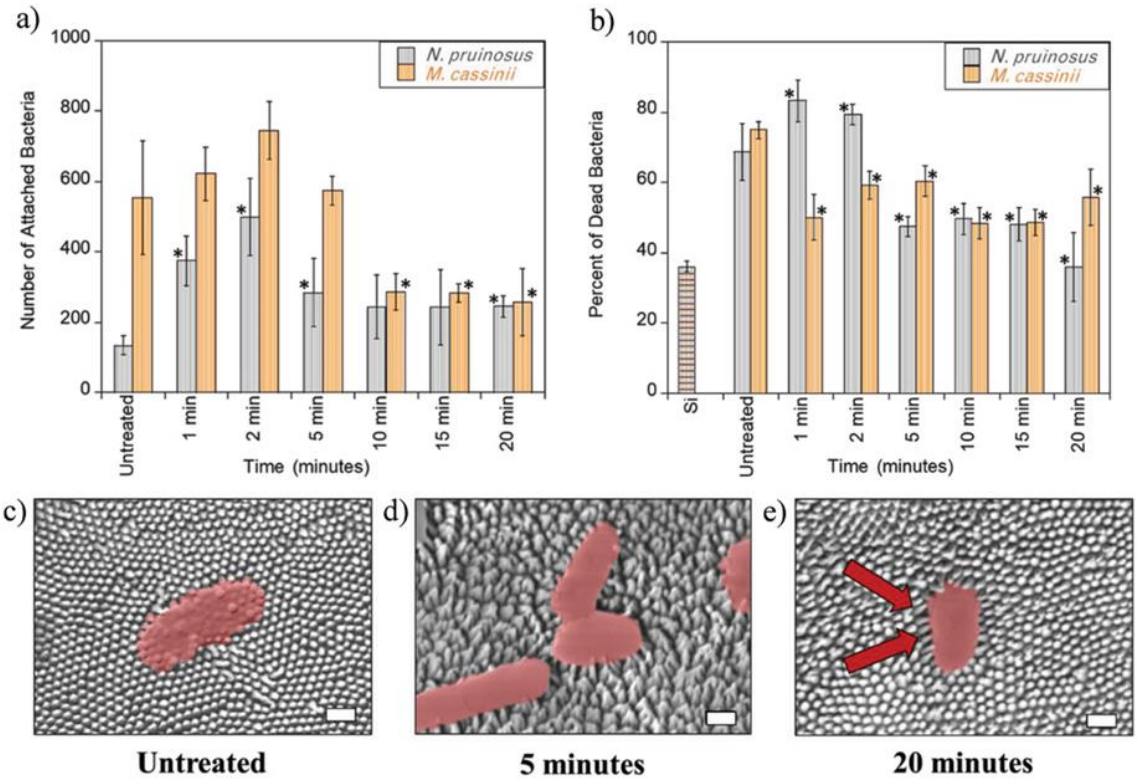

Figure 6. Testing antibacterial properties of cicada wings over the time course of the microwave-assisted extraction (MAE). a) biofouling properies and b) live/dead study (for both the error bars mark the 95 % confidence interval, asterisks mark valus significantly different from untreated wings). SEM images of: c) Untreated wing, d) Wing after 5 minutes MAE, e) Wing after 20 minutes MAE. (Figure altered from Román-Kustas et al., 2020) © 2020 Román-Kustas et al. Published by WILEY-VCH Verlag GmbH & Co. KGaA, Weinheim

In the last two decades, various studies highlighted different techniques in the field of nanolithography. Most of the approaches are quite time-consuming and cost intensive. In contrast, nanostamping holds the potential to replicate nanostructures from biological templates in an efficient and cost-effective way. This makes large nanostructured areas feasible, which opens a vast field of applications. The approaches that have the greatest impact on this study and the developed techniques are presented in this chapter. Zobl and co-workers introduced a fast and cheap approach of soft nanolithography for creating color stamps using the wings of *Morpho peleides* (a tropical butterfly) as a biological template. As a first step, the wing pieces were mounted onto microscope slides and coated with Pioloform® powder dissolved in chloroform (1 % and 0.5 solutions) to flatten the curved wing scales and to have them more closely oriented together on the wing membrane. In the next step, the study used polyvinyl siloxane (PVS)* as a molding material. PVS is widely used for dental impressions and has been used by Kerstin Koch and co-workers for living plant surface impressions. The PVS was gently deposited on the wing and distributed with a metal spatula. After 10 minutes, the PVS template was carefully peeled off the butterfly wing and deposited into a chlorine bath and in a series of five distilled water baths (each lasting 5 minutes) to remove any biological material that was still stuck to the PVS surface after the peeling process. This negative impression of the wings was further used as a master stamp to transfer the nanostructures to a self-mixing 5-minute epoxy resin by simply pressing the template onto a drop of the resin resulting in a positive replica (Figure 7) (Zobl, 2017; Zobl et al., 2016).

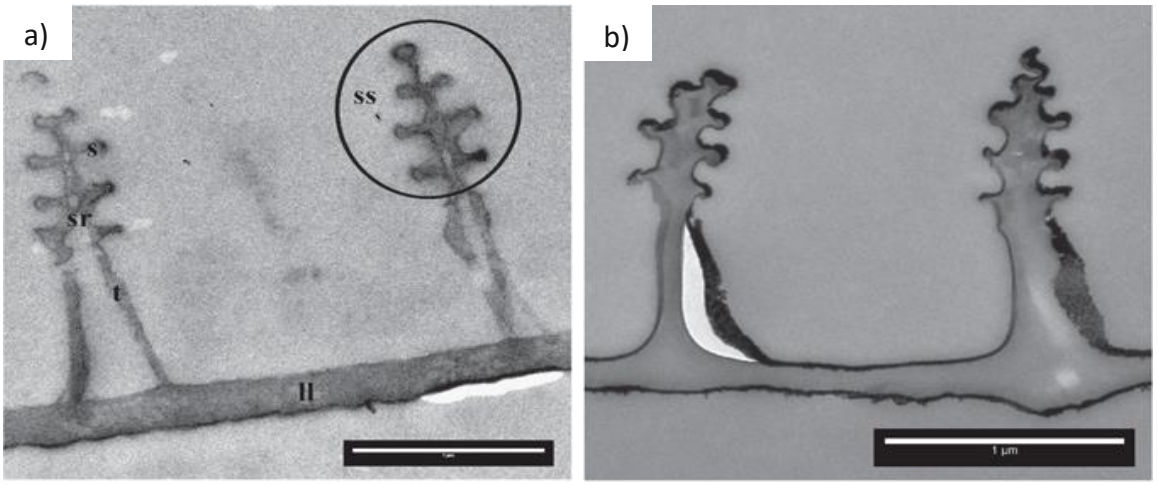

Figure 7. Transmission electron micrographs (length of scale bars: 1 µm). a) A cross-section of a cover scale of a *Morpho peleides* butterfly showing two ridges with the shelf-structures (ss) connected by the lower lamina (ll) with the trabeculae (t). The shelf structures are connected via the subribs (sr), b) A cross-sections of a positive replica in epoxy resin of a cover scale replica. (Figure altered from Zobl et al., 2016) © 2016 IOP Publishing Ltd

As mentioned above, Kerstin Koch and co-workers have previously used PVS to reproduce the surface wax structure of plants (Figure 8). They deposited the molding mass (which was cooled down to 5 °C to extend the polymerization time) on top of the leaves and immediately pressed it down with a glass plate with different pressures. After 5 minutes, the PVS was removed from the biological master surface. To remove the remaining wax crystals in the molding mass, they deposited them into a chloroform bath for another 5 minutes (all performed at room temperature). They estimate the relaxation time of the molding mass as about 30 minutes. Afterwards, they used different liquid resins to create a positive replica. Therefore, they deposited the resins on the PVS templates and put them together on a lab rotator (250 rpm) for 5 minutes. Then they transferred everything into a vacuum chamber (pressure 1 mbar) for 10 seconds per minute. Finally, they let the resin cure at room temperature for 24 hours, but they also accelerated this step by increasing the temperature (3 hours at 50 °C). Their results show that epoxy resin had the best performance in the precision of all the tested molding materials. Moreover, the group found out that the pressure (in the PVS step) should be optimized for each structure. If the pressure was too low, only a few nanostructures were captured; if the pressure was too high, the structure collapsed, and hardly anything was replicated. They state that their method fulfills the most important requirements: high precision and resolution (able to catch three-dimensional details), little effect of shrinking/expanding of the molding mass/template due to different factors and that it is a fast method (Koch et al., 2008; Schulte et al., 2009).

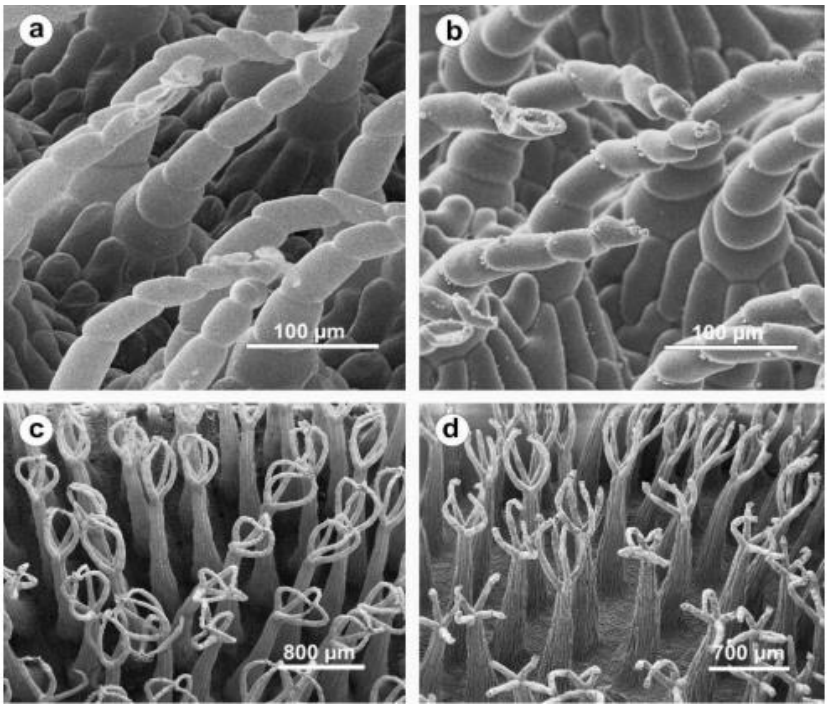

Figure 8. SEM images of the original plant surface structures and their replicas. Trichomes of *Salvinia cucullata* (a) and the respective replica (b). Trichomes of *Salvinia biloba* (c) and their replica (d). (Figure altered from Schulte et al., 2009) © 2009 Acta Materialia Inc. Published by Elsevier Ltd.

Another study developed a Dissolvable Template Nanoimprint Lithography* method (DT-NIL) (Figure 9) to replicate cicada wings (Oh et al., 2020). As a master surface the group used the wings of the Australian cicada species *Neotibicen pruinosus*, which they cleaned beforehand via sequential sonication in acetone, ethanol and deionized water. They dried their probes with a clean Nitrogen stream. After these preparation steps, quick-drying nail polish (top coat) was deposited on the wings. The comparison between spin-coating and simple drop casting showed no significant differences in resolution but only in the layer thickness. After 30 minutes of curing at room temperature the nail polish template was manually peeled off from the wing with forceps. As a next step, the template was put between two microscope glass slides for further curing to prevent warping caused by the residual stresses due to the peeling (Figure 9). The investigation of the used master surface suggested that hardly any damage is caused with this method, allowing to generate additional templates from the same master. With the help of the created template the group tried two different techniques creating a replica: electroplating of copper and a soft lithography approach with polydimethylsiloxane (PDMS) diluted with hexamethyldisiloxane (HMDS). In both methods, the template was dissolved afterwards in an acetonitrile sonication bath and depending on the approach,

additionally washed with ethanol, deionized water or isopropanol. To prevent structural collapse in the case of the softer PDMS (which is a problem in soft lithography), they coated the nail polish template with a 5 nm thick gold layer, which was subsequently transferred to the nanopillars

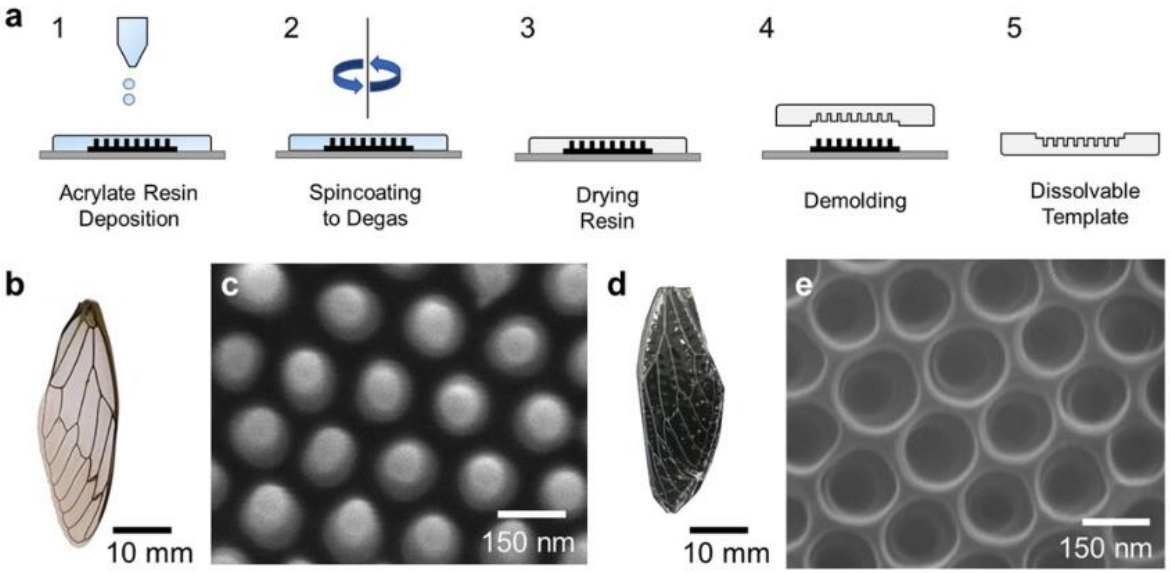

Figure 9. a) Schematic view of the described DT-NIL method, b) Image the original wing of *Neotibicen pruinosus,* c) SEM image of the original wing, d) Photograph of the dissolvable template, e) SEM image of the negative template. (Figure altered from Oh et al., 2020) © 2020 American Chemical Society

Cicadas

It was important for us that no living animal was harmed for this research. Unfortunately, there are no breeders of Cicadidae, which complicated obtaining dead samples. It is unattractive to keep cicadas for the following reasons: Cicadidae have long-lasting life cycles compared to other insect groups: their life cycles vary from 1 to 21 years depending on the species (Simon et al., 2022). While a major part of this time is spent in nymphal stages belowground, the emerged imagines live only for a few weeks to a few months (Simon et al., 2022; Williams & Simon, 1995). During their nymphal stages, they feed on the xylem fluids* of their host plants (Callaham et al., 2000; Cheung & Marshall, 1973). Depending on their emergence behavior, two groups are distinguished: annual and periodical cicadas (Karban, 1986). As the name suggests, annual cicadas emerge each year, although their development takes longer (but the emergence is not synchronized). In contrast, periodical cicadas emerge synchronously in huge numbers in so-called broods every 13 or 17 years (Grant, 2005; Karban, 1997; Simon et al., 2022; Williams & Simon, 1995). Previous studies showed that the wing nanostructures of *Magicicada* sp. have a lower aspect ratio* than other cicadas studied to date and are less efficient in rupturing cells (Nowlin et al., 2014). In this study the differences in structures and properties between *Magicicada* and two other cicada species are compared.

- **Class:** Insecta
  - **Order:** Hemiptera
    - **Family:** Cicadidae
      - **Subfamily:** Cicadettinae
        - **Tribe:** Cicadettini
          - **Genus:** *Kikihia*
            - **Species:** *Kikihia scutellaris*
          - **Genus:** *Amphipsalta*
            - **Species:** *Amphipsalta cingulata*
        - **Tribe:** Lamotialini
          - **Genus:** *Magicicada*
            - **Species:** *Magicicada septendecim*

Figure 10. Taxonomic hierarchy of the investigated cicada species.

More than 50 species in 5 genera live in New Zealand, each belonging to the subfamily Cicadettinae and the tribe Cicadettini (Figure 10) (Marshall et al., 2018; Simon, 2009). These species belong to two different lineages, which colonized New Zealand from Australia independently around 10 - 14 million years ago. One lineage contains the genera *Kikihia*, *Maoricicada* and *Rhodopsalta,* while the other lineage consists of *Amphipsalta* and *Notopsalta* (Marshall et al., 2008, 2012; Simon, 2009).

Amphipsalta cingulata

The genus *Amphipsalta* comprises only three species. This genus split up from the common ancestor with *Notopsalta* about 12.5 million years ago. *A. cingulata** (Figure 11, Figure 18) is restricted to the North Island of New Zealand and can primarily be found living in trees of coastal scrub habitats. Therefore, it sings in the sunlight, in contrast to *K. scutellaris** (Marshall et al., 2012).

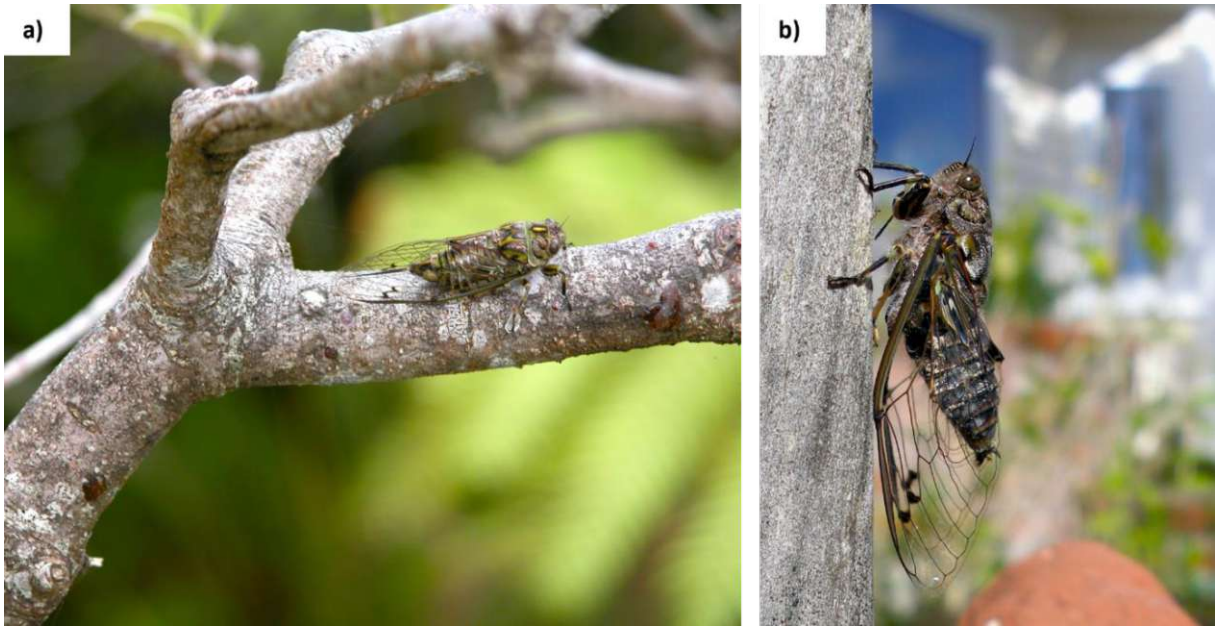

Figure 11. Amphipsalta cingulata (commonly known as clapping cicada), Wellington, Miramar Heights, New Zealand. a) Female *A. cingulata* on a *Pittosporum* tree, © 2008 Chris Simon, b) Male singing on an exposed fence post, on which they can commonly be found. © 2014 Chris Simon. Photos and information kindly provided by Professor Chris Simon (Ecology and Evolutionary Biology Department of the University of Connecticut).

Kikihia scutellaris

The genus *Kikihia* comprises about 30 taxa, such as *K. scutellaris* (Figure 12, Figure 19), found on the North Island of New Zealand. Together with *K. cauta,* it developed from the earliest lineage split in the evolutionary history of the genus about 6 million years ago. Despite most other species of this genus, these live in dense lowland forests, which supposedly predominated in the early Pliocene (about 4 million years ago). Because they prefer singing in deep bushes/forests whereas most other cicadas sing in sunny spots, these species are called „shade singers“* (Arensburger et al., 2004; Marshall et al., 2008).

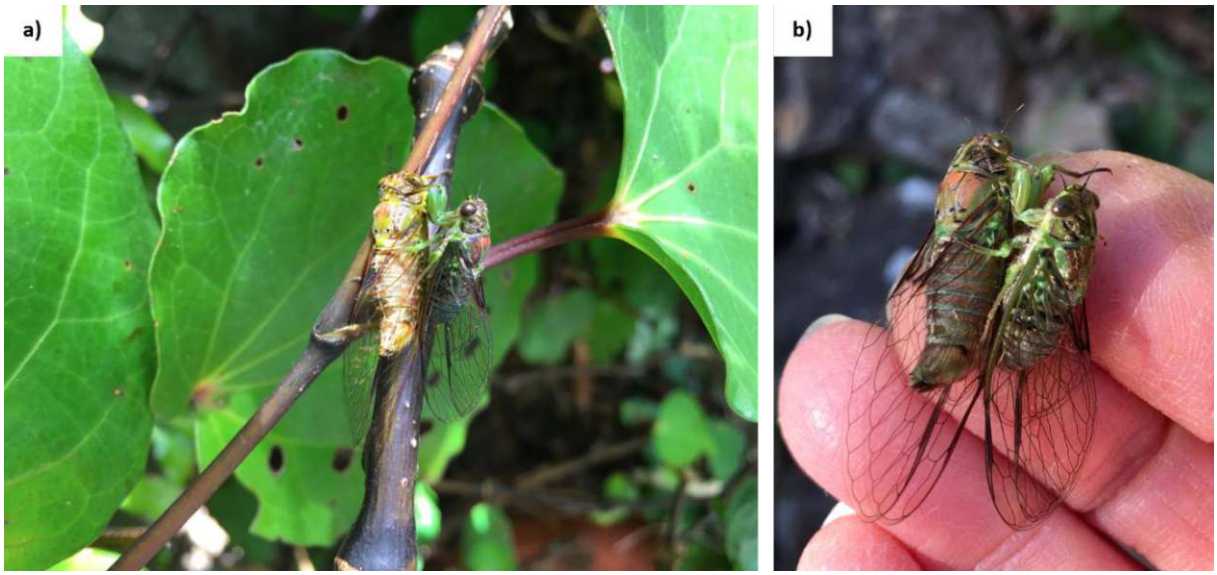

Figure 12. Kikihia scutellaris (commonly known as lesser bronze cicada), Wellington, Miramar Heights, New Zealand. *a)* Mating pair of *K. scutellaris* on a kawakawa (*Macropiper excelsum*), which is a New Zealand tree of the understory. These cicadas prefer to live in this layer of a forest and are therefore called „shade singers”. On the left, a female (pale color probably due to fresh emergence) and on the right a male cicada, © 2019 Chris Simon, b) Mating pair, where the female’s colors (on the left) are more representative, © 2018 Chris Simon. Photos and information kindly provided by Professor Chris Simon (Ecology and Evolutionary Biology Department of the University of Connecticut).

Periodical cicadas of North America

In contrast to annual cicadas, periodical cicadas do not emerge every year but every 13 or 17 years. All periodical cicadas belong to the genus *Magicicada* and are endemic in North America. The genus *Magicicada* belongs to the same subfamily (Cicadettinae) as the New Zealand cicadas (Figure 10) and comprises of seven different species, four of which occur in 13-year cycles and the others in 17-year cycles (Marshall & Cooley, 2000).

Magicicada septendecim

The adults of a *Magicicada septendecim* (Figure 13) population emerge (as the scientific name suggests) every 17 years in synchronized events. While their nymphal stage lasts many years, the imagines* live for four to six weeks. As the time as adults is relatively short, synchronization of emergence is a significant advantage for mating. The different populations emerging at the same time are called a brood. Broods are numbered with Roman numerals (Alexander & Moore, 1962; Simon et al., 2022). The individuals used for our study belonged to Brood X, which emerged in spring 2021.

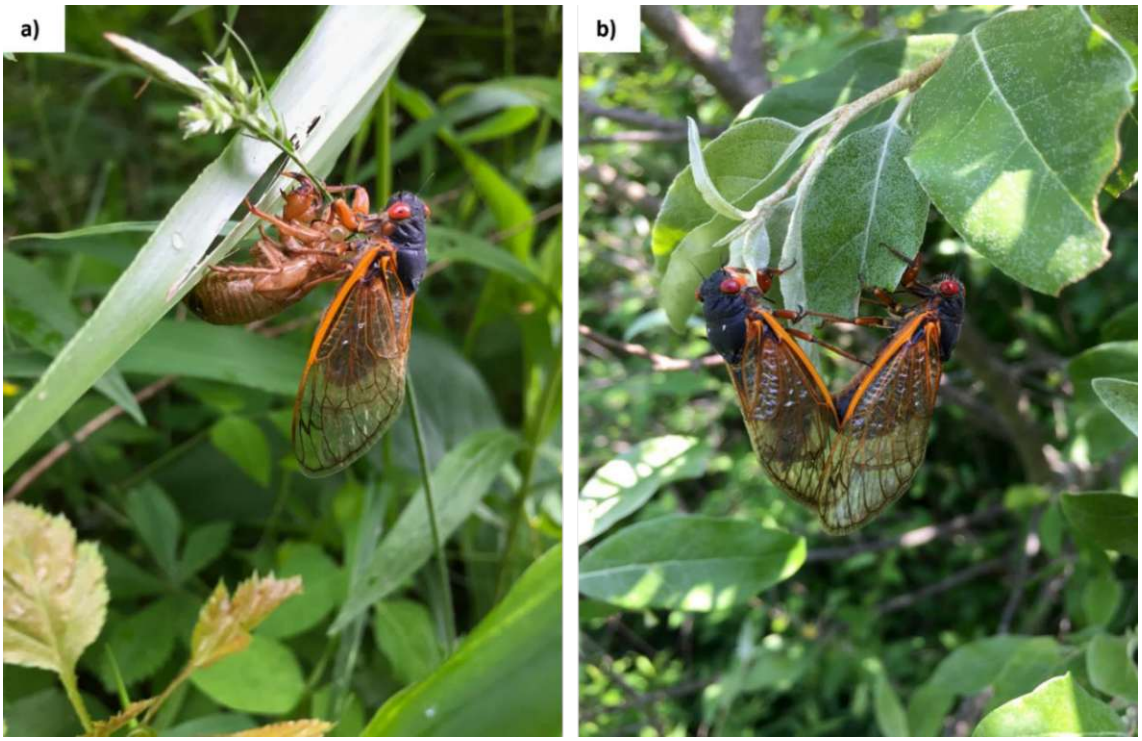

Figure 13. Magicicada septendecim (also known as 17-year cicada), Powdermill Reserve, Rector, Pennsylvania, U.S. a) Freshly emerged *M. septendecim* hanging onto its nymphal skin, © 2019 Chris Simon, b) Mating pair, female on the left, male on the right, © 2019 Chris Simon. Photos and information kindly provided by Professor Chris Simon (Ecology and Evolutionary Biology Department of the University of Connecticut).

Bacteria

Difference between Gram-positive and Gram-negative bacteria

Bacteria can be divided into two major groups, which can be distinguished by the Gram staining method. This staining method was developed by Hans Christian Joachim Gram in 1884, in honor of whom this method was named (Gjertsen & Daintith, 1999). The reason for the reaction to the staining method is caused by a major structural difference of the cell wall. The cell wall of Gram-negative bacteria consists of an outer cell membrane, an inner cell membrane and a thin peptidoglycan layer between both membranes. Gram-positive bacteria have just one cell membrane which is enclosed by a thick peptidoglycan layer (Figure 14). The Gram staining consists of four steps. First the bacteria are stained with crystal violet (CV), a triarylmethane dye, which dissociates into Cl^- and CV^+ ions in aqueous solutions. These ions can cross the cell walls and membranes of both bacteria groups and stain the cells. Next iodine is added. Iodide forms complexes with crystal violet (CV-I), this way the stain is trapped and not soluble in water anymore. In the next step a decolorizer such as ethanol is added. In case of Gram-negative bacteria, the outer cell membrane is removed and the CV-I complexes from the thin exposed peptidoglycan layer are washed out. Therefore, the cells lose their color. Whereas in Gram-negative bacteria the thick peptidoglycan layer traps the staining complexes and the cells keep the typical purple color. As final step a counter stain (such as safranin) is used to mark the Gram-positive bacteria (Fritsche, 2016; Sandle, 2016) (Figure 14).

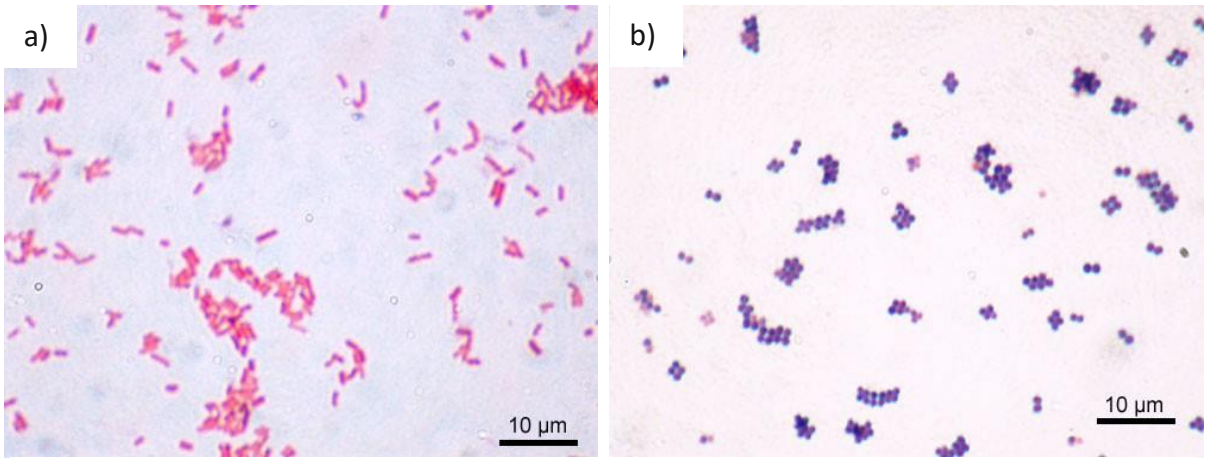

Figure 14. Light microscopy images of Gram-stained bacteria: a) Gram-negative *Escherichia coli* (ATCC 11775), b) Gram-positive *Staphylococcus aureus* (ATCC 25923). (Images taken from https://commons.wikimedia.org, GNU Free Documentation License, 18.03.2022). © 2005 Y_tambe

Gram-positive bacteria

Gram-positive bacteria lack of an outer membrane, instead peptidoglycan builds up the outermost layer. Peptidoglycan consists of glycan chains of repeating disaccharide units (consisting of N-acetyl glucosamine and N-acetyl muramic acid), which are cross linked by peptides (Sun et al., 2022). It forms a rigid polymeric meshwork and determines the shape of the cell. The stiffness of this layer depends on various factors such as the number of cross-links and glycan chain length (Auer & Weibel, 2017). The thickness of the peptidoglycan layer ranges from about 30 nm - 100 nm (Silhavy et al., 2010). Attached to the peptidoglycan wall teichoic acids (WTAs) are found in Gram-positive bacteria. These anionic glycopolymers build up to 60% of the cell wall mass (Brown et al., 2013). Besides WTAs also Lipoteichoic acids (LTAs) exist in Gram-positive bacteria. These are composed of two structural elements: and a polymeric chain and a glycopolymeric head group, which links the LTA to the cell membrane, which is a phospholipid bilayer. Studies showed that WTAs as well as LTAs play a role for the mechanical properties of the cell wall (Auer & Weibel, 2017; Silhavy et al., 2010) (Figure 16).

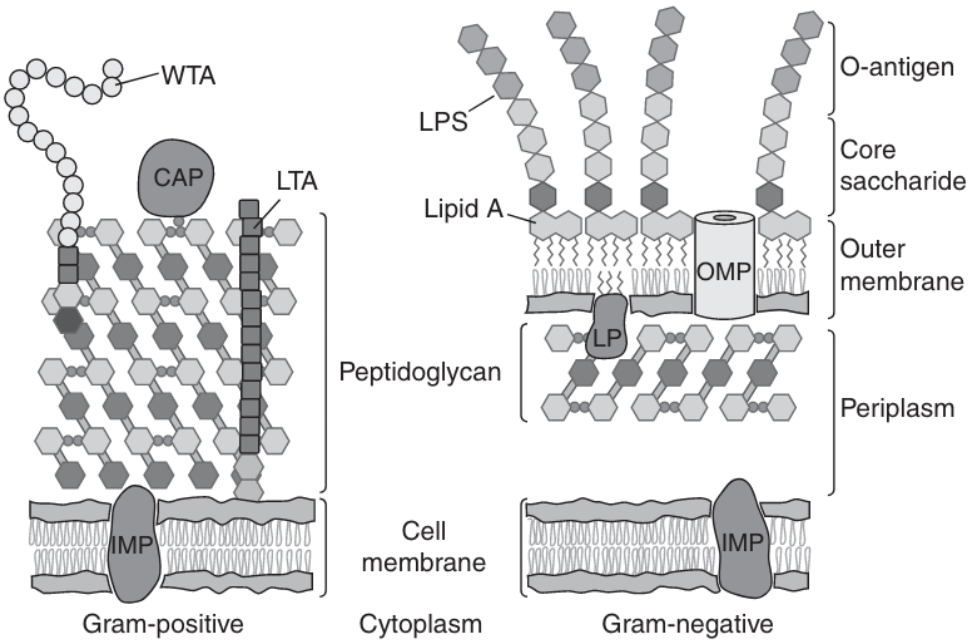

Figure 15. Depiction of Gram-positive and Gram-negative cell envelopes: CAP = covalently attached protein; IMP = integral membrane protein; LP = lipoprotein; LPS = lipopolysaccharide; LTA = lipoteichoic acid; OMP = outermembrane protein; WTA = wall teichoic acid. (Figure taken from Silhavy et al., 2010) ©2010 Cold Springer Habor Laboratory Press

Gram-positive bacteria

Gram-negative bacteria possess an outer membrane which is an asymmetric lipid bilayer. The inner leaflet consists of phospholipids, whereas lipopolysaccharides (LPS) are situated at the outer leaflet (Silhavy et al., 2010; J. Sun et al., 2022). These LPS consist of three major parts: lipid A (also called endotoxin), core oligosaccharides and the distal hydrophilic polysaccharides (also called O-antigen). Lipid A anchors the LPS into lipid bilayer, whereas the polysaccharides with varying lengths build up the outermost layer of Gram-negative bacteria and therefore the interface between bacterium and environment (Raetz & Whitfield, 2002). In addition, the outer membrane contains various proteins and lipoproteins which link the membrane to the peptidoglycan layer. In Gram-negative bacteria the peptidoglycan consists of only one to few layers (thickness of few nanometers). The inner membrane is a phospholipid bilayer containing different proteins and is the interface to the cytoplasm* (Silhavy et al., 2010) (Figure 15).

Mechanics of the bacteria cell wall

Historically the mechanical properties of bacteria cells were mainly derived from the rigid peptidoglycan layer. But studies show that all many compartments play a role in the cell wall mechanics of bacteria. Although bacteria can be distinguished into the two major groups Gram-positive and Gram-negative, a huge variation of mechanical properties can be found within each group. It is caused by many factors such as cell shape and differences in the composition of the layers. Yet, most biophysical models simplify the bacteria cell wall to a homogenous layer and describe the mechanical properties by parameters such as thickness, Young's modulus and bending rigidity (Auer & Weibel, 2017).

Escherichia coli

Escherichia coli (Figure 16) is a rod-shaped Gram-negative bacterium first described in a publication 1885 by the German-Austrian pediatrician and professor Theodor Escherich in honor of whom the genus was named later (Shulman et al., 2007). It is one of the best investigated model organisms and commonly used for scientific studies. It occurs primarily in the gut of vertebrates and the relationship of most strains to the host organism can be described mainly as commensalism* with sometimes even mutualistic* effects (Gordon, 2013; Tenaillon et al., 2010). For example, it is a typical component of the intestinal microflora of a healthy human and colonizes the gastrointestinal tract immediately after birth (Kaper et al., 2004). Beside such harmless or useful strains there are also various pathogenic types of *E. coli.* These may cause several diseases such as diarrheal illness (most common cause of traveler's diarrhea), intestinal and extraintestinal infections. Such pathotypes are responsible for a significant number of deaths worldwide, especially in developing nations (Croxen et al., 2013; Kaper et al., 2004; Smith et al., 2007).

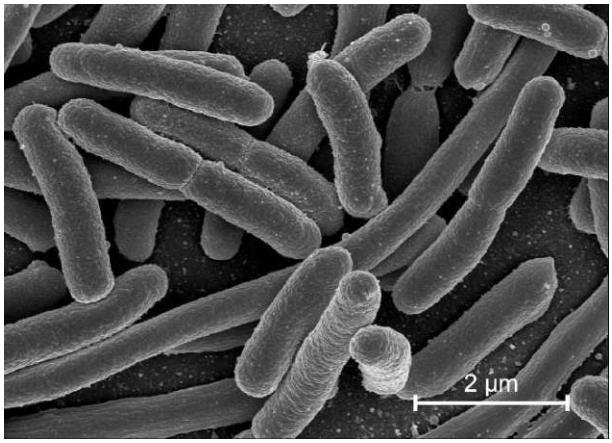

Figure 16. SEM image of *Escherichia coli* adhered to a cover slip. (Altered from NIAD account on *https://.flickr.com*, public domain, 21.02.2022)

Staphylococcus aureus

Staphylococcus aureus (Figure 17) is a spherical shaped Gram-positive bacterium (Thomer et al., 2016). The genus was first described by the British surgeon Alexander Ogston 1882. He named the genus *Staphylococcus* (which origins from the Greek words: σταφυλή meaning grape and κόκκος translating into corn), because it tends to form grape-like clusters in contrast to the chain-forming *Streptococcus* (Ogston, 1882). Later the German physician Friedrich Rosenbach differentiated two different species and named them based on the color of their colonies: *S. albus* (albus (latin) = white) and *S. aureus* (aureus (Latin) = golden) (Rosenbach, 1884). *S. aureus* is a usual part of the human microbiome and occurs as a commensalistic inhabitant of different skin sites such as in the mucous membranes of the anterior nasal passages. Studies showed that about 12-30 % of humans are persistent nasal carriers of the *S. aureus* (Wertheim et al., 2005). However, *S. aureus* can also act as an opportunistic pathogen causing diseases such as endocarditis, skin, soft tissue and bloodstream infections (bacteremia) (Thomer et al., 2016; Tong et al., 2015).

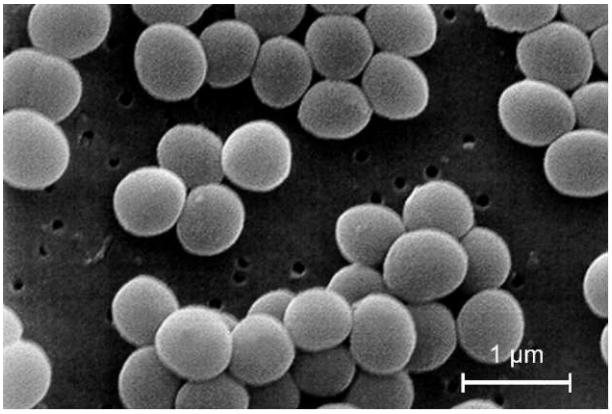

Figure 17. SEM image of Staphylococcus aureus taken from a vancomycin intermediate resistant culture. (Image taken and altered from https://phil.cdc.gov, 21.02.2022) public domain, photo credit Janice Haney Carr

Before the introduction of antibiotics, the mortality due to bacteremia exceeded 80 %. In the 1940s penicillin treatment began, but soon after the first strains developed a resistance through expressing penicillinase. The suffix '-ase' is used for enzymes that have a cleaving effect on a certain chemical substance, which determines the term before the suffix, for example penicillinase inactivates penicillin. Nowadays over 90 % of isolated *S. aureus* produce penicillinase. In 1961 the first penicillinase-resistant penicillin (methicillin) was discovered. Shortly after, the first drug resistant strains were observed. Same problematics arose when other antibiotics such as quinolone and vancomycin were used to treat methicillin resistant *S. aureus* (Lowy, 2003). Today these multidrug-resistant* strains are a major threat to the health system as they are the cause of many clinical infections (Kuehnert et al., 2005; Thomer et al., 2016; Tong et al., 2015).

Aim of this work

This thesis presents studies on the wing membrane surface of three cicada species: *Amphipsalta cingulata*, *Kikihia scutellaris* and *Magicicada septendecim*. Atomic Force Microscopy (AFM)* and Scanning Electron Microscopy (SEM)* are used to study the wing membrane topography on a nanoscale*. In addition, a fast and straightforward 2-step nanoimprinting technique is introduced to transfer the structures found in the insects to versatile technologically relevant materials such as epoxy resin. Qualitative AFM and SEM analyses of the positive impressions are performed.

In a next step the wings are examined regarding formerly reported properties such as hydrophobicity and bactericidal activity. Therefore, contact angle measurements and live/dead staining experiments are performed. To test whether the structure of the bacterial cell wall determines the sensitivity, the bacterial experiments are performed with *Escherichia coli* (Gram-negative) and *Staphylococcus aureus* (Gram-positive). Furthermore, a comparison is drawn to species investigated in previous studies.

Three hypotheses are tested:

1. *A. cingulata* and *K. scutellaris* have different preferences for their living areas. Whereas the former prefers to sing on exposed sunny spots, the latter prefers shady spots in deep bushes. These different ambient conditions lead to different appearance in nanostructures. In humid shady areas it is more important to have hydrophobic wings and therefore the nanostructures have a higher aspect ratio.
2. The higher the nanostructures are, the more efficient are their bactericidal properties.
3. A fast and low-cost nanoimprinting method can be established, with which it is possible to transfer the surface structures on the nanoscale as efficiently as the generally used time-consuming and cost-intensive techniques. Moreover, the produced replicas possess bactericidal properties comparable with the original wing membranes as the killing mechanism is based on mechanical principles rather than chemistry.

Material & Methods

Biological material

Cicada wings

After writing various emails to cicada experts, Dr. Werner Holzinger (Ökoteam® – Institut für Tierökologie und Naturraumplanung, Graz, Austria) recommended contacting Dan Mozgai (Host of the homepage: www.cicadamania.com). Thanks to Dan, I obtained the contact of Professor Chris Simon (Ecology and Evolutionary Biology Department of the University of Connecticut). She helped me to get in touch with David Marshall, Ph.D. (Ecology and Evolutionary Biology Department of the University of Connecticut). He was staying in New Zealand at that time and thankfully he sent me dried and identified specimens (already dead, so no animal was harmed only in purpose of this study) of two cicada species: *Amphipsalta cingulata* and *Kikihia scutellaris* (Figure 19 and Figure 18).

Figure 18. Dried specimen of *Amphipsalta cingulata.* © 2020 Alexander M. Bürger

Figure 19. Dried specimen of *Kikihia scutellaris.* © 2020 Alexander M. Bürger

In addition, Julia Fisher (from the Facebook group Weltfrauen), who lived then in Arlington, Virginia, United States, thankfully collected and sent the cicada wings of several naturally died *Magicicada septendecim* individuals of the population called Brood X, which emerged in a massive event in spring 2021. These wings were air dried in advance.

The wings of the New Zealand cicada species were carefully separated from the body with tweezers. Only the forewings of all three cicada species were investigated in this study and therefore further prepared depending on the experimental design (Figure 20).

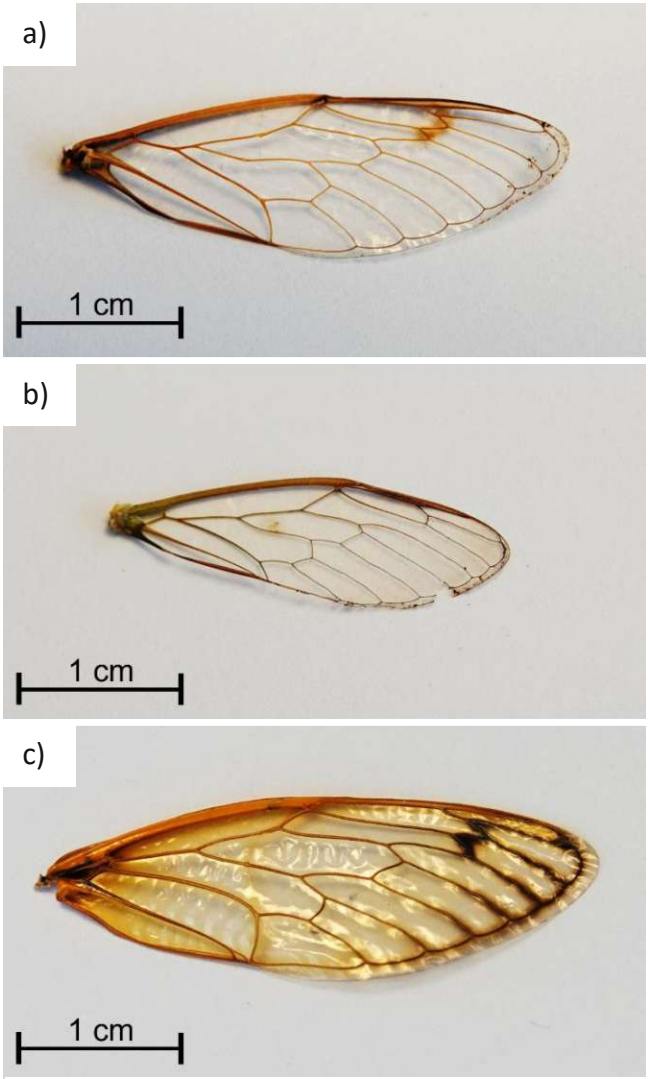

Figure 20. Dissected forewings of all three cicada species investigated. a) *A. cingulata*, b) *Kikihia scutellaris, c) Magicicada septendecim*.

Nanostamping of cicada wings using Polyvinyl siloxane (PVS)

Various experimental designs were developed to transfer nanostructures of cicada wings to replicas based on the former studies discussed in the Introduction (Koch et al., 2008; Schulte et al., 2009; Zobl, 2017; Zobl et al., 2016). The method consists of three major steps:

1. Preparation of the wings
2. Creating a master from the biological template
3. Using the master to create a replica.

An overview of the different methods presented in this study can be found in Table 1.

Preparation of the wings

As a first step, the wings were used as they were or put into an ultrasonication bath in distilled water for 10 minutes (alternatives tried out: acetone [99 %], isopropanol [99 %]). Due to their hydrophobic properties, the wings float on the water surface. Therefore, the wings were placed with the top side down to clean the upper (dorsal)* side, in contrast to pure acetone and isopropanol, where the wings sink down and are fully submerged because of the lower density and surface tension of the fluids. Afterwards, the wings were dried under a nitrogen stream. Furthermore, small discs with 5 mm diameter were cut out of the wings with a biopsy punch (Figure 21, Kai Medical Biopsy Punch 5mm, Kai Industries Co. Ltd., Seki, Japan).

Figure 21. Picture of the biopsy punch used to cut small discs out of the wing. © Alexander M. Bürger

Creating a master stamp

The wing or the prepared discs were mounted (with the dorsal side on top) inside a small plastic petri dish cap (diameter: 35 mm) with double-sided adhesive tapes (Permanent Double Sided Tape from Scotch®, 3M, Saint Paul, Minnesota, U.S.). The negative impressions were obtained with two different PVS dental pastes (President The Original Light body & Xtra light

body, Coltène/Whaledent AG, Altstätten, Switzerland), which were cooled down beforehand to approximately 5 °C as suggested by Koch et al. 2008 to extend the curing process. The two components of the dental pastes were manually mixed in a 1:1 ratio and immediately deposited into the mid of the wing surface. Subsequently, the bottom of the petri dish was placed onto the PVS and was furthermore weighted with standard microscope glass slides (Microscope Slides 76 mm x 26 mm from Henry Schein Inc., Melville, New York, U.S.) (Figure 22). One microscope slide had a mass of 5 g. The tested weights ranged from 5 g to 30 g. The PVS was cured at room temperature or at 4 °C to increase the time for the curing process further. After the PVS was fully cured, it was gently peeled from the biological template and was ready to be used as a master stamp (Figure 24 a & b).

Furthermore, it was attempted to clean the negative impressions in an additional step. They were placed into a formic acid bath [85 %] (AMO Varroxal, Kurdrogerie Resch GmbH, Bad Schallerbach, Austria) to remove any potential biological residuals. Formic acid is an appropriate dissolvent for chitinous components (Roy et al., 2017). After ten minutes, the negative imprint was transferred to an ultrasonication bath in distilled water for another ten minutes.

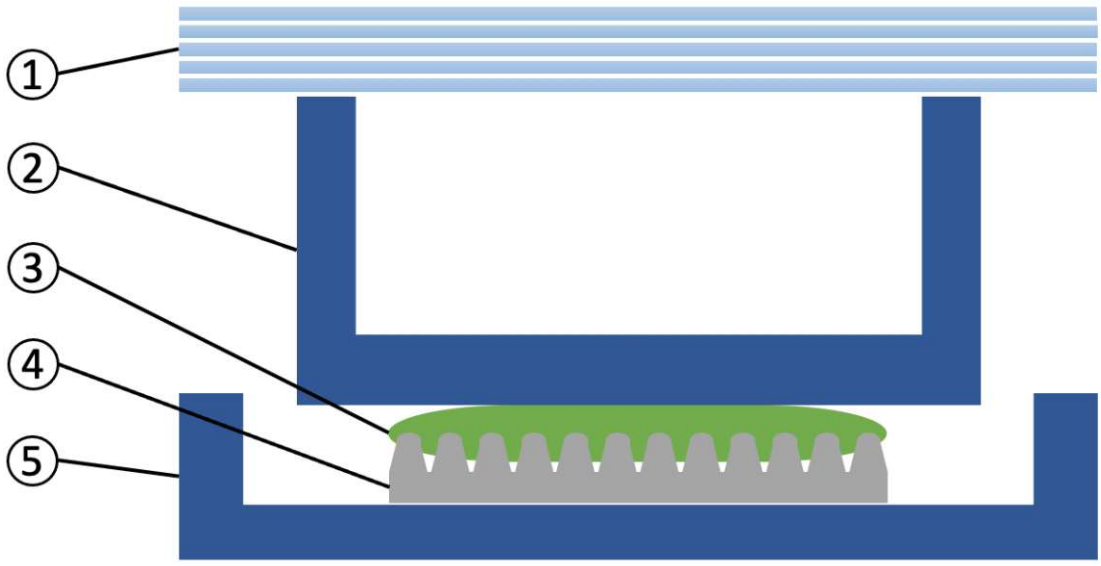

Figure 22. Scheme of the imprinting method: 1) microscope glass slides as weights, 2) Bottom of a petri dish, 3) PVS paste, 4) Wing sample, 5) Cap of a petri dish. ©Alexander M. Bürger

The next step was to fill the negative impression with a molding material to obtain a positive replica. One of the materials selected for the positive replica was epoxy resin (Epoxid-Gießharz Wasserklar + Härter W 300 (Art.-Nr.: 1071060), R & G Faserverbundwerkstoffe®, Waldenbuch, Germany) was chosen as suggested by Koch, Schulte, Zobl and co-workers (Koch et al., 2008; Schulte et al., 2009; Zobl et al., 2016). The negative template was fixed with a double-sided adhesive tape into a cap of a small petri dish. Then the two components (resin and hardener) of the epoxy resin were mixed in the specified ratio and carefully poured over the prepared master stamp. Subsequently, the arrangement was transferred into a vacuum chamber for 5 minutes to prevent air bubbles from being trapped at the interface of the curing resin. The negative template was further fixed with a 3D-printed obstacle to the ground while the air bubbles were sucked out of the resin (Figure 23). After this step, the samples were taken out of the vacuum chamber and cured at room temperature for the time indicated on the label. Finally, the PVS templates were carefully removed. The same method was also performed without putting the resin into a vacuum chamber.

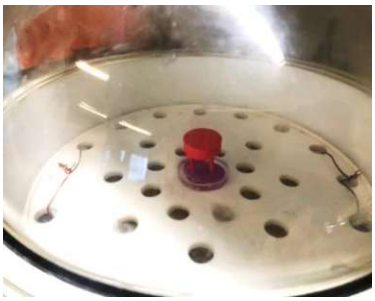

Figure 23. The petri dish with the negative imprint is filled up with epoxy resin and afterwards put into a vacuum chamber. The red obstacle prevents the PVS impression to rise. © 2021 Alexander M. Bürger

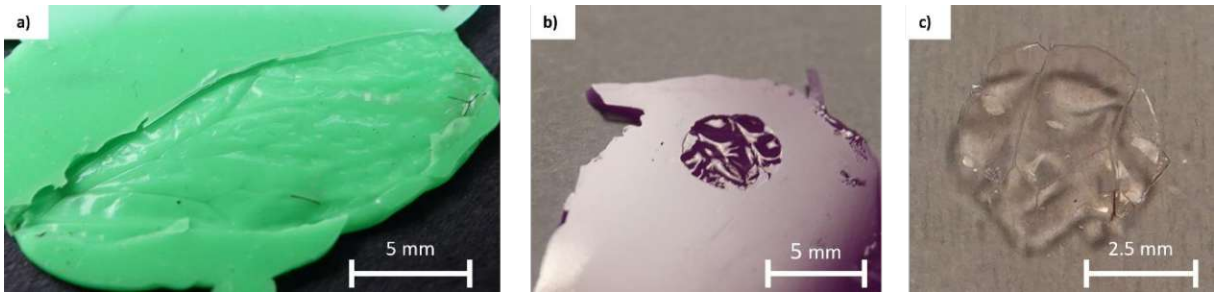

Figure 24. a) Negative impression in PVS Light Body (produced with Method B), b) Negative impression in PVS Xtra Light Body (produced with Method D), c) Replica in UV curing resin (Method D). © 2022 Alexander M. Bürger

In addition, a photopolymer resin (Elegoo ABS-Like LCD UV-curing photopolymer rapid resin, GE-EL-3D-005, Elegoo, Shenzhen, China) was used as a molding material instead of epoxy resin (Figure 24 c). The main advantages of using a UV-curing resin are that initiation of the curing process can be delayed and that there is no need to mix two components together - which reduces the risk of air bubbles trapped into the resin. After casting the resin onto the PVS template, a cover slip was placed on top of the resin droplet to make the replica as thin as

possible (this simplifies the handling for the AFM analysis and bacterial experiments). For the first two hours the resin was protected from light. During this time, the air bubbles have enough time to rise from the liquid resin, which would otherwise disturb the curing process. As a next step, the resin was put under normal light conditions for another three hours to start a slow curing process. Afterwards, it was completely cured with a UV light (UniTak3D UV Light Hardening Lamp, wavelength 405 nm, Shenzhen Redrex Technology Co. Ltd., Shenzhen, China)

Table 1. Overview of the replication methods presented in this a study, where PVS was used as molding material for negative impressions.

	Wing preparation	**Negative impression**	**Cleaning steps**	**Positive impression**
Method A	Ultrasonication in distilled water, whole wing used	PVS Xtra Light Body, cured at room temperature additional weight during molding process 5 g	Formic acid bath, ultrasonication in distilled water	Epoxy resin
Method B	Ultrasonication in distilled water, whole wing used	PVS Light Body cured at room temperature additional weight during molding process 30 g	Formic acid bath, ultrasonication in distilled water	Epoxy resin
Method C	No cleaning steps, 5 mm wing disc	PVS Xtra Light Body, cured at 4 °C additional weight during molding process 15 g	-	UV curing resin/ Epoxy resin, flattened with a coverslip
Method D	No cleaning steps, 5 mm disc	PVS Xtra Light Body cured at room temperature additional weight during molding process 30 g	-	UV curing resin/ Epoxy resin, flattened with a coverslip

Further approaches

Using nail polish for creating a template

Based on a study by Oh et al. 2020, nail polish (ultra quick DRY top coat from Essence, Cosnova GmbH, Sulzbach, Germany) was used instead of PVS. The nail polish was carefully cast on the wing. After approximately 45 minutes, the template was peeled off. The previous study stated that it is essential to wait until the nail polish is semi-cured. If it is undercured, it is still sticky and cannot be removed from the wings without damaging the template structures, but if it is overcured, the nail polish gets brittle (Oh et al., 2020). When the templates were removed from the wings, they were deposited between two microscope slides as described above and fully cured for 6 hours. In addition, a test was conducted in which the nail polish was cured entirely on the wing (6 hours) and then peeled off.

Direct casting of resins

Furthermore, it was investigated if the UV curing resins can be used as stamping material. Therefore, the wing pieces were prepared as described above. Then a drop of the UV-curing resin was cast onto the cicada wing and cured the same way as described above.

Atomic Force Microscopy (AFM)

The surfaces of the cicada wings and their replicas were investigated using an atomic force microscope (Cypher ES AFM from Asylum Research, Oxford Instruments plc, Abingdon, United Kingdom). The samples were washed before in an ultrasonication bath (distilled water) for 10 minutes, dried with a nitrogen stream and mounted on the AFM sample discs with double-sided adhesive tape or with nail polish.

For the investigation of the *K. scutellaris* wings, the AFM was used in tapping and contact mode with an Opus 240 AC-NA AFM cantilever (resonance frequency: 70 kHz; force constant: 2 N/m, probe made of highly n-doped monocrystalline Silicon, backside of the tip coated with Aluminum). Imaging of the wings of *A. cingulata* and the replicas was performed on the AFM

in tapping and contact mode with a ContGB-G AFM cantilever (resonance frequency: 13 kHz; force constant: 0.2 N/m, probe made of monolithic Silicon with an overall Gold coating) from BudgetSensors© (Innovative Solutions Bulgaria Ltd., Sofia, Bulgaria).

In addition, a standardized setting was used to compare the wing topography of all three cicada species. The scans were performed at the same Cypher ES in tapping mode (device provided by Prof. Markus Valtiner, head of the Applied Interface Physics division at the Institute of Applied Physics, TU Wien). All measurements were performed with a Tap300-G probe from BudgetSensors© (resonance frequency: 300 kHz; force constant: 40 N/m, probe made of uncoated monolithic Silicon). The samples were this time cleaned in an ultrasonic bath in distilled water and dried under a (warm gaseous) nitrogen stream.

The replicas were investigated with an MFP-3D-BIO AFM (Asylum Research, Oxford Instruments plc) due to the more accessible chamber (provided by Prof. Markus Valtiner). The measurements were also performed with a Tap300-G probe from BudgetSensors© in tapping mode. An overview of the different settings used in this study is provided in (Table 2).

Table 2. Overview of the Atomic Force Microscopy (AFM) settings used.

	AFM	Cantilever	Mode	Samples analyzed
Setting CY_C (Cypher_Contact) Optimized for contact mode	Cypher ES	ContGB-G force constant: 0.2 N/m, monolithic Silicon with Gold coating	contact & tapping	*A. cingulata* wings
Setting CY_A (Cypher_Allround) Allround setting for both modes	Cypher ES	Opus 240 AC-NA force constant: 2 N/m n-doped monocrystalline Silicon, backside Aluminum coating	contact & tapping	*K. scutellaris* wings
Setting CY_T (Cypher_Tapping) Optimized for tapping mode	Cypher ES	Tap300-G force constant: 40 N/m uncoated monolithic Silicon	tapping	*A. cingulata*, *K. scutellaris*, *M. septendecim* wings, replicas
Setting MFP_T (MFP_Tapping) Optimized for tapping mode short sample switching time	MFP-3D-BIO	Tap300-G force constant: 40 N/m uncoated monolithic Silicon	tapping	replicas

AFM image analysis

AFM measurements were analyzed with the open-source software Gwyddion (Nečas & Klapetek, 2012). To evaluate the heights of the nanopillars, first, the base plane was flattened. In addition, the ground level of the AFM image was set to the minimum, justified by the assumption that at this point, the tip was able to come closest to the actual base in between the nanopillars. As a next step, the so-called watershed operation was performed with Gwyddion to mark the peak of each nanopillar, which is suitable for detecting local extremes (Klapetek et al., 2009). This way, the hills of the nanopillars were marked in each image (Figure 25). The maximum of each marked area (which refers to the absolute top of a hill) was measured. This was performed on with two or three 25 µm^2 areas to calculate an average height distribution. For the tip-to-tip spacing, distances between 200 nanopillars were measured and averaged.

Furthermore, the height data of the nanopillars was tested for normal distribution with the software package RStudio (RStudio Team, 2015).

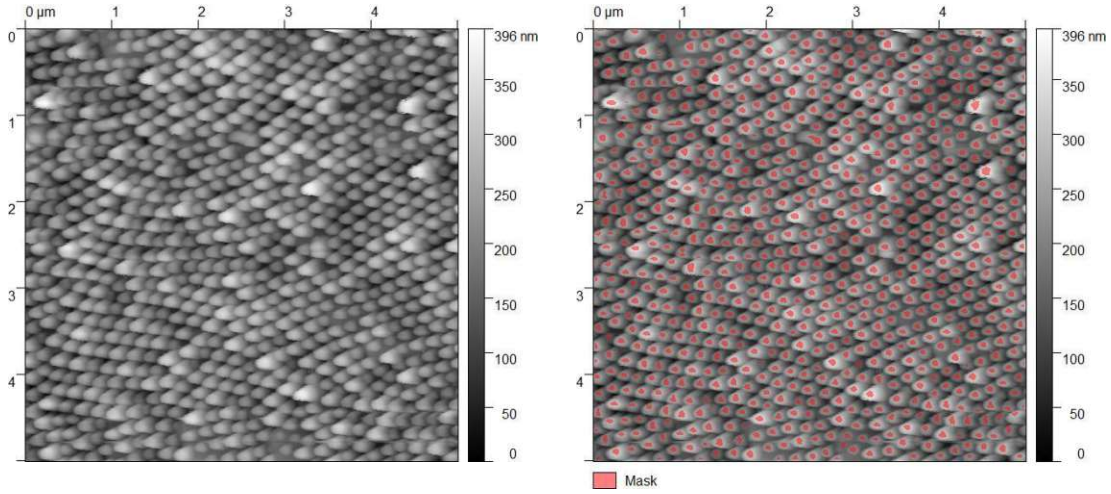

Figure 25. Example of using the watershed approach in Gwyddion to mark the nanopillar tops as grains. (Cypher ES AFM from Asylum Research, tapping mode, Opus 240 AC-NA AFM cantilever; image size: 5 µm x 5 µm, imaging parameter: height). Own images

Scanning Electron Microscopy (SEM)

For a better understanding of the nanopillar structure and to evaluate the nanostamping technique, an SEM analysis was performed in addition to AFM scans. The SEM imaging was carried out using facilities at the University Service Centre for Transmission Electron Microscopy, Vienna University of Technology, Austria (operator Karin Whitmore). The microscopes used were a Scios 2 DualBeam and an FEI Quanta 250 FEG (both from Thermo Fisher Scientific GmbH, Waltham, Massachusetts, U.S.).

The cicada wings were washed in distilled water ultrasonic bath for 10 minutes and afterwards put under a stream of nitrogen to remove the water residuals. Furthermore, some PVS impressions, as well as some replicas, were investigated. In addition, imaging was also performed on a wing of each species with attached *E. coli* bacteria. To prepare such a sample, the wings were incubated in a bacterial suspension for one hour, as described in the next section. After this time, the suspension was removed. All samples were air-dried in a petri dish with silica gel for two days. Finally, the samples were mounted on the sample holder with double-sided adhesive carbon tape (Thermo Fisher Scientific GmbH, Waltham, Massachusetts, U.S.) and sputtered with a 4 nm Gold/Palladium layer.

In addition to the regular SEM mode, a focused ion beam (FIB)* investigation was performed to investigate the nanopillar structure further. As a first step, the area of interest was coated with a protective Carbon layer. Next, a thin layer of Wolfram was applied, followed by another thicker layer of Wolfram. These layers protect the surface from the Gallium ion beam, which is used was used to cut the sample vertically layer by layer (Young & Moore, 2005).

The images were analyzed with the open-source platform Fiji (Schindelin et al., 2012). For the height, base diameter, and tip diameter 100 measurements were taken by hand and averaged. The tip-to-tip spacing was calculated between the centroids* of a nanopillar to its 6 nearest neighbors (as the base unit of the nanopattern is hexagonal). The measurement was performed for 200 nanopillars and the results were averaged.

Bacterial testing

For the examination of bactericidal properties of the cicada wing membrane, bacterial live/dead tests* were performed. The bacterial test procedures were developed together with Richard van Nieuwenhoven (diploma student at the Institute of Applied Physics at TU Wien) with the advice of Philip Kienzl from the Department of Dermatology at Medical University of Vienna. The initial cultivation of the bacteria and measurements at the fluorescence microscope were performed by the latter two.

Bacteria used

As a previous study reported that the susceptibility of Gram-positive and Gram-negative bacteria regarding the killing mechanism differ (Hasan et al., 2013), it was decided to use one of each kind. *Escherichia coli* (DSM 5698/ATCC 25404) was used as a Gram-negative representative and *Staphylococcus aureus* (DSM 1104/ATCC 25923) as Gram-positive representative, both were obtained from the Leibnitz Institute (DSMZ-German Collection of Microorganisms and Cell Culture GmbH, Braunschweig, Germany).

Cultivation

The initial cultivation of the freeze-dried bacteria was performed in Lysogeny broth (LB-medium), which was produced after the standard protocol developed by Giuseppe Bertani (Bertani, 1951). After an overnight growth, the suspension was mixed 1:1 with a 50 % glycerol solution in phosphate-buffered saline (PBS). The suspension was carefully intermixed and distributed to Eppendorf tubes® (Eppendorf SE, Hamburg, Germany). They were stored in succession at -80 °C (Ultra-Tiefkühlbox B 35-85, Fryka-Kältetechnik GmbH, generously provided by Professor Markus Valtiner).

Preparation of bacterial suspension

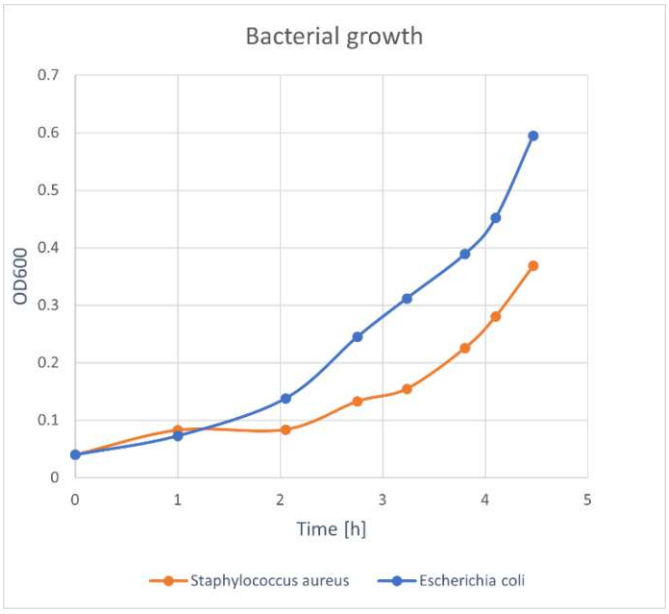

Figure 26. Growth experiment of both bacteria (*E. coli* and *S. aureus*) used with OD_{600} measurements over the time.

Before each experiment, the bacteria were carefully thawed up and suspended in LB medium. The suspension was carefully mixed and split into 1.5 ml tubes. These were put into a shaker (Thermomixer Compact, Eppendorf®, Hamburg, Germany) at 37 °C and 800 rpm to provide optimal growth conditions regarding temperature and oxygen supply. The suspension was grown until it reached an optical density at 600 nm wavelength (OD_{600}) of around 0.25 for a wavelength. The OD_{600} value is commonly used as a rough estimation of the bacterial density*. The measurements were performed with a BioTek EL800 Absorbance Microplate Reader (Agilent Technologies, Santa Clara, California, United States). OD_{600} = 0.25 marks the early logarithmic growth stage, in which the viability of cells is optimal (Figure 26). A previous study showed that this density is well suited for live/dead experiments (Robertson et al., 2019). Higher densities would complicate the counting of bacteria during the experiment. Former studies about the antibacterial properties of cicada wings used densities in the range of 0.1 and 0.3; therefore, the used OD_{600} (0.25) lies within this range and increases the comparability between studies (Hasan et al., 2013; Ivanova et al., 2012; Kelleher et al., 2016; Román-Kustas et al., 2020).

Cicada wing preparation

As a first step, the cicada wings were placed in an ultrasonic distilled water bath and afterwards dried in the air. As preparation, a black 3D-printed ring was glued to microscope slides with nail polish so that it would form a watertight seal (Figure 27 a). The container thus created is used for the further steps. A small slice (5 mm diameter) was cut from each wing using a biopsy punch. These pieces were mounted with nail polish onto the prepared microscope slides.

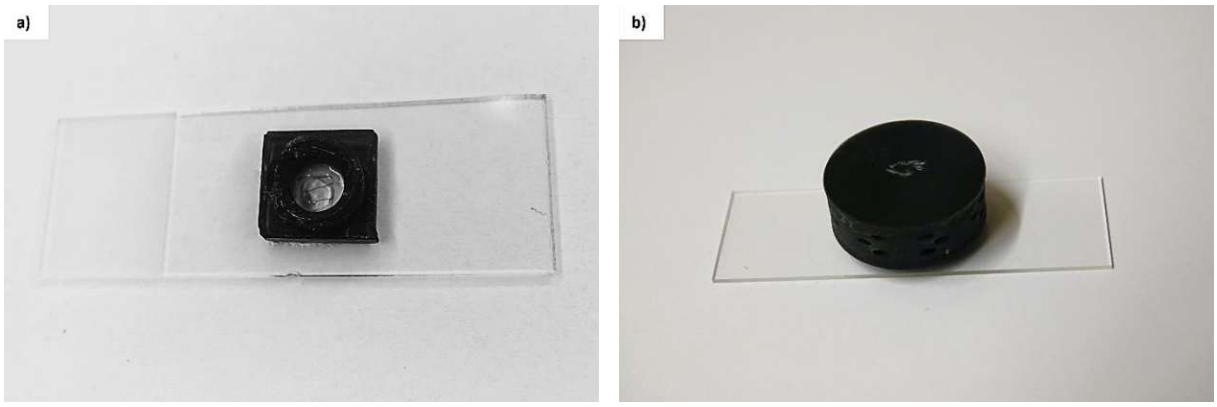

Figure 27. Microscope slides (76 mm x 26 mm) prepared for bacterial testing. a) Prepared chamber with mounted wing piece, b) Light protection case for staining steps. © 2022 Alexander M. Bürger

Fluorescence dyes

To perform a live/dead experiment, it is essential to differentiate between living and dead cells. One common way to achieve that is using fluorescence stains with different properties. In this study Propidium Iodide (PI) (≥ 94.0 % (HPLC), P4170 Sigma-Aldrich) and Bisbenzimide Hoechst 33343 (≥ 98.0 % (HPLC and TLC), B2261 Sigma-Aldrich) both obtained from Merck KGaA (Darmstadt, Germany) were used. PI is a nucleic acid stain that does not permeate intact membranes. It is only able to enter dead cells in which the integrity of the membranes is damaged. In comparison, Bisbenzimide is a DNA stain, able to pass intact cell membranes. In this way, all bacterial cells should be stained with Bisbenzimide, but only dead cells should include PI. Both dyes were used as the protocol stated. As a stock solution, PI powder was dissolved in water [1 mg/ml]. In the experiments, it was further diluted in PBS [40 µl/ml]. Bisbenzimide was initially dissolved in water [0.5 mg/ml] and, for usage, diluted in PBS with 25 % ethanol [6 µl/ml]. The ethanol was used as a fixation to improve the stability of the stained samples, as suggested by a former study (Ciancio et al., 1988).

Bacterial incubation and live/dead staining

350 µl bacterial suspension was added to each prepared glass slide and incubated for one hour at room temperature. Two poly-L-lysine coated microscope slides* (obtained from Electron Microscopy Sciences, Hatfield, Pennsylvania, U.S.) without cicada wings were used as a control

group for each bacterium species. Poly-L-lysine coating was chosen to increase the number of attached bacteria compared to normal glass. This is an advantage as it provides a more comparable reference for the rough surface of the cicada wings. After one hour, the suspension was carefully removed. To obtain a control (dead) group, one of the incubated slides was heated to 95 °C for four minutes to kill all bacteria after the incubation period. This control (dead) group is used to analyze the live/dead staining. In addition, methanol was used to create a control (dead) in the experiment carried out with the replica in UV curing resin. 100 µl of the bacterial suspension was removed and replaced with 100 µl methanol 15 minutes before the end of incubation time. In this experiment an impression in the same UV curing resin was used as control (live) to exclude differences in chemistry.

The first staining step was performed with PI. 110 ml of the PI/PBS solution was filled in each container and incubated for 15 minutes. A black cap was put over the container to protect the fluorescence dyes from bleaching. As the next step, the samples were carefully washed with 110 µl PBS to remove unbound stain and unattached bacteria. 110 µl Bisbenzimide/PBS solution was added and exposed for 30 minutes, again shielded from light (Figure 27 b). Afterwards, the suspension was removed, as well as the surrounding plastic ring. A coverslip was put on every sample with Fluoromount-G™ (00-4958-02, Thermo Fisher Scientific GmbH, Waltham, Massachusetts, U.S.) to enhance the stability of the fluorescence stains. The edges of the coverslip were further sealed with nail polish to prevent the Fluoromount-G™ from evaporation.

Fluorescence Microscopy

The imaging of the live/dead staining experiment with cicada wings was performed from Richard van Nieuwenhoven at the Medical University of Vienna (device provided by Prof. Adelheid Elbe-Bürger, Department of Dermatology, under the supervision of Philip Kienzl, Ph.D., Department of Dermatology) on an Olympus IX73 inverted microscope (Olympus Corporation, Tokyo, Japan). PI was excited at 561 nm and the emission measured at 640 nm. Whereas Bisbenzimide Hoechst 33343 was excited at 405 nm and measured at 488 nm.

The live/dead staining experiment with the replica was performed by Richard van Nieuwenhoven at the Core Facility Imaging of the Medical University of Vienna on a Zeiss LSM 880 Airyscan (Carl Zeiss AG, Oberkochen, Germany).

Image analysis

The pictures were analyzed with the software Fiji (Schindelin et al., 2012). Since PI is impermeable to the living cell membrane, only dead bacteria are stained. On the other hand, Bisbenzimide stains all cells, whether dead or alive. In this way all cells with excitation in the red and blue light are counted as dead. All bacteria with excitations only in the blue light are counted as alive. The color channels were separately analyzed. As a first step, the contrast and brightness were consistently optimized. Each image was converted into a binary image in the next step (applying a threshold to exclude noise). Afterwards a segmentation analysis was performed to count the number of cells with a suitable cell size threshold to additionally exclude noise (Figure 28). For each sample, three images were analyzed and averaged.

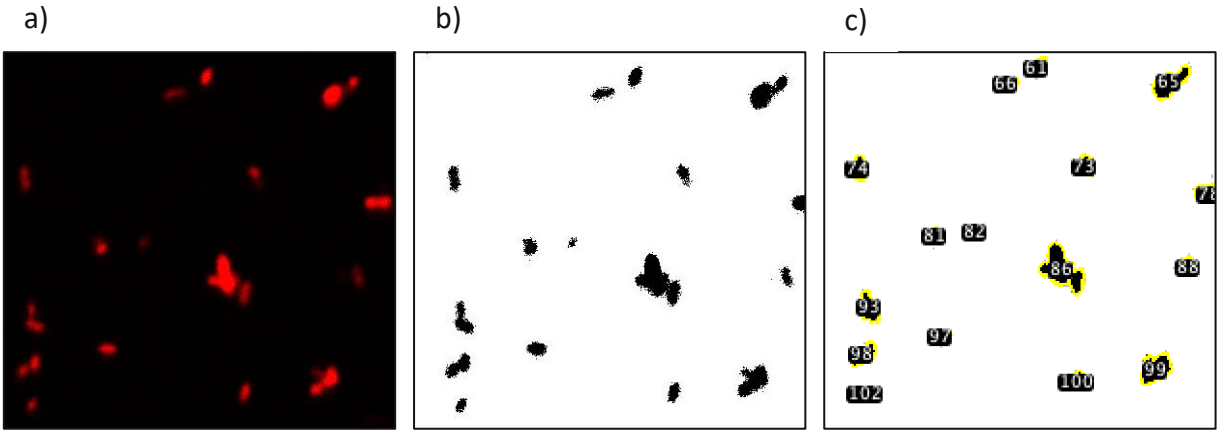

Figure 28. Image analysis steps shown on the basis of a picture section. a) Fluorescence image, b) Image converted into a binary with a suitable threshold, c) Particle analysis run, cells get numerated. All steps performed with open source software Fiji.

Contact angle measurements

To investigate the hydrophobic properties of the cicada wing, a contact angle measurement was performed. The cicada wings were cleaned with a nitrogen stream to remove particles. A biopsy punch was used to cut 5 mm discs out of the wings so that most of the surface was covered by the wing membrane. The wing veins disturb the measurement as they are not nanostructured like the membrane and therefore are not hydrophobic. If water drops adhere to the veins, the surface tension of the water drop is altered and consequently, the shape changes. The pieces were mounted with double-sided adhesive tape on cover glasses. In this step, it is essential that the wings are mounted as flat as possible. The prepared sample was placed on a sample table, which lies at one level with the camera. As studies report that the drop size affects the contact angle (Drelich, 1997), it was decided to use the same amount of water for each experiment. Previous studies on cicada wings used drop sizes in the range of 0.1 µm to 10 µm for contact angle measurements (Hu et al., 2011; Ivanova et al., 2012; Nowlin et al., 2014; Román-Kustas et al., 2020; M. Sun et al., 2009). It was decided to use 3 µl of deionized water, which lies in the recommended range and ensures better comparability to the former cicada wing studies. The water drop was carefully cast with a pipette in the middle of a wing cell, so no vein was touched by the water drop. A picture of the drop was taken with a USB 2.0 CMOS Camera (Thorlabs, Newton, New Jersey, U.S.) with a telecentric lens (0.5x, 65 mm WD CompactTL™ Telecentric Lense, Edmund Optics Inc., Barington, New Jersey, U.S.). The images were analyzed with the open-source software OpenDrop (Huang et al., 2021).

Results

Topographical analysis of cicada wings

AFM investigation

As different settings were used, the calculations for the nanopillar characteristics were performed separately for each measurement setting. A summary of the set-ups used can be found in Materials & Methods (Table 2). The images depicted in Figure 29 are taken from the same standardized measurement setting for better comparability between the species (Figure 29). As the contact mode images were blurred and the pillars seemed to move in the scanning direction, only tapping mode images were used for analysis.

AFM measurements show that the surface of the cicada wing membranes is composed of numerous nanopillars, which are regularly arranged in hexagonal arrays (Figure 29). The heights of the nanopillars differ significantly between species and different measurement settings used, even for the same wing with different instruments and different places of investigation on the wing. *K. scutellaris* shows the highest nanostructures of the three investigated species, followed by *A. cingulata*. The lowest nanostructures were found on *M. septendecim.*

In case of *K. scutellaris* the average height was 266 ± 42 nm for the first setting (Setting CY_A, which was suitable for contact and tapping mode, but not optimized for any of them, Table 3). The average height of setting specialized for tapping mode (Setting CY_T) showed an average of 328 ± 54 nm, which is about 60 nm higher (smallest pillar measured at 175 nm, highest pillar at 560 nm, Figure 30). *A. cingulata* shows less pronounced structures with a mean of 233 ± 42 nm (for the tapping optimized Setting CY_T). In the Setting CY_C (optimized for contact mode but measured in tapping mode as contact mode produced blurred scans) the average was about 100 nm (136 ± 30 nm). In contrast, the tip-to-tip spacing distance was more robust, showing only a slight, non-significant variation depending on the different settings. Both cicada species showed a spacing of roughly 180 nm between neighboring nanopillar tips on the wing surface (Table 3).

Table 3. Nanopillar parameters of the cicada wing membrane as determined by AFM scans. The peak-to-peak distances of 200 randomly measured nanopillar neighbors were averaged to calculate the tip-to-tip spacing.

	Average height of nanopillars [nm]	Number of nanopillars	Total area investigated [µm²]	Tip-to-tip [nm]
		Setting CY_C		
Amphipsalta cingulata	136 ± 30	1723	50	177 ± 18
		Setting CY_A		
Kikihia scutellaris	266 ± 42	1839	50	181 ± 41
		Setting CY_T		
Amphipsalta cingulata	233 ± 42	2705	75	175 ± 18
Kikihia scutellaris	328 ± 54	2348	75	188 ± 30
Magicicada septendecim	54 ± 12	2117	75	201 ± 25

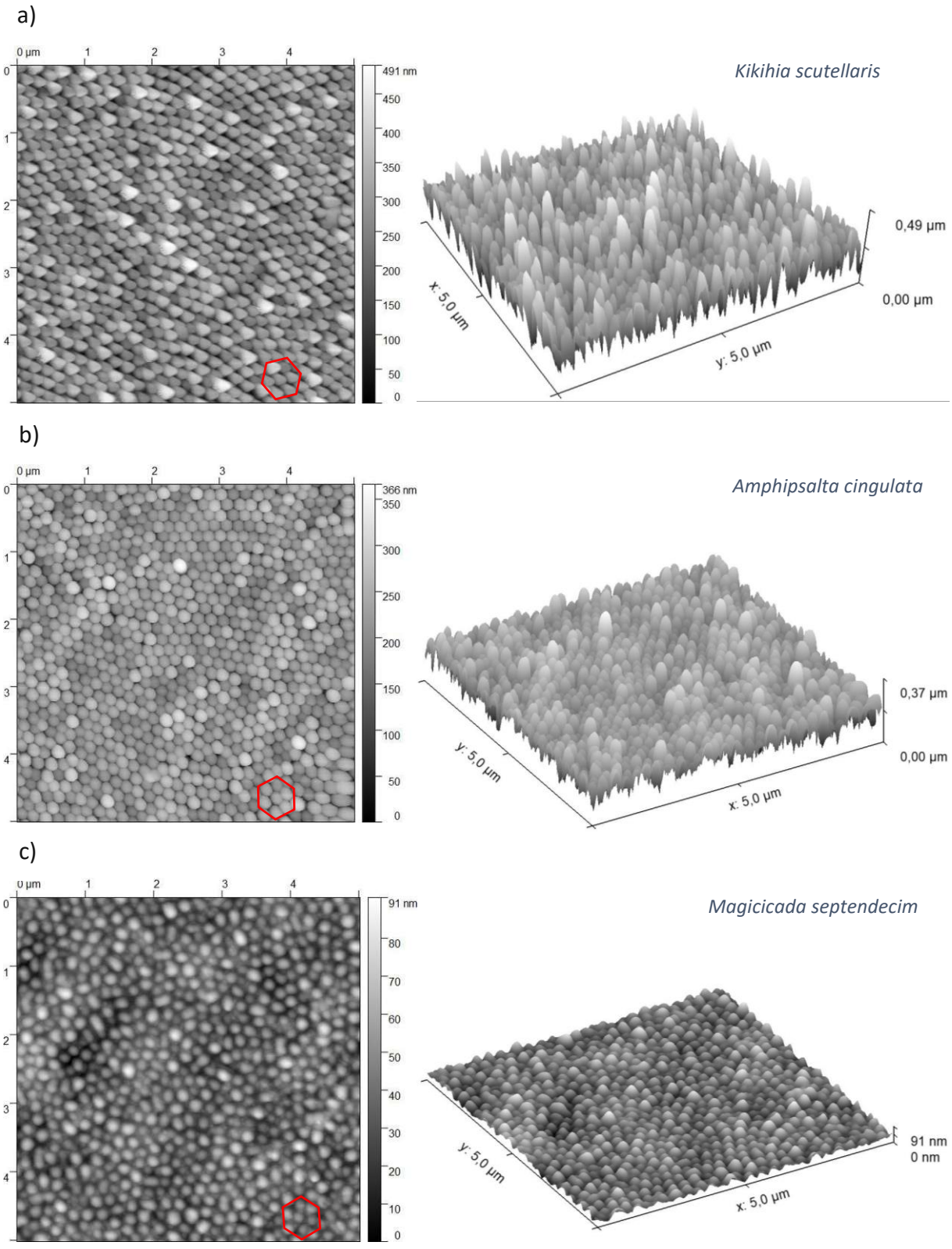

Figure 29. Selected AFM scans (Setting CY_T, image size: 5 µm x 5 µm, imaging parameter: height) of cicada wings with their respective three-dimensional reconstruction (height depicted three times higher compared to length and width): a) *Kikihia scutellaris*, b) *Amphipsalta cingulata*, c) *Magicicada septendecim.* Own images

The height distribution of the nanopillars on the wing surfaces of both New Zealand cicada species is symmetrical and shows that a variation occurs on the same wing. This can also be seen in the reconstructed three-dimensional images (Figure 29).

The Shapiro-Wilk test* is commonly used to test whether samples originate from normally distributed population. The null hypothesis assumes a normal distribution, if the calculated test statistic for a sample set exceeds a critical value, the hypothesis is rejected (Shapiro & Wilk, 1965). Alternatively, the p-value can be used. It resembles the probability that values, which are equal or more extreme as the samples, are obtained from random drawing out of the population under the assumption that the null hypothesis is true. If the p-value lies below the significance level (α-level, mostly set as 0.05 in this use case), the null-hypothesis should be rejected, which means in the case of the Shapiro-Wilk test that no normal distribution can be assumed (Timischl, 2013).

In addition, the quantile-quantile plot* (Q-Q plot) is often used as graphical measure to compare the sample distribution with the standard normal distribution. The x-axis shows the quantiles of the normal distribution, whereas the z-axis shows the quantiles of the distribution of interest. If the population of the samples is normally distributed, the quantiles should show a linear relation to the standard normal distribution (Timischl, 2013).

In the cases of both New Zealand cicadas, the Shapiro-Wilk test suggests rejecting the assumption of a normal distribution for a significance level of 5 % (α = 0.05): *K. scutellaris* (p-value = 9.36 e^{-11}), *A. cingulata* (p-value = 0.025).

In contrast, the Q-Q plot shows only a slight deviation from the normal distribution of the nanopillar heights of the wing surface in the Zealand cicada species, mainly caused by the extreme values (Figure 30). In both New Zealand cicadas, the shape of a single nanopillar can be described as cone-like with a rounded cap with a decreasing radius from the bottom to the top radius. Due to their more considerable height, the nanopillars of *K. scutellaris* seem sharper (Figure 29).

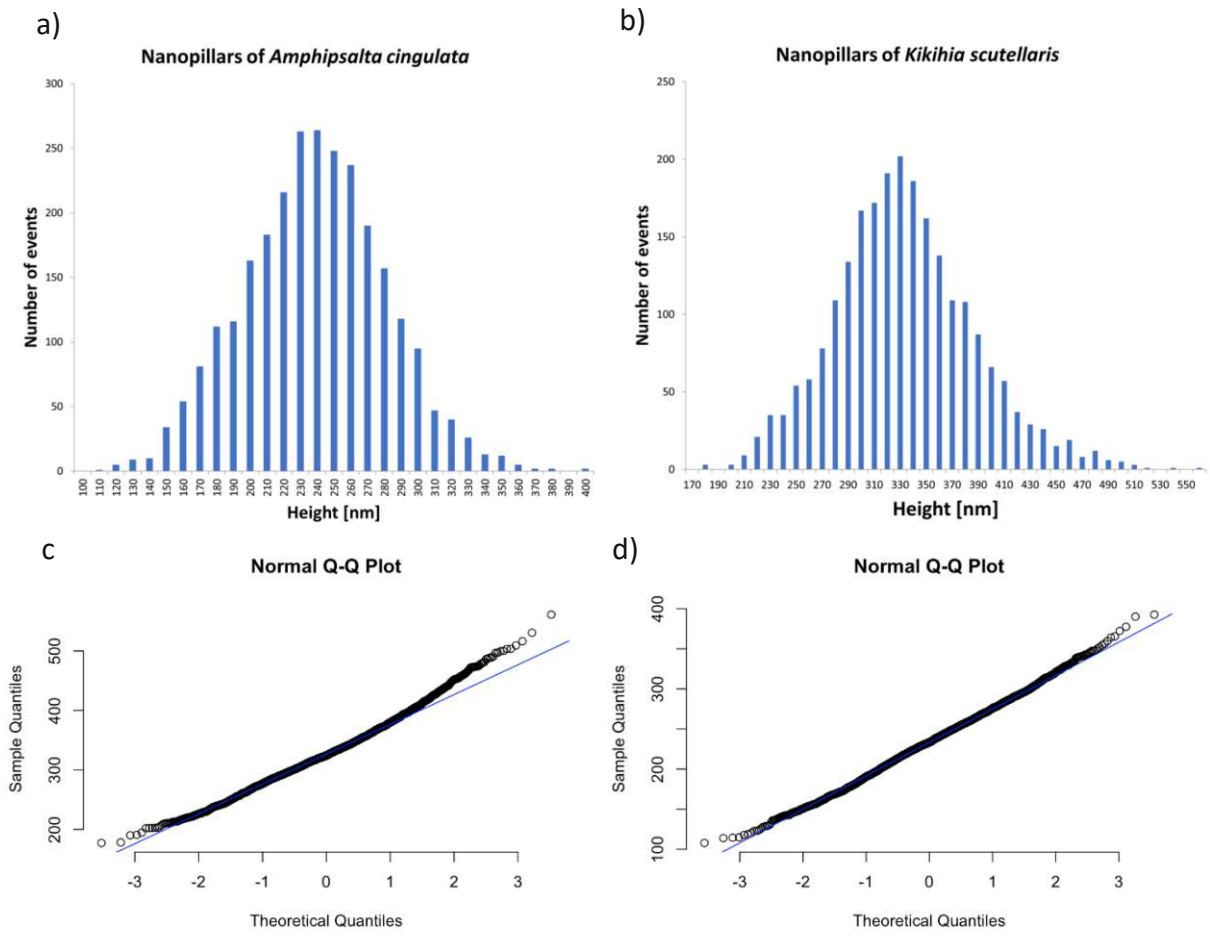

Figure 30. Histograms depicting nanopillar heights on the wing membrane of the investigated New Zealand cicada species based on AFM scans (Setting CY_T): a) *Amphipsalta cingulata,* b) *Kikihia scutellaris.* Respective Q-Q plots shown below: c) *Amphipsalta cingulata,* d). *Kikihia scutellaris.*

In *M. septendecim* (the periodical cicada), the smallest nanostructures were found. They cannot be described as nanopillars but rather nanodomes, which would be a more accurate term. The average height of the structures was 54 ± 12 nm (lowest value measured at 22 nm, highest at 90 nm). Furthermore, the periodical cicada shows the largest distances between the tips of neighboring nanopillars, about 200 nm (Table 3, Figure 29 c). The nanodomes are also hexagonally arranged, but apparently less regular with a large variation of the base radius (Figure 29 c). The height distribution has graphically a similar shape as in the other cicada species. Again, the Shapiro-Wilk test rejects the assumption of a normal distribution (p-value = 0.036). However, the Q-Q plot indicates that a normal distribution could be used as a rough approximation (Figure 31). As a note, it was observed that the surface of *M. septendecim* is generally more corrugated on a microscopic level with rather pronounced valleys and elevations.

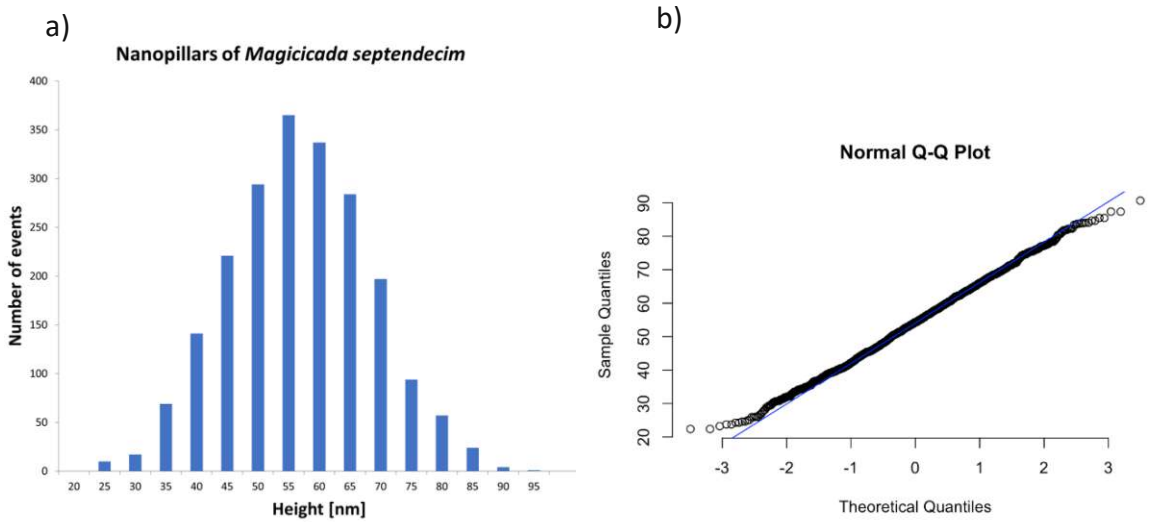

Figure 31. a) Histogram depicting nanopillar heights on the wing membrane of *Magicicada septendecim* based on AFM scans (Setting CY_T), b) Respective Q-Q plot.

SEM investigations

In addition to the AFM scans, SEM imaging was performed to improve the understanding of the nanostructures. The regular arrangement of the nanostructures on the New Zealand cicada wings can clearly be seen in the overview images (Figure 32 a, Figure 33 a). In *M. septendecim,* the pattern seems to be a little more irregular. At a closer look, the same hexagonal base unit can be found, which was already visualized in the AFM section (Figure 29 c, Figure 35). It should be noted that no angular correction was applied to the height measurements as it was assumed that the wing edges were approximately orthogonal to the electron beam. However, the actual angles most likely deviate from 90°, which could lead to a small difference between the actual and measured heights.

Based on SEM imaging the heights in of the cicada wings deviate slightly from the AFM measurements (Setting CY_T) but significantly from the other AFM settings (Setting CY_C & Setting CY_A). In addition, also the tip-to-tip distances were not significantly different from the AFM scans (compare Table 3 & Table 4). Since the results of the AFM and SEM scans coincide well, the assumption that no angular corrections have to be made seems to be justified.

Furthermore, the SEM images allow for a closer investigation of the shape of the nanostructures. In contrast to the AFM scans, the SEM images reveal a different shape of the nanopillars of both New Zealand cicada species, more structured than a simple capped cone.

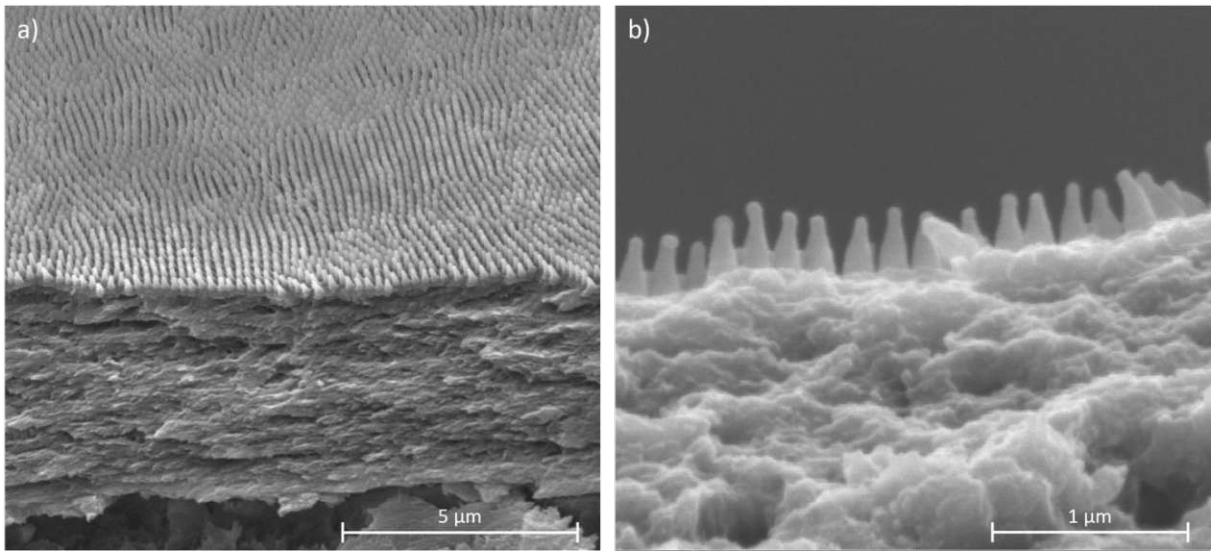

Figure 32. SEM images of a fracture edge of a *Amphipsalta cingulata* wing (High voltage used: 5 kV): a) Overview of the wing membrane (working distance: 7 mm), b) Sideview on the nanopillars of the wing membrane (working distance: 7.4 mm). Own image, taken with K. Whitmore, USTEM TU Wien, 2021

The nanopillars have a broader base (135 ± 16 nm in *A. cingulata* and 150 ± 13 nm in *K. scutellaris*) and narrow towards the tip. At the top, they widen again, forming a head-like structure. The narrowest point is located below this head (Figure 32 b, Figure 33 b). Despite the height difference, the nanopillars of both New Zealand cicadas show the same tip diameter (60 ± 6 nm, 60 ± 7 nm). However, the diameter slightly deviates at the base (Table 4). In addition, the SEM scans support the hypothesis that the nanopillars show a variation in height within the same wing. For example, in Figure 33 b, a few nanopillars are considerably larger than the others. Furthermore, it was observed that certain regions on the same win have less or more pronounced nanostructures.

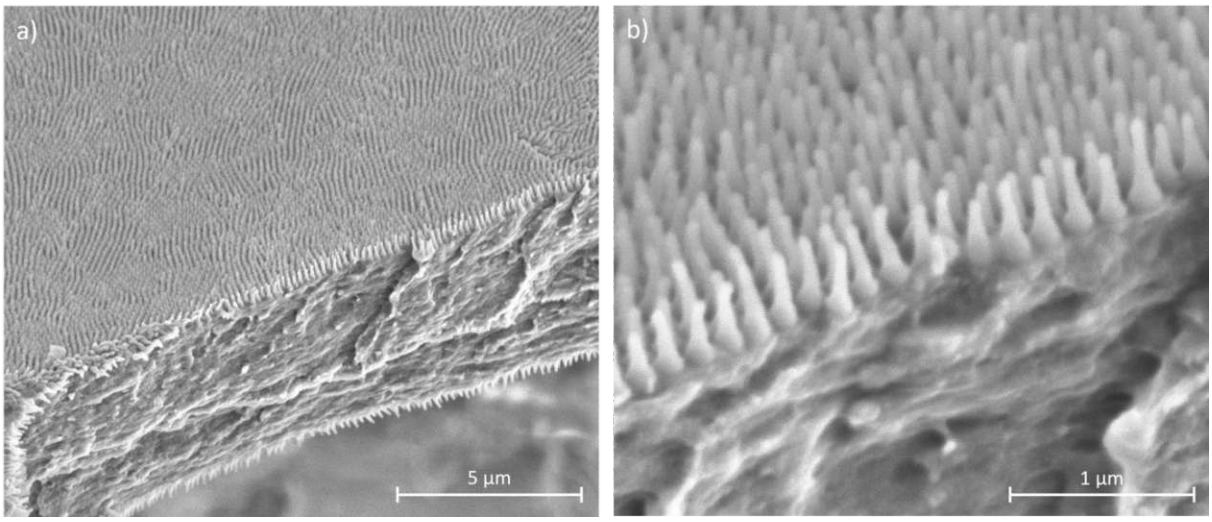

Figure 33. SEM images of a fracture edge of a *Kikihia scutellaris* wing membrane (High voltage used: 3 kV, working distance: 11.8 mm): a) Overview of the wing membrane, b) High resolution zoom on the nanopillars of the wing membrane. Own image, taken with K. Whitmore, USTEM TU Wien, 2021

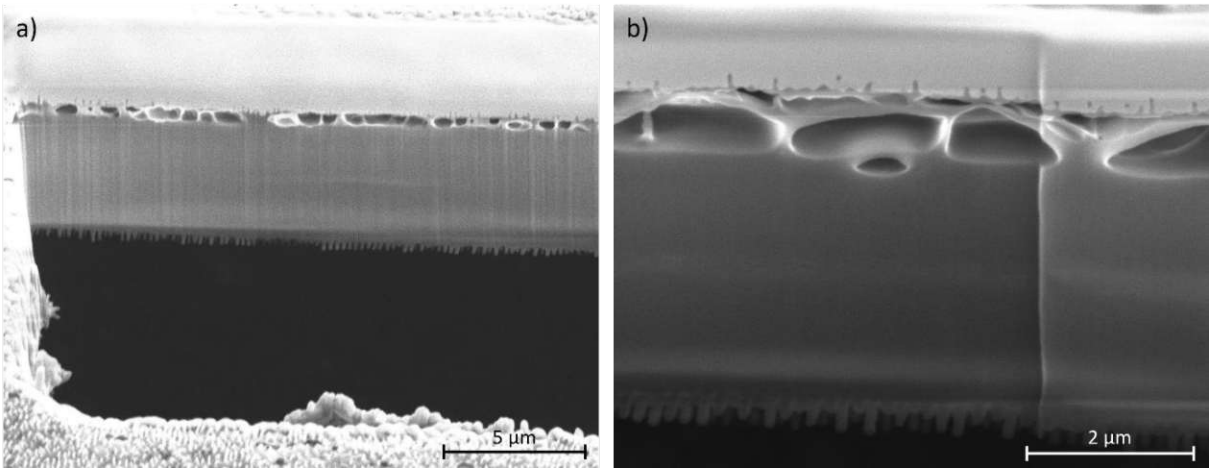

Figure 34. SEM image of a Focus Ion Beam (FIB-SEM) cross-section of a *Kikihia scutellaris* wing: a) Overview of the cut, on top of the wing is the applied Wolfram layer, b) High resolution zoom on the cross-section. Own image, taken with K. Whitmore, USTEM TU Wien, 2021

The FIB cross-section revealed that the whole wing membrane of *K. scutellaris* is about 3.5 µm thick (Figure 34). To protect the surface from taking uncontrolled damage by the focused ion beam in a first step a thin carbon layer was applied. Next a thin Wolfram layer was applied followed by a thicker one (Figure 34). As the nanopillars on the dorsal side are structurally damaged, it seems as if the carbon layer was not thick enough and the deposition of the Wolfram might have destroyed these nanofeatures. Therefore, no reliable structural information can be obtained. Below the base of the nanopillars, a layer with large chambers is visible (Figure 34). This layer was not found at the fracture edge SEM scan (Figure 33). However, Figure 34 shows that the ventral* side of the wing possesses similarly shaped structures as on the dorsal side, which can also be observed in Figure 33. In contrast to the upper side, the nanopillars there are not damaged.

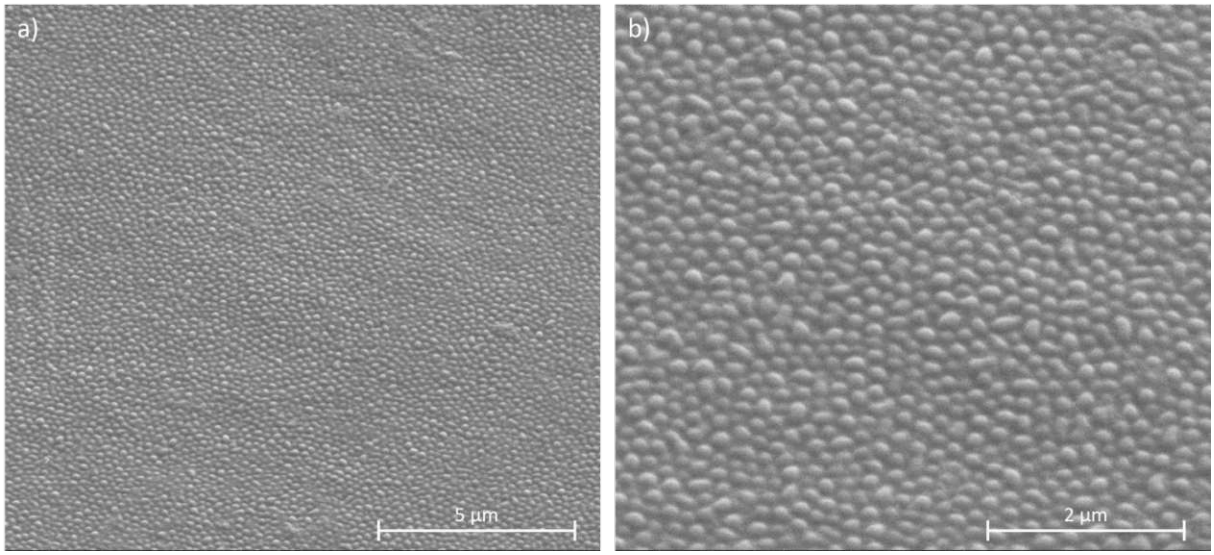

Figure 35. SEM images of a *Magicicada septendecim* wing (High voltage used: 3 kV, working distance: 9.8 mm): a) Overview of the wing membrane, b) Zoom on the nanopillars). Own image, taken with K. Whitmore, USTEM TU Wien, 2021

In the case of *M. septendecim,* the wing surface nanopillars were too small to obtain reliable measurements of their height and height distribution with the SEM. As mentioned above, their shape can be described as dome-like. They are not as differentiated as the nanopillars of the two New Zealand cicadas (Figure 35). On average, the base has a diameter of about 150 ± 30 nm, but the standard deviation is about twice as high compared to the New Zealand cicadas (Table 3). This irregularity can also be observed by analysis of the SEM images. It seems as if the nanodomes have a rather irregular shape and size (Figure 35).

Table 4 Nanopillar parameters of the cicada wing membrane determined via SEM image analysis with Fiji. As the nanopillars were too flat, average height and tip diameter were not measured for *Magicicada septendecim*. The tip-to-tip distance was calculated via a nearest neighbor algorithm which was applied to the centroid of the nanopillars.

	Average height of nanopillars [nm]	Base diameter [nm]	Tip diameter [nm]	Tip-to-tip spacing [nm]
Amphipsalta cingulata	249 ± 42	135 ± 16	60 ± 7	182 ± 44
Kikihia scutellaris	332 ± 43	153 ± 13	60 ± 6	182 ± 29
Magicicada septendecim	-	150 ± 30	-	215 ± 45

Nanoimprinting

Using PVS as master stamp material

The AFM scans of the nanopillars on the cicada wings showed significant differences in quality and detail depending on the imprinting techniques. A selection of the best replicas of each method is presented in this section. The replicas are named with capital letters of the respective fabrication procedure (Table 1), a number indicating the how often the corresponding PVS stamp has been used (only specified if the master template was used several times) and an abbreviation of the filling material used (EP = epoxy resin, UV = UV curing resin). Detailed information about the different techniques used is found in the Material & Methods section (Table 1).

Two AFM surface scans of the best replica produced with Method A and Method B (Table 1) are shown in Figure 36. The difference between these two methods is the type of PVS paste used and the weighting, when the PVS is cast onto the wing. Compared to the original surface (Figure 29 a), the structures of both replicas are significantly smaller in size. Replica A_EP has more outstanding nanopillars accumulated in one corner. Some of them have comparable height to the original, but the shape differs significantly. It gives the impression of fused pillars (Replica A_EP: Figure 36 a & b). Replica B_EP showed an almost identical pattern (hexagonally arranged arrays of nanopillars) but differed significantly in size (Replica B_EP: Figure 36 c & d).

The number of nanopillars per area detected in the positive imprints is about half the one of the original wing surface. The average height of nanopillars in Replica B_EP is about twice as high as in Replica A_EP (Table 5).

In addition, the absolute range of occurring heights is much broader in Replica A_EP. In contrast, Replica B_EP shows a rather symmetrical distribution resembling the shape of the height distribution on a *K. scutellaris* wing (Figure 37). The average distance between two nanopillar peaks is about 20 nm larger in Replica A_EP than in Replica B_EP, which has a spacing about 192 ± 41 nm. This is very close to the original tip-to-tip spacing (188 ± 30 nm). Moreover, the tip-to-tip values of Replica A_EP do show a high scattering (Table 5). All in all, Replica A_EP shows higher nanopillars, but the surface structure of Replica B_EP resembles the original nanostructures better regarding arrangement and pattern.

Table 5. Nanopillar parameters of the cicada wing membrane replicas. For the calculations of the spacing, the peak-to-peak distances of 200 nanopillars were analyzed.

	Average height of Nanopillars [nm]	Number of nanopillars	Total area investigated [µm²]	Tip-to-tip spacing [nm]
Replica A_EP	127 ± 42	453	25	213 ± 100
Replica B_EP	63 ± 21	470	25	192 ± 41

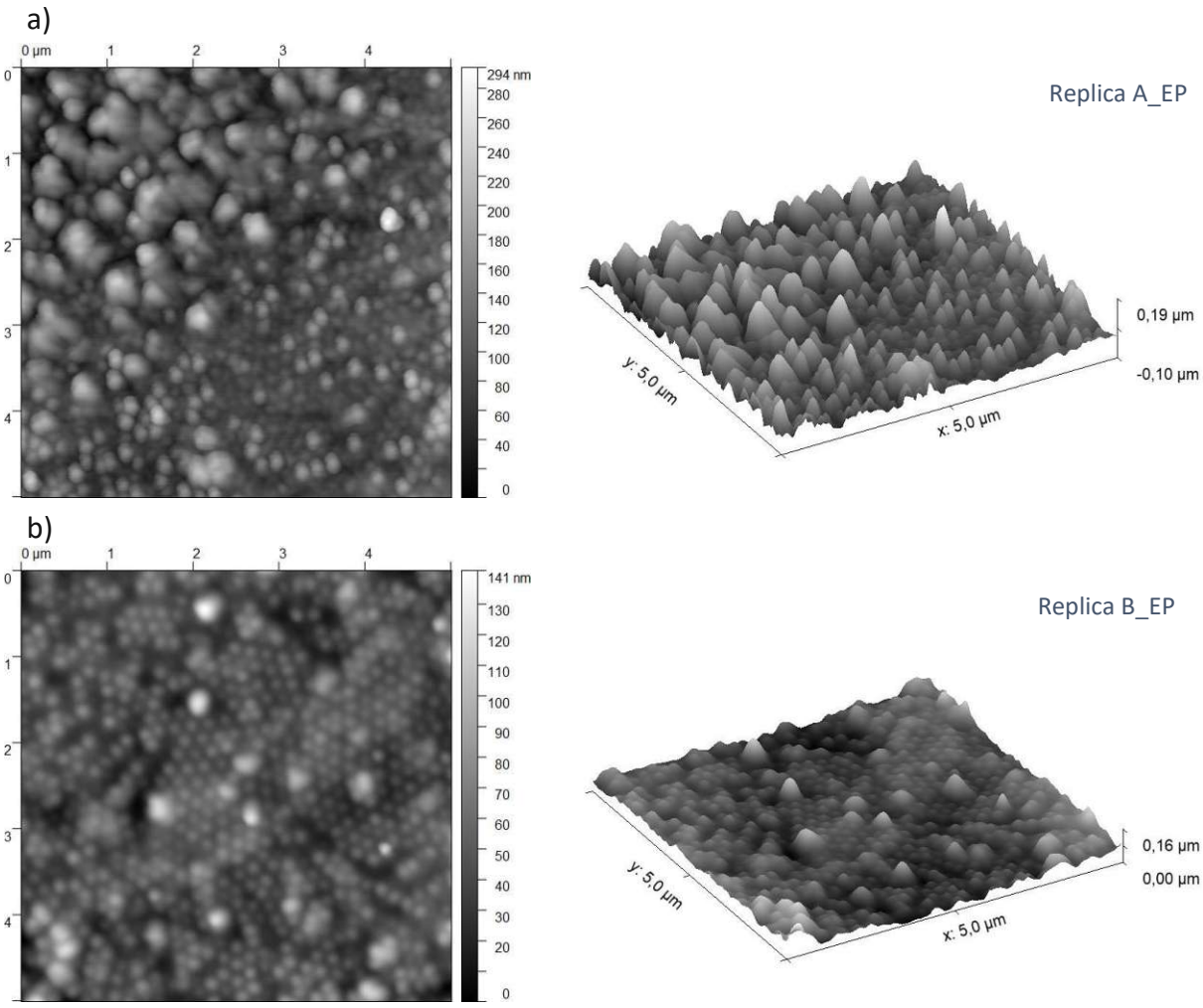

Figure 36. AFM scans of two *Kikihia scutellaris* wing replicas (Setting CY_T, image size: 5 µm x 5 µm, imaging parameter: height) with their respective three-dimensional reconstructions (height depicted three times higher compared to length and width): a) Replica A_EP (Produced with Method A), b) Replica B_EP (Method B). Own images, 2021

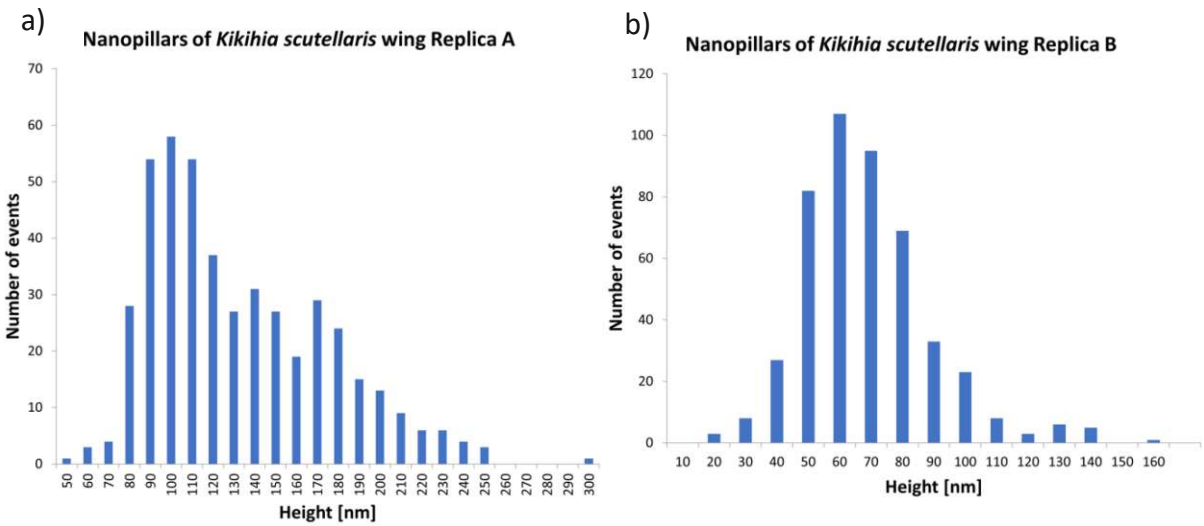

Figure 37. Histograms depicting nanopillar heights on *Kikihia scutellaris* wing replicas in epoxy resin: a) Replica A, b) Replica B

The three replicas presented below (Replica C1_UV, Replica C2_EP, Replica C3_UV) were produced with the same PVS master stamp (fabricated with Method C, Table 1). Replica C1_UV is the first produced after the master stamp was created and was formed with UV curing resin. This replica shows nanopillar characteristics very similar to the original wing (Figure 38). The height (mean: 295 ± 39 nm), the nanopattern as well as the tip-to-tip distance between neighboring nanopillars (184 ± 25 nm) was precisely transferred to the replica. Moreover, the number of nanopillars detected by the algorithm suggests a similar density of nanopillars compared to the biological template (compare Table 3 & Table 6). Comparing the height distributions of the original wing (Figure 30) to the Replica C1_UV (Figure 39) highlights the accuracy of the replica. As in the case of the cicada wing, the Shapiro-Wilk test rejects the assumption of a normal distribution ($p < 2.2\ e^{-16}$). Especially, outliers in the region of about 70 nm to 160 nm cause a significant deviation from a normal distribution (Figure 39 b).

Table 6 Nanopillar parameters of the *Kikihia scutellaris* replicas, produced with the same master stamp. The PVS template was cured at 4 °C and no cleaning steps were performed. For the calculations of the spacing, the peak-to-peak distances of 200 nanopillars were analyzed.

	Average height of nanopillars [nm]	Number of nanopillars	Total area investigated [µm²]	Tip-to-tip spacing [nm]
Replica C1_UV	295 ± 39	2357	75	184 ± 25
Replica C2_EP	100 ± 30	1440	75	185 ± 69
Replica C3_UV	177 ± 43	1442	75	224 ± 22

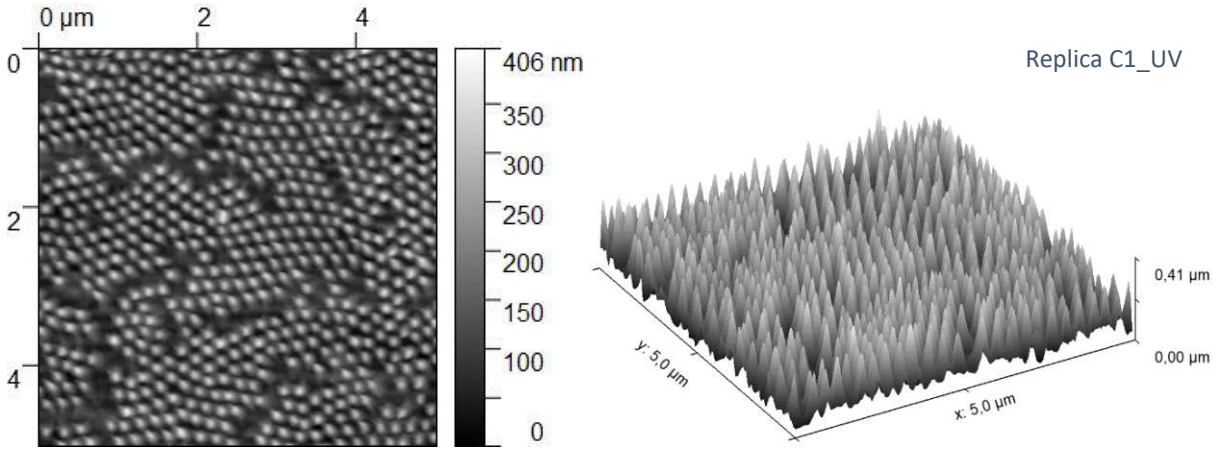

Figure 38. AFM scan (Setting MFP_T, image size: 5 µm x 5 µm, height measured) of a *Kikihia scutellaris* wing replica (fabricated with Method B) stamp with the respective three-dimensional reconstruction (height depicted three times higher compared to length and width).

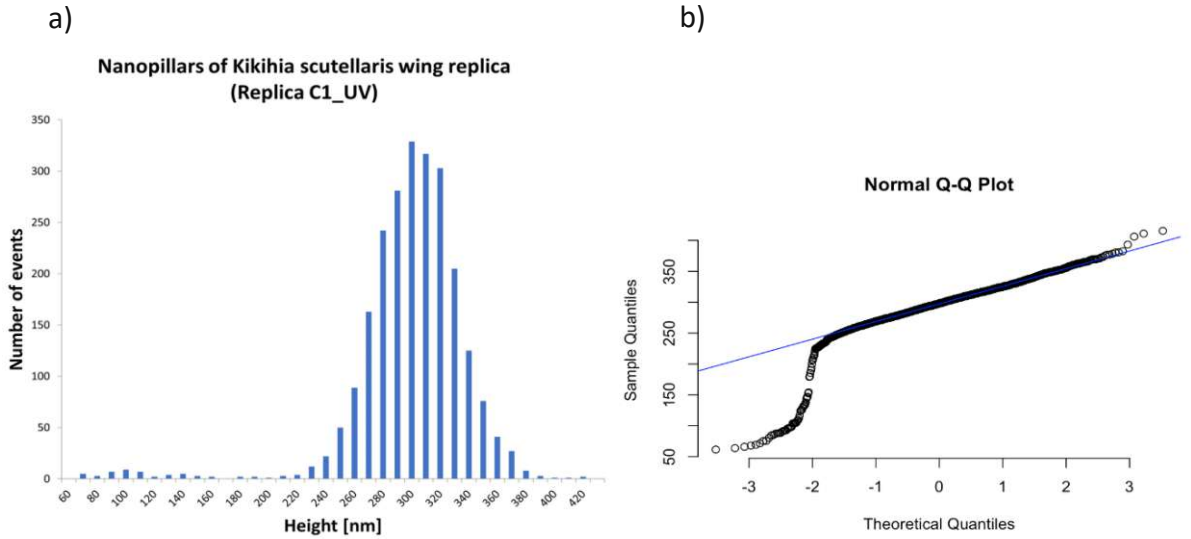

Figure 39. a) Histogram depicting nanopillar heights of the *K. scutellaris* wing Replica C1_UV based on AFM scans (Setting MFP_T), b) Respective Q-Q plot.

After creating the first positive impression, the master stamp was reused. This time, epoxy resin was used as a molding material. The surface nanostructures deviate significantly from the original template. Generally, the replica surface looks irregular, with many nanopillars sticking together or getting lost during the replication process. The average height of the nanopillars (100 ± 30 nm) is only about a third compared to the nanostructure on *K. scutellaris*. Furthermore, the detected nanopillar density is only about half of the biological template (Table 6). Especially, the height distribution differs significantly and cannot be approximated with a normal distribution (Figure 40).

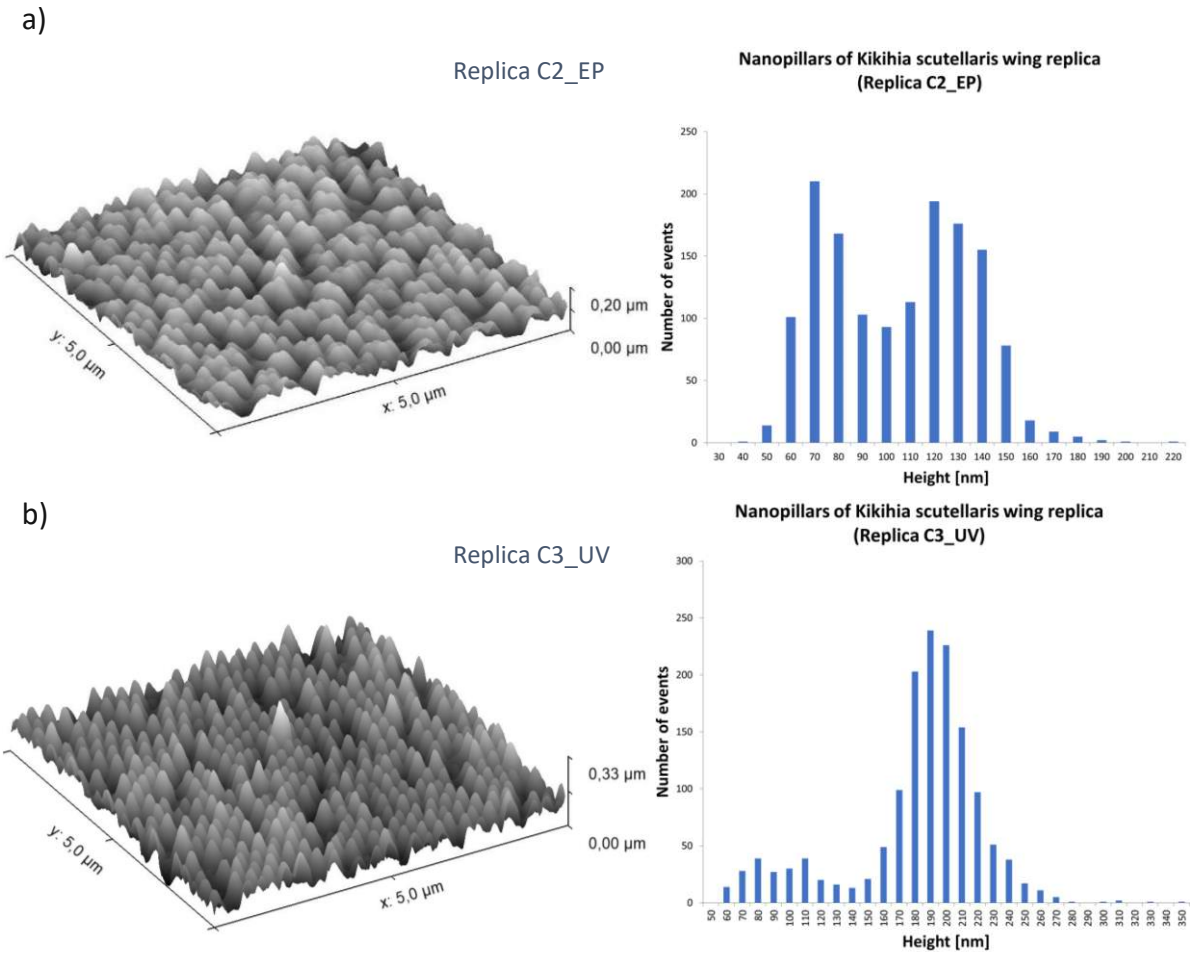

Figure 40. Three-dimensional reconstruction (height depicted three times higher compared to length and width) based on an AFM scan (Setting MFP_T, image size: 5 µm x 5 µm, imaging parameter: height) of two replicas created with the same PVS stamp (Method B): a) Replica C2_EP (epoxy resin), b) Replica C3_UV (UV curing resin). Own images

A third positive impression was fabricated from the same PVS template with a UV curing resin to investigate whether the quality stamp decreases due to type of molding material or because of reuse. The AFM investigation shows that the nanostructures of this replica are significantly higher compared to the second impression but still significantly lower compared to the first replica produced (177 ± 43 nm, Table 6). The basic nanostructure pattern was efficiently transferred and the single nanopillars are well resolved (Figure 40 b). A major deviation from the height distribution of the original template is caused by a group of low nanopillars in the range of about 60 nm to 130 nm, which is a significant deviation from the normal distribution (Figure 40 b). In Figure 41 a comparison of representative line scans is displayed.

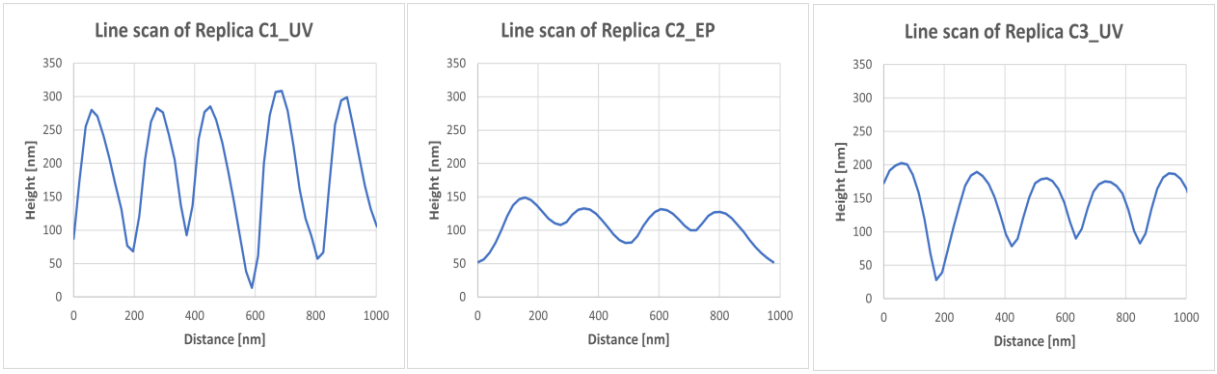

Figure 41. Comparison of representative line scans of three replicas made from the same PVS template (Method C).

As it was decided to use Replica C1_UV for the bacterial experiments, the SEM investigation was instead performed on Replica C3_UV. The overviews illustrate the regularity of the transferred structures with few gaps occurring, where nanostructures potentially got lost during the replication process (Figure 42 a & b). Furthermore, the close-ups show that the nanostructure arrangement of the replica is composed of the same hexagonal base unit (Figure 42 d). In some regions, replication errors occur in which the tips of two to four nanopillars stick together (Figure 42 c). Compared to their biological counterparts, the nanopillar shape is not as differentiated. They can be described as simple cones with a rounded cap, but no head-like structure is found as in the original nanopillars (compare Figure 33 and Figure 42 d).

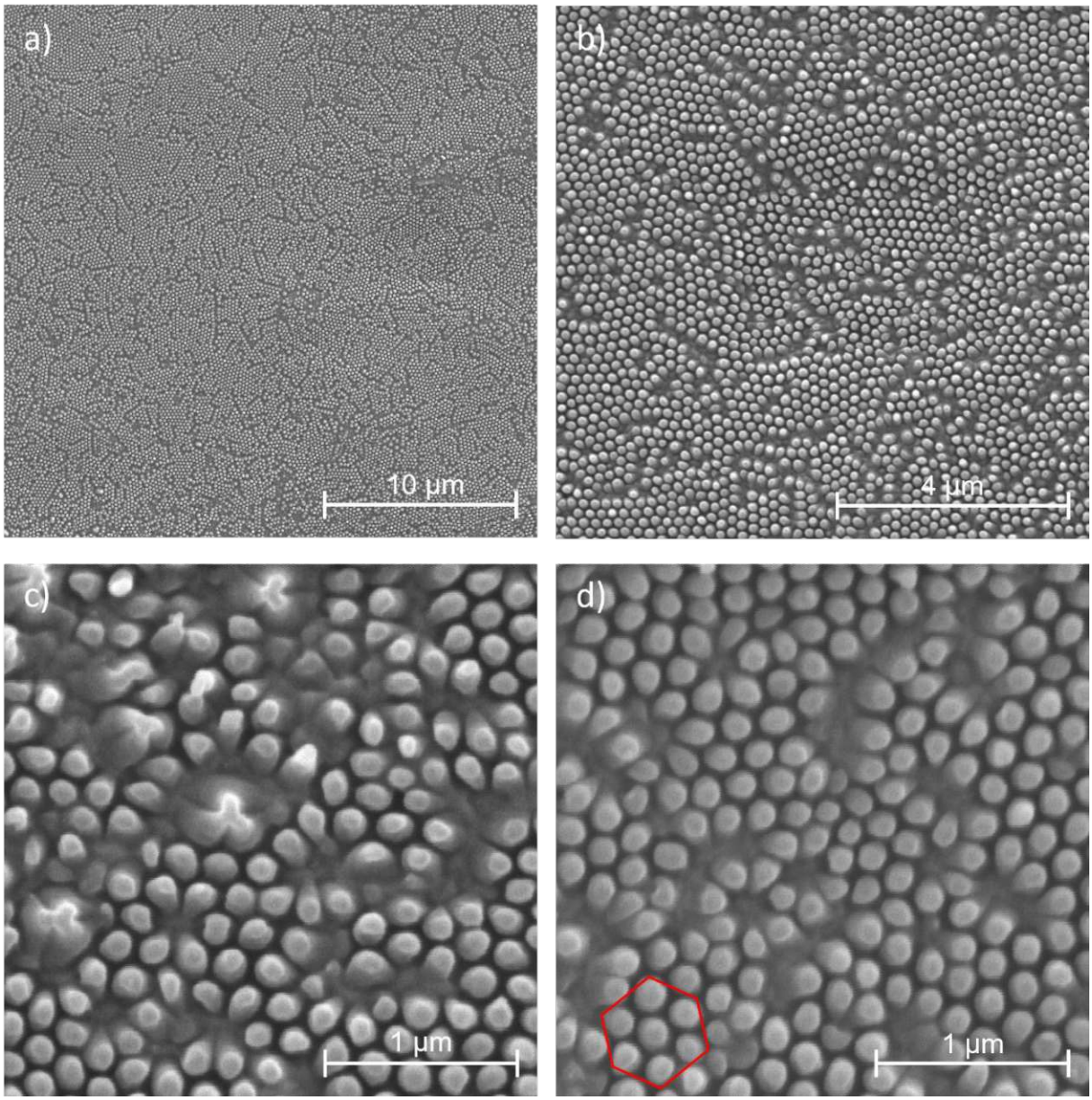

Figure 42. SEM images of a *Kikihia scutellaris* wing replica (Replica C3_UV). Negative impression was performed with PVS Xtra Light Body on a wing disc (5 mm) at 4 °C (Method C). The replica was the third one made from this master stamp: a) & b) Overview of the transferred structures, c) Slight transferring defects, where the tips of nanopillars stick together, d) Hexagonal base unit of the nanopillar arrangement marked. Own images, taken with K. Whitmore, USTEM TU Wien, 2021

Further approaches

Besides using PVS as stamping material, two alternatives were tested: casting of UV curing resin and nail polish directly on the biological template. For the low aspect ratio nanodomes of *M. septendecim,* the negative impression fabricated captured the nanostructures sufficiently regarding arrangement and depth. In the case of *K. scutellaris,* it was hardly possible to remove the negative impression without damaging it. The wing ruptured when the resin and nail polish were peeled off and parts kept stuck in the filling material. Moreover, the structures were only partly transferred.

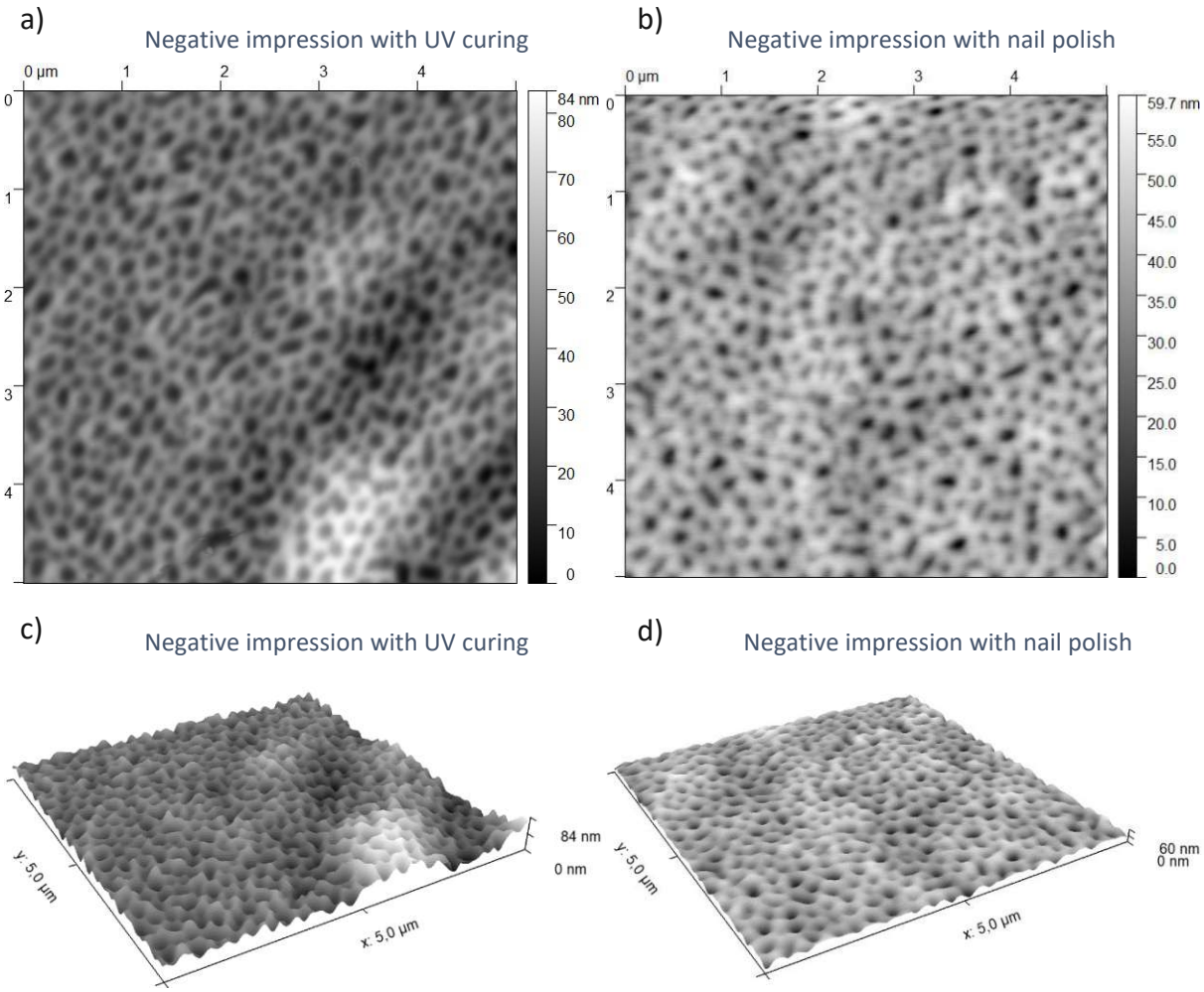

Figure 43. AFM scans (Setting C, image size: 5 µm x 5 µm, height measured) of negative impressions. Two different molding materials were directly casted onto a *Magicicada septendecim* wing: a) UV curing resin, b) Nail polish. Own images, 2021

Bacterial experiments

Live/dead staining experiments

The live/dead staining experiments were performed with two species of bacteria: the Gram-negative *E. coli* and the Gram-positive *S. aureus.* In the case of the former, all three cicada species showed a significantly higher number of dead cells stained with propidium iodide (PI) compared to the control (live) group (Figure 44 a), which is the blank poly-L-lysine coated microscope slide. *K. scutellaris* and *A. cingulata* performed with about the same efficiency, whereas in *M. septendecim,* the percentage of viable cells was higher (Figure 45).

On the New Zealand cicada species wings, about 80% of the bacteria detected were stained as damaged cells, which is about 60 % more than in the control. In the case of the periodical cicada, around 70 % of the bacteria observed were counted as dead, which is 50 % more than in the reference group. The control (dead), where the bacteria were killed beforehand (through heating up to 95 °C for four minutes) was included in the experiments to evaluate the quality of the staining and image analysis method used. About 96 % of the dead *E. coli* were correctly detected (Figure 44 a).

Using *S. aureus* as a bacterial testing agent revealed also bactericidal properties (Figure 44 b). In this case, the highest percentage of dead cells were found on the American cicada, around the same value as the negative reference (96 % of bacteria were dead). *K. scutellaris* showed a slightly lower killing efficiency of around 90 %. The lowest percentage of damaged cells was detected on *A. cingulata* (80 %). Compared to the control (live), all cicada wings showed a significantly higher percentage of dead cells (at least twice as high) (Figure 45).

In addition, a separate experiment was performed to evaluate if a replica with transferred nanostructures shows a similar bactericidal effect as the original wings. As Replica C1_UV showed the highest nanopillars, it was used for a live/dead staining test with *E. coli* bacteria. As a reference, the same resin was cured on the impression of a smooth glass microscope slide to exclude the influence of different chemical materials. In comparison to the smooth cured resin, a higher proportion of dead bacteria were detected on the replica. While in the control group (UV resin), around 55 % of the bacteria were counted as labeled with PI, the percentage in Replica C1_UV lay about 70 % (Figure 47). Generally, it was observed that more bacteria

were able to attach to the rough positive impression compared to the smooth reference (Figure 48). In the control (dead) group, where all bacteria were killed in advance to staining, 90 % percent were detected as dead (Figure 47).

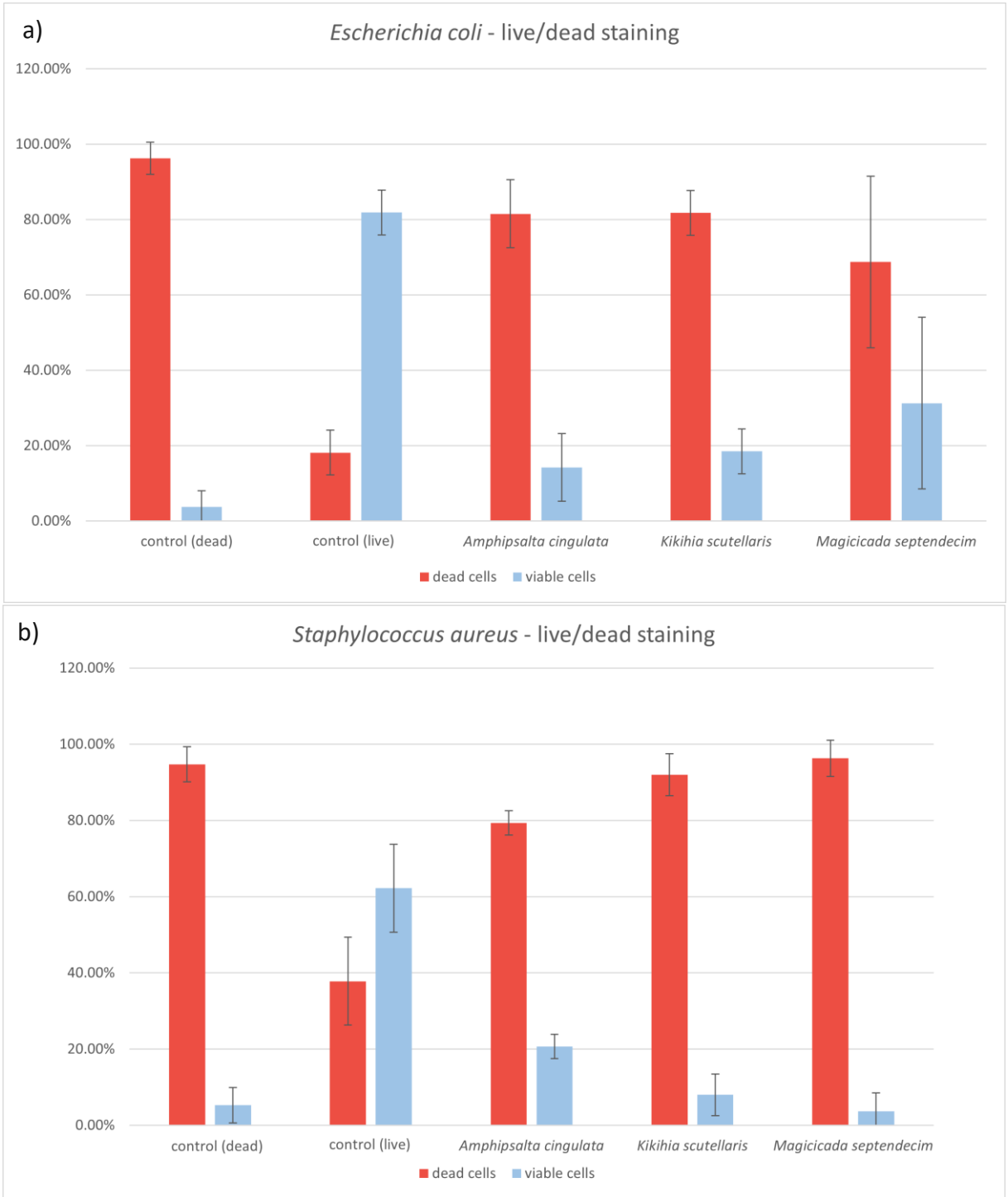

Figure 44. Results of the image analysis of the live/dead staining experiments performed with two bacterium species on the wings of three cicada species. In the control (dead) group the bacteria on a poly-L-lysine coated microscope slide were killed prior to staining (heated at 95 °C for 4 minutes). Control (live) was a poly-L-lysine coated microscope slide incubated with bacteria. a) Test performed with *Escherichia coli,* b) Test performed with *Staphylococcus aureus.*

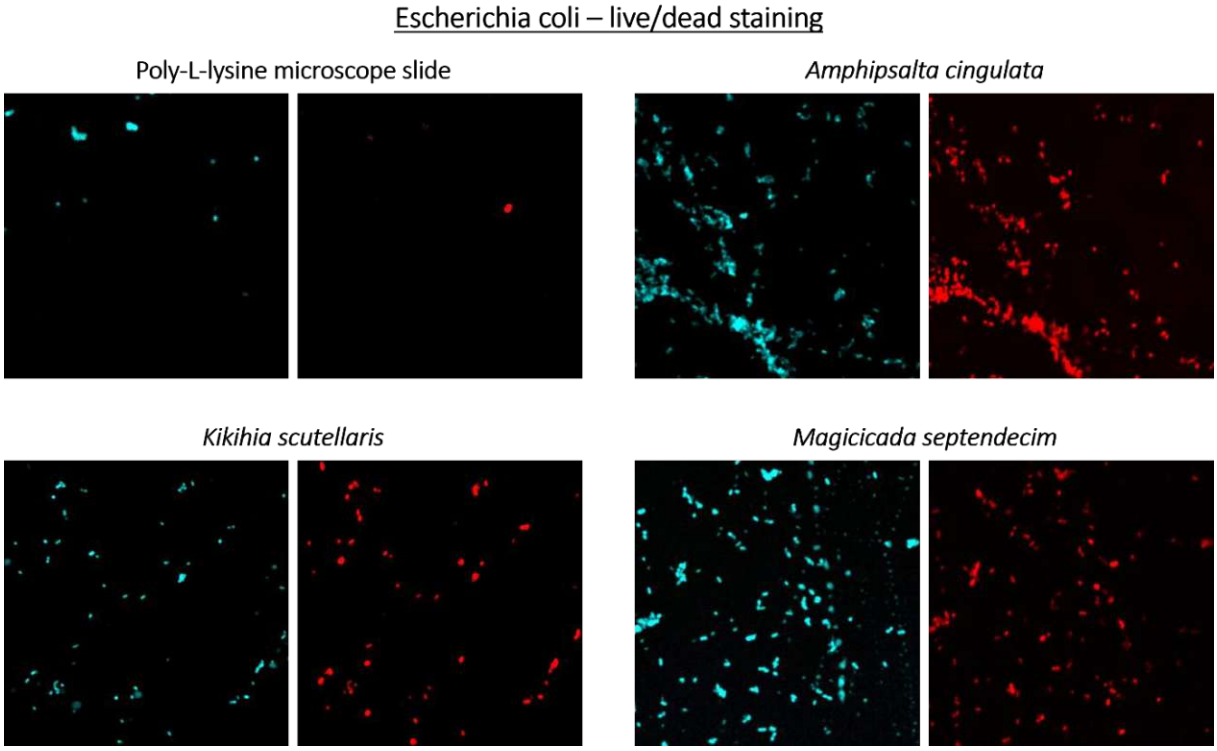

Figure 45. Fluorescence microscopic images of the live/dead staining experiment performed with *Escherichia coli* on various cicada wings and a control group (image size 100 µm x 100 µm). All cells are stained with Bisbenzimide Hoechst 33343 (shown on the left). Dead cells are stained with Propidium Iodide (shown on the right). A poly-L-lysine microscope slide was included as neutral reference. Images taken by Richard W. van Nieuwenhoven, 2021

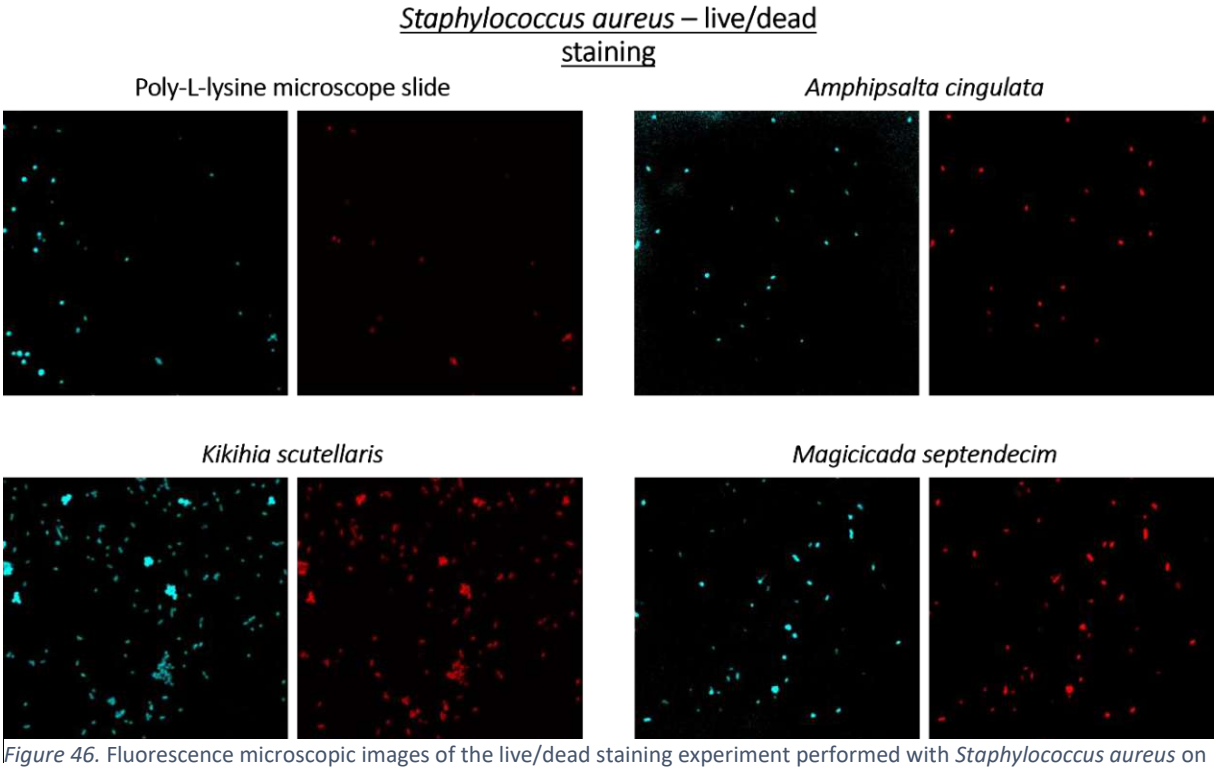

Figure 46. Fluorescence microscopic images of the live/dead staining experiment performed with *Staphylococcus aureus* on various cicada wings and a control group (image size 100 µm x 100 µm). All cells are stained with Bisbenzimide Hoechst 33343 (blue). Dead cells are stained with Propidium Iodide (red). A poly-L-lysine microscope slide was included as neutral reference. Images taken by Richard W. van Nieuwenhoven, 2022

Figure 47. Results of the image analysis of the live/dead staining experiments performed with *Escherichia coli* on a *Kikihia scutellaris* wing replica (Replica C1_UV). In the control (dead) group the bacteria on a poly-L-lysine coated microscope slide were killed prior to staining (in 50 % methanol for 15 minutes). Control (live) was a UV curing resin, replica of a smooth glass surface to exclude chemical differences between test and control (live) group.

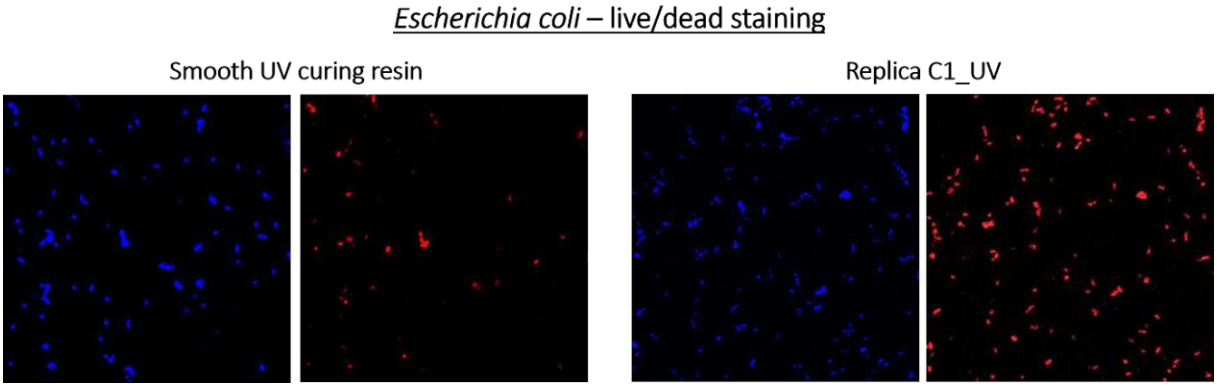

Figure 48. Fluorescence microscopic images of the live/dead staining experiment performed with *Escherichia coli* on a *Kikihia scutellaris* wing replica and a control group (image size 100 µm x 100 µm). All cells are stained with Bisbenzimide Hoechst 33343 (blue). Dead cells are stained with Propidium Iodide (red). A poly-L-lysine microscope slide was included as a neutral reference. Images taken by Richard W. van Nieuwenhoven, 2022

SEM investigation of bacteria-nanopillar interaction

Besides the bacterial live/dead experiments, SEM investigations of *E. coli* cells attached to the wings of each cicada species were performed. The bacterial density on the *A. cingulata* was relatively high. A high percentage of the surface was covered by bacteria (Figure 49 a). Although some cells were completely sunken into the nanopillars (Figure 49 b, blue mark), quite many were only partly stuck into the nanostructures. In Figure 49 d, one can see the interaction between the bacterial cell and the nanopillars. The membrane adheres to the heads of the nanopillars and the nanostructures are slightly bent towards the bacterium.

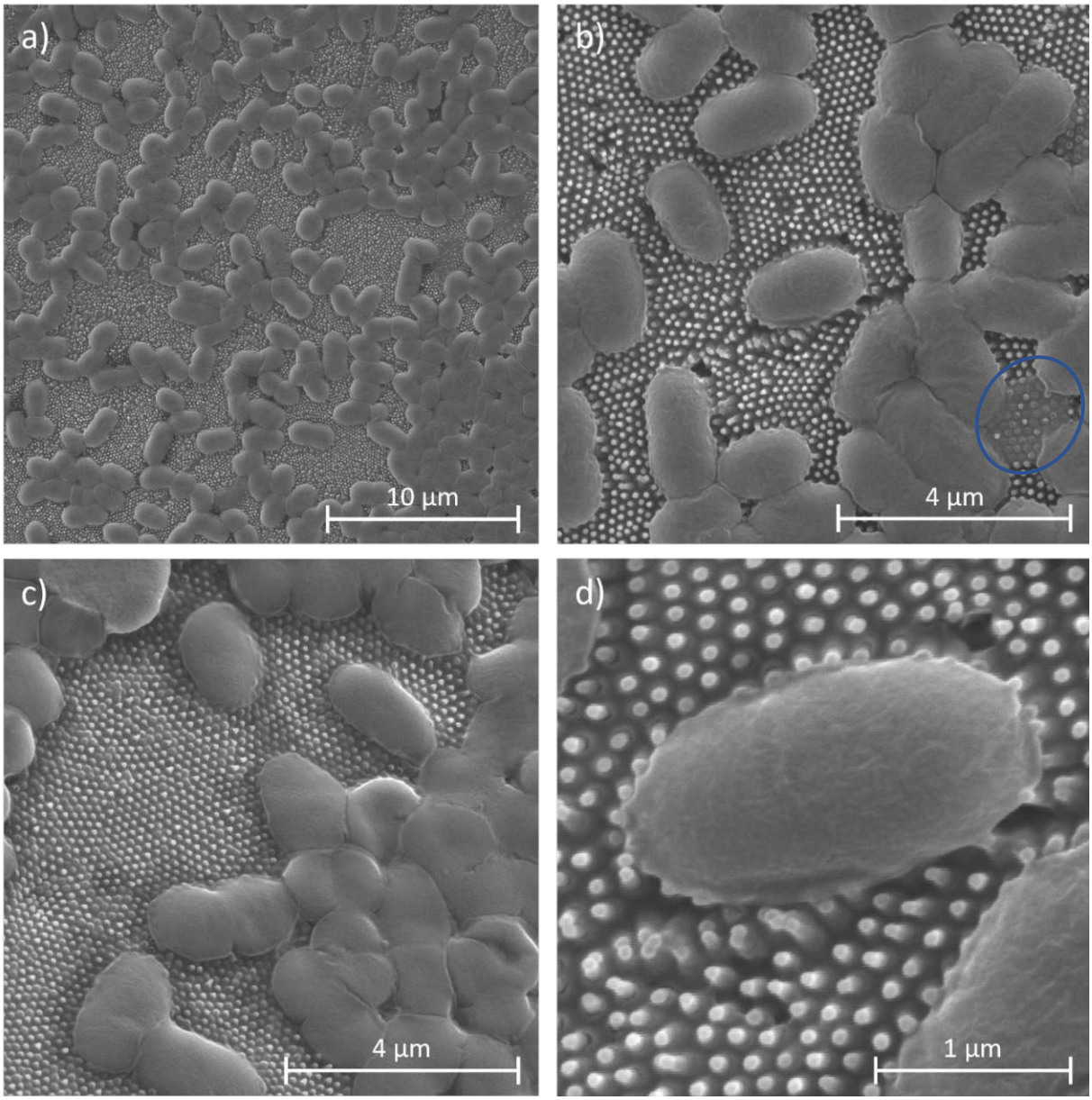

Figure 49. SEM images of *Escherichia coli* bacteria on a *Amphipsalta cingulata* wing: a) Overview of the wing with attached bacteria, b) Blue mark shows a cell completely impaled by the nanostructures, c) Various *E. coli* cells on the wing membrane with a cluster of deformed cells (in the lower right corner), d) High resolution zoom on the interaction between nanopillars and bacteria. Own images, taken with K. Whitmore, USTEM TU Wien, 2021

Many cells show indications for structural damage, such as wrinkled cell walls or shape deformations, but some seem intact (Figure 49 b & c). It must be noted that the samples were air-dried, leading to potential related desiccation damage.

A similar interaction between cells and wing is displayed in the SEM images of the *K. scutellaris* wing. Some parts of the wings were clustered with bacteria cells and in other areas, the wing is not as densely populated (Figure 50 a). The blue mark in Figure 50 b shows two examples where the cell wall (in contact with the nanopillars) is ruptured and cytoplasm leaked out. Moreover, the nanopillars of *K. scutellaris* seem elastic and the tips of the surrounding structures are bent towards the bacterial cells. It seems as if the caps, once in contact with the cell, get tightly adhered and become engulfed by the membrane (Figure 50 c & d).

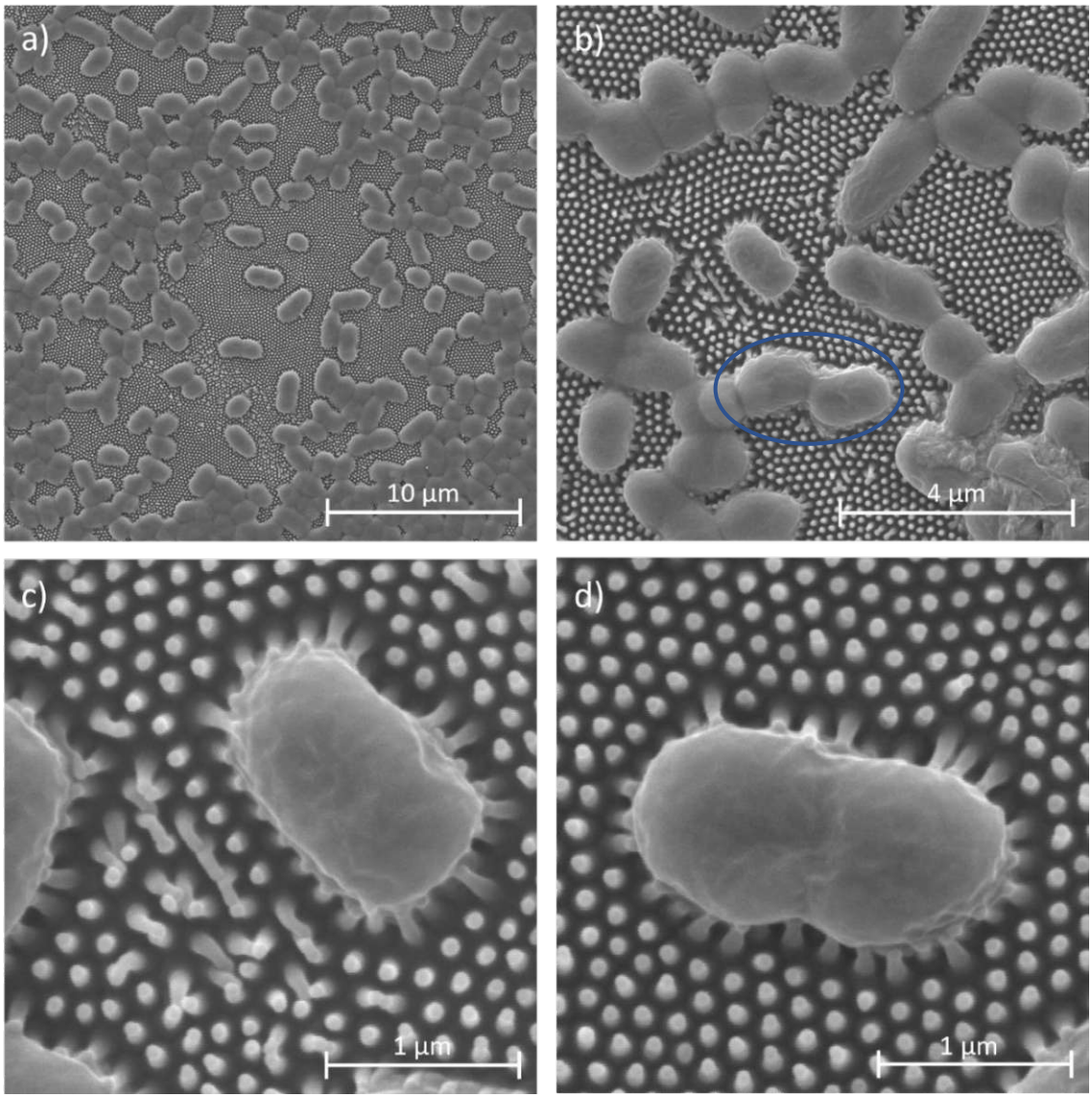

Figure 50. SEM images of *Escherichia coli* bacteria on a *Kikihia scutellaris* wing: a) Overview of the wing with attached bacteria, b) Various *E. coli* cells on the wing membrane, with examples of ruptured cells (blue mark), c) & d) High resolution zoom revealing the interaction between nanopillars and bacteria in more detail. Own images, taken with K. Whitmore, USTEM TU Wien, 2021

On the *M. septendecim* wing, hardly any individual bacteria were found at the wing surface. Most of them were clustered together (Figure 51 a) and large parts of the wings were uncovered. This is a major difference compared to the wings of the two New Zealand cicadas. Within these clusters, the bacterial cells were tightly compressed to each other. Most of them were collapsed in the middle and consequently, their shapes remotely resemble erythrocytes (Figure 51 b). At the edge of the cell clusters, it seems as if parts of the nanostructured surface were torn off and stuck to the bacteria (Figure 51 c). In addition, a few single cells were found the surface. One example is depicted in Figure 51 d, where the cell is impaled by the nanodomes and leakage of the cytoplasm can be observed.

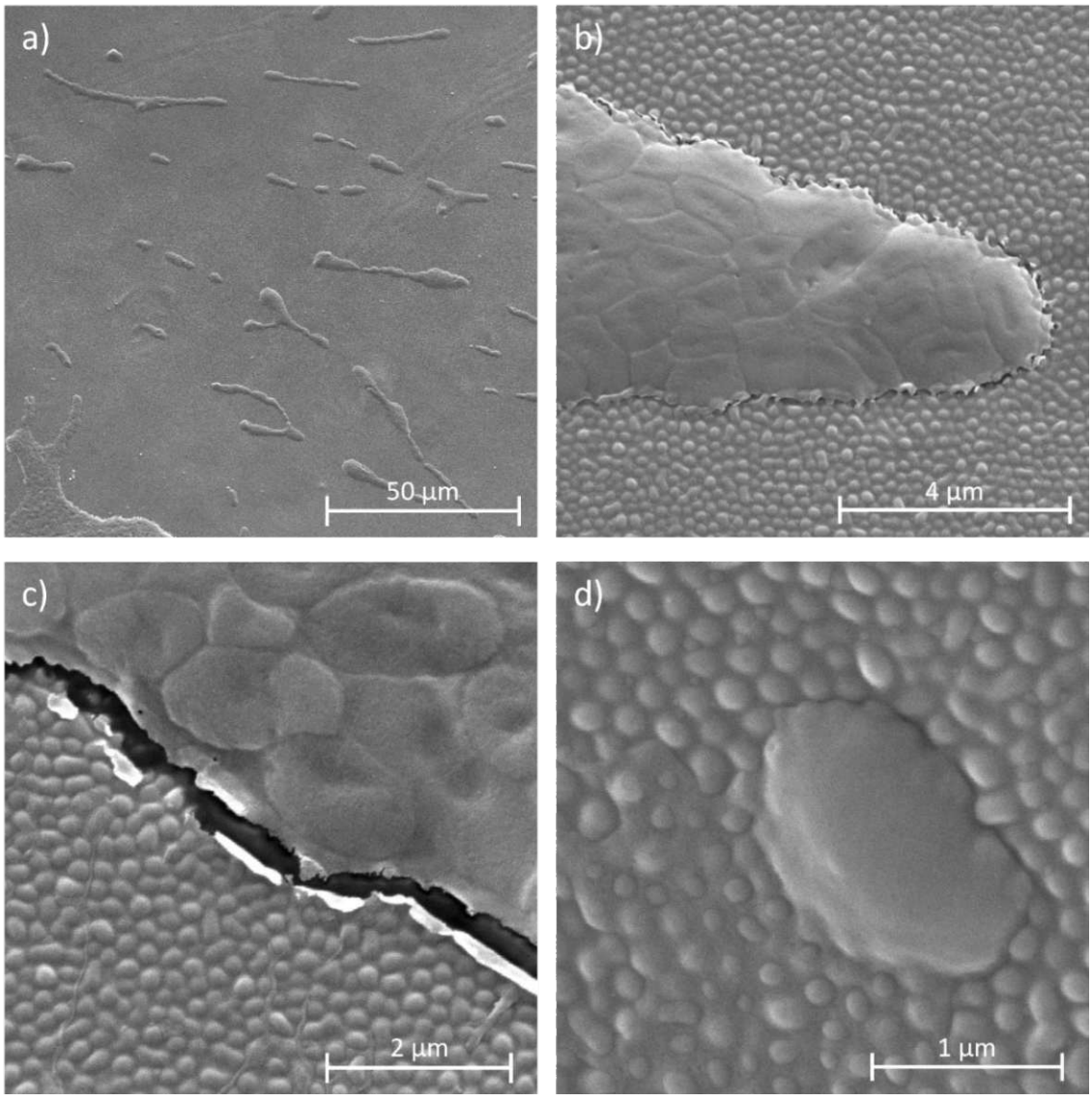

Figure 51. SEM images of *Escherichia coli* bacteria on a *Magicicada septendecim* wing: a) Overview of the wing with various bacterial clusters, b) One bacterial cluster, c) Edge of an *E. coli* cluster, d) High resolution zoom onto an individual bacterium cell. Own images, taken with K. Whitmore, USTEM TU Wien, 2021

In addition to the wings, also Replica D_UV (fabricated with Method D, Table 1) was incubated with bacteria and investigated with an SEM. Although it represents a replica of a *K. scutellaris* wing, it shows significantly smaller nanopillars than its biological template. However, the regular arrangement of the nanostructure was transferred sufficiently. The bacteria were similarly distributed over the surface compared to both New Zealand cicada wings, with single cells and clusters occurring (Figure 52 a). Despite the reduced height, damaged cells impaled by the nanostructures were observed (Figure 52 b).

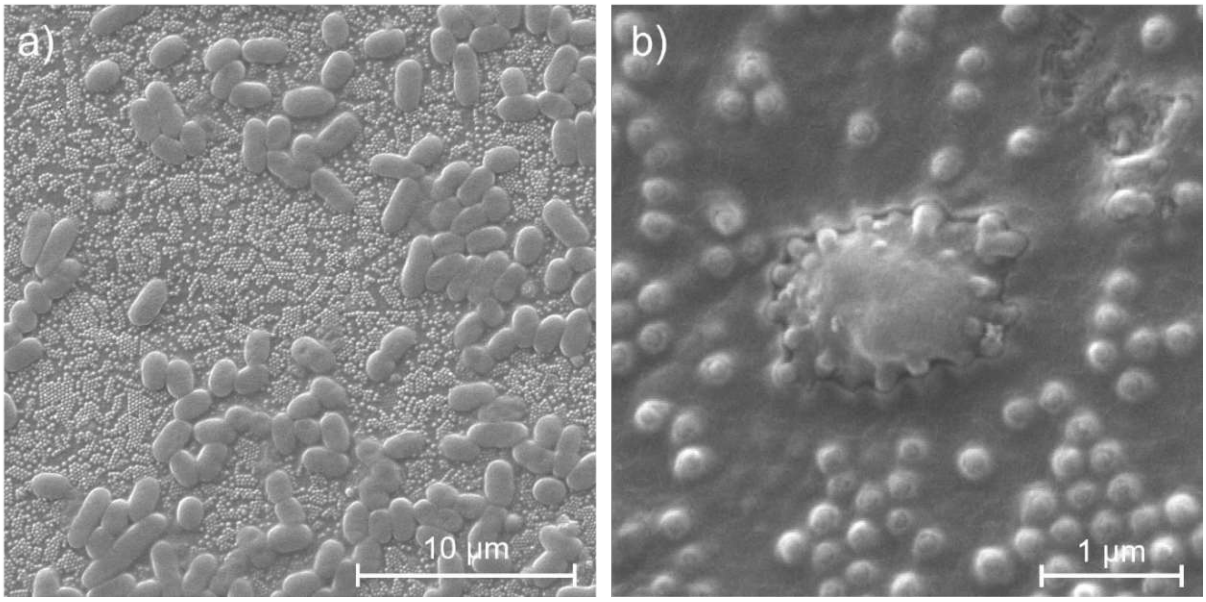

Figure 52. SEM images of *Escherichia coli* bacteria on a *Kikihia scutellaris* wing replica (Replica D_UV: a) Overview of the bacteria on the replica, b) Single impaled cell. Own images, taken with K. Whitmore, USTEM TU Wien, 2021

Contact angle measurements

Previous studies reported hydrophobic and superhydrophobic properties of cicada wings. Therefore, static contact angle measurements were performed in the present study. In *A. cingulata,* the largest angles of about 165° were observed, followed by the *K. scutellaris* wing with values of about 147°. The smallest contact angles (around 105°) were found in *M. septendecim* (Figure 53).

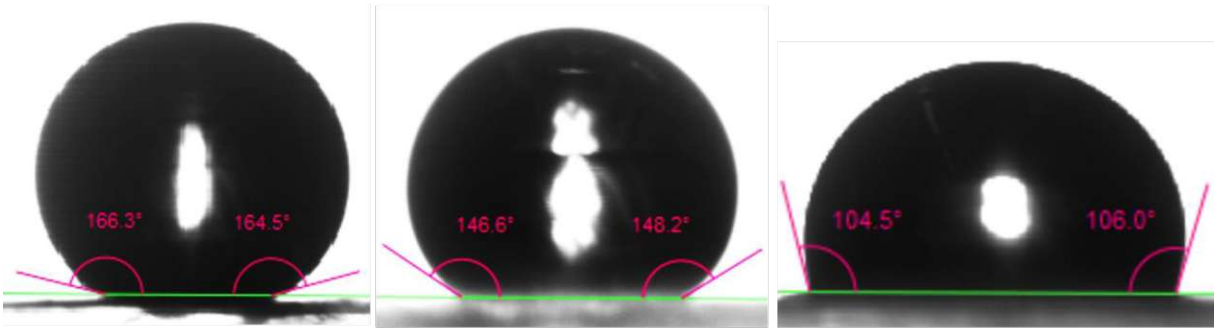

Figure 53. Contact angle measurements of water drops (3 µl) casted on the wings of three cicada species. The images were analyzed with the open-source software OpenDrop. © 2022 Alexander Bürger

Discussion

Morphological analysis

Comparison of topographical investigation methods

In this study different AFM settings were used, optimized for contact mode, tapping mode or suitable for both. In comparison, the results for the various AFM settings show significant differences, especially concerning the height resolution. The AFM setting optimized for tapping mode delivered the results most similar to the SEM investigation. As the findings of these two approaches are comparable, they are identified as the most reliable results and will be discussed further. Using the other settings in AFM (which were not optimized for the tapping mode used) did apparently not result in images that resolve the space in between the nanopillars, leading to an underestimation of the nanopillar heights. The main reason these settings were tried out was the possibility of using contact mode (which would allow for much faster scanning velocities). However, it was revealed that contact mode was not suitable for the investigation of the wing membrane surface. It was observed that the elastic nanopillars were dragged along with the scanning direction when measured in contact mode. This introduced measurement artifacts to the scan and the data could not be used for further analysis.

To sum up, the best AFM results can be achieved with the settings optimized for tapping mode as the results are well supported by the SEM investigation. It is assumed that the resolution could be further improved by using a high aspect ratio cantilever with a high aspect ratio tip.

Cicada wing topography

The topological analysis revealed that the wing surface structures of all three cicada species share common attributes. All are densely packed with hexagonally arranged arrays of pillar-like nanostructures (Figure 29). Despite this similarity, some differences were observed. Most apparently, the differing heights of the nanopillars. As assumed, the wing surface of the New

Zealand „shade singer", *Kikihia scutellaris,* shows the highest nanopillars (average around 330 nm) among the investigated species (Table 3, Table 4). In comparison, the New Zealand cicada *Amphipsalta cingulata* has nanopillars about 100 nm smaller (average about 240 nm) whereas the structures of the American cicada *Magicicada septendecim* (average about 55 nm) would be more appropriately described dome-like rather than pillar-like. Moreover, the nanopillar height within the same wing is not constant but follows approximately normal distributions in the case of all three species (Figure 30, Figure 31).

Based on the three-dimensional reconstructions of the AFM scans of the wings of the New Zealand cicada species, one would describe the nanopillars as relatively simple cones with rounded caps (Figure 29). However, the SEM imaging revealed that the nanopillars have a differently structured shape. In addition, parameters such as the diameter (which varies over the height) could be measured (Figure 32, Figure 33). The bases of the nanopillars are the broadest parts, with a diameter of about 135 nm for *A. cingulata* and 150 nm for *K. scutellaris*. The shape of the nanopillars on *Kikihia scutellaris* wings reminds of the elephant's foot plant (*Beaucarnea recurvata*). The diameter first decreases rapidly with the height and then the nanopillar forms a neck-like structure with a slowly decreasing radius. At the top, the nanopillar gets slightly broader again, forming a head-like tip (Figure 33 b). In *A. cingulata,* a similar shape can be observed without such a prominent foot-like structure (as the radius decreases more constantly over height) (Figure 32 b).

In contrast, the nanostructures of *M. septendecim* remind of domes (Figure 35). It was observed that these nanodomes showed a rather significant variation in their shape and also in the size of the base diameter (Figure 35).

Compared to previously investigated species, *K. scutellaris* showed some of the largest nanopillars, whereas *A. cingulata* can be classified as mid-tier (Table 7). *M. septendecim* shows the smallest nanostructures similar to the ones of *M. Cassinii*. Remarkably, the results of one study (Oh et al., 2017) coincide very well with the results obtained in this study. In contrast to another group (Nowlin et al., 2014), which observed significantly different results (Table 7). This could be an indicator that also differences within species occur. This was also suggested by another group, which investigated the nanostructures of the same cicada species but from different locations (Sun et al., 2018).

Table 7. Summary of selected studies about nanostructures of cicada wings and their properties.

	Average nanopillar height [nm]	Tip-to-tip nanopillar distance [nm]	Reported properties	References
Magicicada cassinii	≈50	-	Bactericidal, hydrophobic	(Román-Kustas et al., 2020)
Magicicada septendecim	54 ± 12 (AFM) 84 ± 14[a] 50[b]	201 ± 25 (AFM) 215 ± 45 (SEM) 252 ± 8[a] 227 ± 30[b]	Bactericidal, fungicidal (low extent)[a], hydrophobic[a,b]	This work [a] (Nowlin et al., 2014), [b] (Oh et al., 2017),
Mogonnia conica	159 ± 13	115 ± 15 (base-to-base)	Hydrophobic (low extent)[a,b], anti-reflective[b]	[a] (Sun et al., 2009), [b] (Sun et al., 2011)
Cryptotympana aguila	182	187 ± 13	Bactericidal, hydrophobic	(Kelleher et al., 2016)
Ayuthia spectabile	182	251 ± 31	Bactericidal (low extent), hydrophobic	(Kelleher et al., 2016)
Psaltoda claripennis	200[a,b]	170[a,b]	Bactericidal[a,b,c], superhydrophobic[a, d], self-cleaning[d]	(Ivanova et al., 2012), (Pogodin, Hasan, Baulin, Webb, Truong, et al., 2013)[a] (Hasan et al., 2013) (Wisdom et al., 2013)[b]
***Ewartia oldfieldi* (syn. *Cicadetta oldfieldi*)**	200 ± 28	200	Superhydrophobic, ultra-low particle adhesion	(Hu et al., 2011)
Amphipsalta cingulata	233 ± 42 (AFM) 249 ± 42 (SEM)	177 ± 18 182 ± 44 (SEM)	Bactericidal, superhydrophobic	This work
Megapomponia intermedia	241	165 ± 8	Bactericidal (high extent), hydrophobic	(Kelleher et al., 2016)
Megatibicen dorsatus	250	227 ± 32	Superhydrophobic, self-cleaning	(Oh et al., 2017)
Meimuna durga	257 ± 24	89 ± 9 (base-to-base)	Hydrophobic [a,b], anti-reflective[b]	[a] (Sun et al., 2009), [b] (Sun et al., 2011)
***Neotibicen tibicen* (formerly *Tibicen tibicen*)**	183 ±32[a] 332 ± 28[c]	175 ± 11[a] 224 ± 35[b]	Fungicidal (high extent)[a] Superhydrophobic[b], self-cleaningb	[a] (Nowlin et al., 2014), [b] (Oh et al., 2017), [c](Oh et al., 2020)
Kikihia scutellaris	328 ± 54 (AFM) 332 ± 43 (SEM)	188 ± 30 182 ± 29 (SEM)	Bactericidal, (super)hydrophobic	This work
Terpnosia jinpingensis	339 ± 24	46 ± 4 (base-to-base)	Hydrophobic (high extent)[a,b], anti-reflective[b]	[a] (Sun et al., 2009), [b] (Sun et al., 2011)
Cryptotympana atrata	400[a], 253 to 464[b]	190[a], 67 to 92 (base-to-base)[b]	Hydrophobic (different levels)[b], anti-reflective[a]	[a] (Xie et al., 2008) [b] (M. Sun et al., 2018)[b]
Neotibicen pruinosus	405[a] ≈350[b]	218 ± 33[a]	Bactericidal[b], superhydrophobic[a,b], self-cleaning[a]	[a] (Oh et al., 2017), [b] (Román-Kustas et al., 2020)

Hydrophobicity of cicada wings

Several previous studies focused besides to the bactericidal effect of cicada wings on their hydrophobic properties. Generally, hydrophobicity is determined by the static contact angle (CA) between the surface and the waterdrop (S. Wang & Jiang, 2007). Depending on the contact angle, water repelling surfaces can be divided into hydrophobic (CA ≥ 90°) and superhydrophobic (CA ≥ 150°) (M. Sun et al., 2009; S. Wang & Jiang, 2007). Based on this definition, the results of the measurements classify only *A. cingulata* as superhydrophobic (CA ≈ 165°, Figure 53). A contact angle of 165° is comparable with the contact angle found on the leaves of sacred Lotus (Barthlott & Neinhuis, 1997). Although *K. scutellaris* shows the highest nanopillars, the contact angles measured were just below 150° (CA ≈ 147°), which lies at the border of superhydrophobicity. *M. septendecim*, as expected, showed the lowest hydrophobicity (CA ≈ 105°). This contact angle slightly deviates from the result of the group of Miljkovic (115.2° ± 5.5°) but coincides with the angles found for *M. cassinii* (102.8° ± 5.2°) by the group of Alleyne (Oh et al., 2017; Román-Kustas et al., 2020).

It was expected that *K. scutellaris* would show the highest level of hydrophobicity as it prefers to live in shady areas (as mentioned in the Introduction). Furthermore, the topographical characterization showed that this species possesses the highest nanopillars and previous literature showed a positive correlation between pillar height and contact angle (Oh et al., 2017). However, another group showed the dependency of the contact angle on chemical components of the surface (Sun et al., 2009), which could be an explanation for the lower contact angle despite the more pronounced nanopillars.

However, it needs to be mentioned that it was actually most difficult to place the water droplets on the wings of *K. scutellaris.* First of all, this species has the smallest wing cells (areas between veins). Moreover, the adhesion force of the water droplet to the pipette was much stronger than the gravitational force combined with the adhesion to the cicada wing. Therefore, a second pipette tip was used to push the droplet off. In most of the tries, the water drop rolled off the wing membrane or adhered to a vein. The only time when the drop was successfully deposited on the wing, the measurement was taken. This was the reason why for each species only the best image was selected and analyzed. It gives a first insight in the hydrophobic properties of the wings of the investigated cicada species.

Replication by two-step nanoimprinting

After testing various variations of fabricating the negative and positive impressions, a method was developed, with which it was possible to efficiently capture the nanopillar structure very efficiently. Different factors play a role in the quality of the replication. Initial cleaning of the wings was not necessary. On the contrary, washing with acetone altered the transparency of the cicada wings, indicating some sort of chemical reaction. Ultrasonication in Isopropanol caused ruptures in the more fragile wings of *K. scutellaris*. The ultrasonication in distilled water did not seem to alter the wing structures, but also showed no beneficial effect.

The most efficient master stamp was fabricated with the Xtra Light Body PVS paste. Before applying the PVS a 5 mm disc was cut out of the wing. Thereby, the negative influence of larger veins could be excluded. Furthermore, it helped to reduce the curvature of the wing to a minimum. To give the PVS the time to capture all details, it is suggested to perform the molding process at 4° C to extend the curing period. Three microscope slides (total mass of 15 g) were used to put an additional pressure on the PVS during the molding process (Figure 22). Moreover, it was found that after peeling the wing off no cleaning steps are necessary to remove organic residuals. On the contrary, the formic acid seemed to react with the PVS and alter its surface as the reflectivity and color changed. In addition, the ultrasonication with water could also have a negative effect as water residuals could be gathered at in the wells of the negative impression. This could result in a reduced quality of the replica as the resin for the positive replica then cannot fully fill out the wells.

Finally, the UV curing resin proved as the most efficient filling material for the master stamp. The testing series, where the master stamp was used first with UV curing resin (Replica C1_UV), followed by epoxy resin (Replica C2_EP) and again with UV curing resin (Replica C3_UV), clearly showed the dependency on the filling material. Replica C1_UV was a nearly perfect replication of the original wing structure. The surface was densely packed with the hexagonal arranged arrays of nanopillars and the spacing was precisely captured (Figure 30 & Figure 37). Only the nanopillar height showed a slight deviation from the original (compare Table 3 & Table 5).

Replica C2_EP could not compete with the results obtained with the UV curing resin. The structures were only irregularly captured and many pillars seemed fused (Table 6, Figure 40 a). The third replica produced with the same master stamp (Replica C3_UV) showed more regular structures than the epoxy resin replica. In addition, the nanopillar arrangement is similar to the original wing as well as the height distribution (except for a larger group of outliers in the height range of 60 to 130 nm, (Figure 40 b). However, the height deviates significantly (about half of the original structures, Table 6). One possible reason for the reduced replication efficiency could be residuals of the epoxy resin that remained in the wells of the master stamp. This would prevent the UV resin from capturing the nanopillars in full height. This could also explain the shape of the nanopillars in the SEM scan of Replica C3_UV, which looks like the upper part with the head-like structures was cut off (Figure 42). However, the images show how well the hexagonal arrangement was transferred (Figure 42 d). At some areas, small replication errors were found as some pillars stuck together with their tips. A direct comparison of the three replicas is displayed in Figure 41 with help of representative line scans.

The other approaches using PVS as molding mass could not provide a similar efficiency (Table 5, Figure 36). In addition, the alternatives to PVS (casting of resin and nail polish directly onto the wing surface) worked only for the low aspect ratio structures of *M. septendecim* but were nearly impossible to remove from the *K. scutellaris* wing (Figure 43).

To sum up, the developed method is a fast and efficient low-cost technique, with which one can precisely replicate the nanostructures of cicada wings. Therefore, the method developed in this study can compete regarding quality with the time-consuming and cost-intensive approaches used in other studies.

Cicada wings as a mechanical bactericide

Antimicrobial action is one of the most remarkable properties of cicada wings. This property has repeatedly been reported by several studies in recent years (Ivanova et al., 2012; Hasan et al., 2013; Kelleher et al., 2016; Nowlin et al., 2014; Román-Kustas et al., 2020). As mentioned in the Introduction, these studies were one of the primary inspirations for this work. Especially since surfaces capable of killing attached bacteria hold great potential for biomimetic applications. To verify that the cicadas examined in this study exhibit similar properties, live/dead staining experiments were performed. Previous studies observed that Gram-negative and Gram-positive bacteria (due to their structural differences regarding the cell wall) react differently sensitive to the nanopillars of the cicada wing membranes (Hasan et al., 2013; Nguyen et al., 2019). This was the reason why one species from each of the two major groups was selected for the experiments performed in this study.

Live/dead staining experiments

In the case of *E. coli*, the two cicada species with high nanopillars (*A. cingulata* and *K. scutellaris*) showed a greater percentage of propidium iodide (PI) stained cells attached to their wing membrane (Figure 44 a). PI is a dye impermeable for intact membranes and stains only cells with damaged membranes, which can be considered as dead. The periodical cicada *M. septendecim*, on the other hand, which has significantly lower nanostructures, also showed a lower efficiency against the Gram-negative bacteria (about 10 % less). Compared to the control group with living bacteria, even on the wing surface of the periodical cicada with nanodomes of only 50 nm, three times as many damaged cells were found. This is surprisingly, to say the least. Both New Zealand cicada species showed approximately the same killing efficiency (Figure 44, Figure 45).

For bacterial tests, it is very important to include a reference group (bacteria on a poly-L-lysine coated microscope slide was used in the present study) as the results between different experiments can vary significantly. First of all, unfortunately, there is no clearly defined

standard protocol for live/dead tests yet. The previous studies used different bacteria, different staining methods, varying incubation times and several analysis tools. Furthermore, various parameters could determine the viability of bacteria, such as different sensitivity of bacterial strains, different environmental conditions and bacterial density. Several additional factors could influence the outcome of the experiment and not all of them are controllable to the extent one might wish for. These are some reasons why comparisons of bactericidal efficiency (percentage of attached bacteria that become killed by the surface nanostructures) over different studies are not reliable. Only the comparison to a control group makes the results meaningful as the reference is investigated exactly under comparable conditions.

The results show that around a third of all bacteria were detected as dead in the positive control group, which is a remarkably high number (Figure 44). Without this reference, the efficiency of the nanopillars could be overestimated. A standard glass slide was used as a control for the first time, but the bacterial count was relatively low, making the results very sensitive for counting errors and also for staining errors. Therefore, it was decided to use poly-L-lysine coated microscope slides instead. This coating, which is commonly used to attach cells to, increases the number of bacteria attached, leading to better comparability with the attachment to the cicada wings.

In addition, a negative control (with only dead bacteria on it) was used to evaluate the quality of the staining and analysis methods. Therefore, the microscope slide with the attached bacteria was heated to 95° for 4 minutes (cicada wing tests) or killed with 50% methanol (replica test). For both bacterium species, about 96 % of damaged cells were correctly classified as dead and 4 % were counted as viable (Figure 44 a). All in all, it is a high percentage of correctly detected bacteria, which shows that the results obtained can be assumed as reliable.

To sum up, all three cicada wings exhibit significant bactericidal properties against *E. coli*. Moreover, the outcome supports the hypothesis that nanopillars with a higher aspect ratio show a stronger antimicrobial effect (Figure 44 a). This is further supported by former studies (Kelleher et al., 2016; Nowlin et al., 2014).

The *S. aureus* tests showed significantly different results (Figure 44 b). The cicada wings with the least pronounced nanostructures, *M. septendecim*, showed the highest percentage of killed bacteria. This percentage was almost about the same as the negative control group

(around 96 %). Furthermore, 90 % of the bacteria on the *K. scutellaris* wing were classified as dead. In *A. cingulata* this number amounts to about 80 %, which is about as twice as much as in the control group (Figure 44 b).

However, it needs to be mentioned that only three randomly selected 100 µm^2 areas were analyzed, which might be a too small sample size for reliable and reproducible results. Moreover, the used image analysis could introduce some errors into the results. The original fluorescence microscope image needs to be converted into a binary image to perform the particle analysis with the software Fiji. Therefore, a certain pixel value must be set as a threshold to distinguish between signal and no signal. As some of the original images showed not the same intensity for the fluorescence signals, the threshold had to be set individually. Thereby one has to take care, not to set the threshold for the PI signal too low. PI shows the tendency to gather around the outside of bacteria, which can cause some false low intensity signal. This was another reason why a control group with dead bacteria was included in the experiments as it enables a reference to distinguish between these false signals and true signals from dead bacteria. It was tried to be as consistent as possible within an experiment with the threshold setting, but it needs to be mentioned, that this could introduce a certain bias. Moreover, the segmentation algorithm showed difficulties to identify the number of bacteria if clusters were formed. This highlights the urgent need of a general standard for bacterial live/dead staining tests.

Several studies stated that Gram-positive bacteria are not or only modestly susceptible to the nanopillars of cicadas due to their thick peptidoglycan layer (Hasan et al., 2013; Nguyen et al., 2019). The group of Ivanova tested the effect of the Australian cicada *Psaltoda claripennis* on another strain of *S. aureus* than that one that was used in this study (Hasan et al., 2013). It could be the case that the susceptibility for mechanical stress varies amongst different strains. In contrast to these previous findings, the experiment performed in this work indicates that all three cicada species show an effect against *S. aureus* in comparison to the control group. However, in 2019 the group of Yarlagadda found that their investigated cicada wings showed an antibacterial effect against *S. aureus*, which would support the findings of the present study (Shahali et al., 2019). To validate these results, further studies should be performed with various Gram-positive bacteria. If the results could be reproduced, it could be shown that cicada wings indeed affect Gram-positive bacteria, which was previously only reported for

nanostructures with a very high aspect ratio as are found on black silicon*, dragonfly wings or on gecko skins (Ivanova et al., 2013; Watson et al., 2015)

SEM investigation of bacterium-nanopillar interaction

Scanning Electron Microscopy scans were performed to investigate the interaction between the bacterial cells and wing surfaces. These scans showed that the bacterial membrane is attached to the nanopillars and partly engulfs their heads (Figure 49, Figure 50). As consequence, the membrane gets stretched and stress is induced. The high nanopillars of both New Zealand cicada species stretched the bacterial membranes (Figure 49 d, Figure 50 c & d). Moreover, some bacteria were found completely sunken into the bed of nanopillars (Figure 50 b).

Interestingly, the density of the bacteria seems higher on the wing surfaces with more pronounced structures. On *M. septendecim,* most bacteria were concentrated in clusters and only a few solitary cells were found (Figure 51 a). Several of these single cells found were damaged and a leaked fluid could be observed, possibly part of the cytoplasm (Figure 51 d). This clustering could be caused by the method of the sample preparation and therefore be an artifact. After the incubation in the bacterial suspension, the wings were air dried. As already mentioned above, the wing membrane is not flat but shows elevations and depressions. This could result in the formation of suspension residuals during the evaporation, where the remaining fluid converges. It seems as if the bacteria were either able to move actively into the flow direction or were passively dragged along with it. This could explain the compact clustering of the bacterial cells due to the final desiccation process during which the bacteria are compressed together (Figure 51 b & c).

In addition, the observed collapse of the cells could also be caused by desiccation rather than caused by interaction with the nanopillars. This form of clustering was only observed in the American cicada. It is proposed that the high aspect ratio nanopillars of the New Zealand cicada species immobilize the bacteria as the cells partly sink into the nanostructures, which is not possible for the nanodomes of *M. septendecim*.

Bactericidal properties of the replicas

In addition, a live/dead staining experiment was performed on the replica that showed the highest similarity to the *K. scutellaris wing* (Replica C1_UV, Figure 38). *E. coli* was chosen as a testing agent as the experiment on the cicada wings revealed more expected results.

The positive impression of a *K. scutellaris* wing showed a higher proportion of PI-stained bacteria as the unstructured control group (which was produced with the same UV curing resin to exclude a potential difference of the results due to chemistry). About 15 % more bacteria were inactivated. It must be noted that about 50 % of the bacteria found on the control group were classified as dead. A possible explanation could be that some chemical components in the resin had an influence on the viability of the cells. As this experiment was performed on another fluorescence microscope (which used slightly different excitation wavelengths), differences in resolution and intensity could have influenced the image analysis. This is further reason why it is of great importance to include a reference in each test (as it was done in this study).

Moreover, the negative control group reveals that only 90 % of the damaged cells are classified as dead (Figure 47). In addition, more attached bacteria were found on the rough replica than in the smooth reference (Figure 48). This supports the findings of former studies that the nanopillars do not prevent attaching but rather damage adhered bacterial cells (Hasan et al., 2013; Ivanova et al., 2012).

In addition, SEM scans were taken from a replica prepared in the same way as the wings (incubated for one hour in an *E. coli* suspension and afterwards air dried). It has to be noted that the replica used (Replica C3_UV) is made from the same PVS stamp as the replica used for the live/dead staining (Replica C1_UV) but showed significantly lower nanopillars (Figure 41, Figure 42). Despite this fact, the bacteria showed similar behavior as on the original wing. No large clusters as in *M. septendecim* were detected. In addition, some cells were completely sunken into the nanopillars (Figure 53).

Although further testing series should be performed to verify the results, the experiments clearly show an effect of the nanostructure on bacteria. The replica produced with the developed nanostamping technique showed the ability to reduce the number of viable cells.

Challenges of live/dead experiments

One of the major criticisms on established literature in this field of research is the little available comparability of results between studies. Each group had its own protocol for the bacterial experiments and used different bacteria species, different incubation times, different bacterial concentrations, different staining approaches and different analysis methods (Hasan et al., 2013; Ivanova et al., 2012; Kelleher et al., 2016; Román-Kustas et al., 2020). There are no standardized settings for testing mechanical bactericides yet. That is the reason why only the comparison to the control group is reliable for the time being. It would be important to introduce a testing protocol for bactericidal surfaces with standardized settings and protocols. Only this way, it will be possible to compare the efficiency of different structures to previously investigated ones without including them all into the same measurement series.

Furthermore, it should be noted that these tests do not resemble natural conditions. In Nature, there are rarely bacterial populations composed of only one species but indeed many different species interacting with each other. In addition, a former study raised the awareness that many potential applications (for example vascular prostheses) would be better simulated with experiments under flowing conditions. Moreover, colleagues state that the rinsing step performed to remove loosely attached bacteria could introduce a bias as undefined shear forces are applied which could alter the proportion of living and dead bacteria (Senevirathne et al., 2021).

Despite this weakness, bacterial live/dead experiments are still an important tool to investigate bactericidal surfaces and provide valuable results if compared to a control group.

The underlying principle of bactericidal properties of nanopillars

Various studies investigated the underlying mechanism of the bactericidal property of nanopillars. The first biophysical model was proposed by the group of Ivanova (Pogodin et al., 2013). This group proposed that due to the adherence of the bacterial membrane to the nanopillar tips, non-uniform stress is induced in the parts that are located between two pillars (Figure 4). As consequence, cytoplasm leaks and the bacterial cell dies.

They suggested that the bactericidal effect is just determined by physical properties and not by chemical interactions. As a control, bacterial testes with gold-coated wing membranes performed – they showed about the same killing efficiency and therefore point towards mechanical rather than chemical reasons for bactericidal properties (Ivanova et al., 2012; Pogodin et al., 2013).

In 2020 the group of Alleyne stated that not only the topography plays a role in the bactericidal effect of the nanopillars, but also the chemical constituents of the wing surface. They used a chemical layer extraction approach and observed a change in bactericidal depending on the components of the chemical layer at the surface (see Introduction, Figure 6, for detailed description). Especially, this seems to be the case for *Magicicada cassinii*, which has low nanopillars, but possess an antibacterial effect (Román-Kustas et al., 2020). As this cicada species is closely related to *M. septendecim* and possesses similar structures, the reported bactericidal effect of *M. cassinii* coincides well with the results observed for *M. septendecim* (Figure 6, Figure 44). Another study suggested that additional mechanisms such as the effect of cell division and movement, which enhance the mechanical stress induced by nanopillars on the bacterial cell wall, might be relevant for the bactericidal properties (Köller et al., 2018). Furthermore, Jenkins and coworkers suggested that the interaction of the bacteria with nanopillars could lead to the production of reactive oxygen species (ROS)*, which could play a role in the bactericidal effect of such nanostructures (Jenkins et al., 2020). In addition, Ishak and coworkers recently investigated the role of bacterial surface proteins in interaction with fabricated nanopillars on a polyethylene terephthalate (PET) surface (Ishak et al., 2021).

To sum up, the mechanisms underlying the bactericidal property are continuously being refined by scientific investigations and many different aspects are discussed. Bacterial cell walls are not a homogenous layer, but consists of many different components (see Introduction, Figure 15). Therefore, the interactions with the nanopillars most likely take place on a physical as well as on a chemical level. This could be an explanation, why small nanostructures as in *M. septendecim* show bactericidal properties as well. However, it will still take further investigations to fully understand the interactions between nanostructured surfaces and bacterial cells.

Potential for biomimetic applications and challenges

As the experiments showed, the nanostructures of the cicada wing membranes possess significant bactericidal properties. In contrast to traditional antibiofouling* surfaces, cicada wings do not prevent the attachment of bacteria, but instead induce cell wall damage in adhered bacteria. This raises a major question. What happens over time on the surface? Will the dead bacteria clog the nanostructures and inhibit the killing mechanism for new arriving bacteria or is the surface self-cleaning regarding the impaled bacteria?

There are some groups that discussed these problematics in previous studies. The group of Yarlagadda stated that under static conditions (which would resemble the live/dead experiment setting) remains of the lysed bacteria will compromise the nanopillars and build up a suitable substrate for newly attaching bacteria. At the same time, they mention that under flow conditions, the bacteria could be removed and the surface would keep their bactericidal property. This would apply for several biomimetic applications, such as bioimplants, where body fluids exhibit shear forces and additionally phagocytes would digest the lysed bacteria (Senevirathne et al., 2021).

The group of Ivanova proposed a model of a self-cleaning cycle based on their investigation of bacteria on a Silicon nanopillar surface for a static bacterial solution. They investigated that the lysed bacteria disappeared after a certain time from the surface and seemed to be removed into the solution again (Nguyen et al., 2019).

Another problem of biomimetic surfaces is friction, which is damaging the nanostructures over time. Therefore, it must be investigated how resistant these structures are regarding mechanical forces. If they are durable enough it would open a vast field of applications. Especially, in combination with efficient and low-cost methods such as the developed nanoimprinting technique, which would enable upscaling on large areas and could also be applied in developing countries with little technical infrastructure.

Moreover, several studies showed these nanopillar surfaces harmless and non-cytotoxic for eukaryotic cells (such as mammalian cells). Furthermore, there are indications nanopillar-induced growth promoting properties for certain cell types (Pham et al., 2016; Shahali et al., 2019; Watson et al., 2015). In combination with their function as mechanical bactericide this would lead to an immense advantage in medical applications such as implants. Furthermore,

another group discussed the potential in regenerative medicine, in terms of guided cell growth which could be used for example in ophthalmology (Green et al., 2012).

However, even with the limiting factors of bacterial clogging and friction, nanopillar surfaces bear a huge potential in time-limited and low friction applications, such as implants (Hosseinpour et al., 2021; Jaggessar et al., 2017) or in fluidic systems (X. Wang et al., 2016).

Conclusion

All three investigated cicada species show the same hexagonal arrangement of nanopillars on the wing membrane surface. However, the height varies significantly between the species. As assumed the „shade singer" *Kikihia scutellaris* possesses the highest nanostructures (about 330 nm). This could have resulted from an adaptation to the ambient conditions. The second highest nanofeatures were found in *Amphipsalta cingulata* (about 240 nm) and the lowest in *Magicicada septendecim* (about 50 nm). Interestingly, despite all investigated wings being hydrophobic, superhydrophobic contact angles (i.e., contact angle ≥ 150°) were reported in *A. cingulata.* The results for the wing membrane of *K. scutellaris* were at the threshold to superhydrophobicity. This is contrary to the expectations that nanopillars with a higher aspect ratio result in higher contact angles, so maybe the wings have a different chemical composition. The wing membranes of *M. septendecim* show the lowest value for hydrophobicity among the investigated species.

Bacterial experiments showed that all three cicada species show significant bactericidal properties against attached bacteria of the two species investigated: *E. coli* (Gram-negative) and *Staphylococcus aureus* (Gram-positive). This result was unexpected as previous studies suggested a mechanical insensitivity of Gram-negative bacteria against cicada nanopillars. Astonishingly, *M. septendecim* showed the highest efficiency against *S. aureus*. This is opposite to the traditional opinion that higher aspect ratio nanostructures are more efficient in terms of their bactericidal effect. This leads to the suggestion that chemistry might also play a substantial role in the antibacterial properties of certain cicada wings such as in *M. septendecim*. In contrast, the results for *E. coli* support the positive relationship between higher nanopillars and bactericidal efficiency.

The unexpected findings regarding hydrophobic and bactericidal properties need to be tested in further experiments to see if they reflect the actual situation or if they occurred due to some measurement issues.

An interesting question for future topographical investigations could be to which extent environmental adaption affects the shape of nanopillars. First indicators were found in this study comparing the „sunny singer" *A. cingulata* and the „shade singer" *K. scutellaris.* As expected, the highest nanopillars were found in *K.* scutellaris, but it is contradictory that the

„shade singer" *K. scutellaris* shows smaller contact angles compared to *A. cingulata* as superhydrophobicity would be a tremendous advantage in shady humid areas. Further investigations of closely related cicada species could reveal if differences in the height of nanopillars occur due to environmental adaption.

Furthermore, this study showed that the developed nanoimprinting technique proved to be capable of producing replicas with the same height and spacing of nanopillars as the original wings. No difference could be seen compared to more time-consuming and cost-intensive fabrication methods used in previous studies. In addition, the bacterial experiments revealed that the replica showed a significant bactericidal effect compared to the smooth control group.

As the nanoimprinting technique is cost-efficient, fast and straightforward, it opens a vast field of applications (even for large areas) such as hospital surfaces, medical devices, door handles and mobile phone displays. In particular, nanopillar surfaces could provide valuable solutions for temporarily limited and low friction applications such as medical bioimplants and fluidic systems. The use of mechanical bactericides could be an immense step to reduce the application of chemical microbicides, which often result in strains with multi-resistances, as bacteria cannot develop chemical resistance against structures. Thereby, a nanopillar-based structure-centered approach might be one of the ways to go to successfully address multidrug resistance in bacteria.

Nature comprises millions of species, which developed over millions of years under selection pressure. This led to a huge variability of tissues. As surfaces are the first protective layer and the outermost interface with the environment, they stand under high selection pressure. This led to natural surfaces with multiple amazing properties, which can inspire technical interfaces. The surfaces of most plants and animals are still not investigated on a physical level, resulting in a huge potential for future studies.

Acknowledgments

First of all, I would like to thank Professor Ille C. Gebeshuber (Research Unit of Atomic and Plasma Physics at the Institute of Applied Physics, TU Wien), who introduced me to this exciting topic and supported me greatly with her expertise in biomimetics. Since I was a child, I have always been fascinated about the basic principle of learning from Nature to solve technical challenges, which was one of the reasons why I studied technical physics and biology. When I first heard about Prof. Gebeshuber and her research field, I immediately wished I could work with her. I am very thankful she accepted me as a diploma student and introduced me to biomimetics. She will always be scientific a role model for me.

Of course, this thesis would not have been possible without cicadas. My special thanks goes to the cicada experts Professor Chris Simon and her colleague David C. Marshall, Ph.D., who sent me cicadas from New Zealand and furthermore provided me with information about these fascinating animals. Their help marked the beginning of my research and I am really grateful for that! Moreover, Prof. Chris Simon provided me with great photos of the cicada species, showing these amazing animals alive in their natural environment.

My sincere thanks goes to Julia Fisher (from the Facebook group Weltfrauen) who collected many wings of the periodical cicadas and sent them to Vienna. This way we had another species for our investigations - with surprising results!

Many thanks go to my colleague Richard van Nieuwenhoven, BSc (graduated computer scientist and diploma student of Prof. Ille C. Gebeshuber working on his Biomedical Engineering degree). who did joint research with me on this topic. We discussed endless hours how to optimize the different experimental settings. Moreover, he carried out major parts of the bactericidal experiments and shared his fluorescence microscopy images.

I want to thank the director of the Institute of Applied Physics, Vienna University of Technology, Professor Friedrich Aumayr, who provided us with funding.

I want to express my gratitude to Professor Markus Valtiner (head of the Applied Interface Physics division at the Institute of Applied Physics, TU Wien) who provided Richard and me access to his laboratory and AFM instruments. Without him the scope of this thesis would not have been possible, as AFM scans were a crucial part in the investigation of nanostructures of the cicada wing membranes and their replications. In addition, thank you to Laura L. E. Mears, who introduced me to the AFM handling and supported me wherever she could. I also want to thank Dominik Dworschak who solved several issues that occurred using the AFM.

Furthermore, I want to thank Prof. Adelheid Elbe-Bürger (Department of Dermatology, Division of Immunology, Allergy and Infectious Disease, Medical University of Vienna) who provided access to a confocal fluorescence microscope. Furthermore, thanks to Philip Kienzl, Ph.D. (Department of Dermatology, Division of Immunology, Allergy and Infectious Disease, Medical University of Vienna), who helped us with his expertise and supervised the bacterial tests.

Thank you to Karin Whitmore who took with me the beautiful SEM images, giving more detailed insight about the shape of the nanopillars and the bacterial interactions with the cicada wing surface. It is a great pleasure to work with such a seasoned expert.

Particularly, I want to thank the most important people in my life, my family. First of all, I want to thank my mother, who is always here when I need someone to talk to and encourages me to follow my dreams. Furthermore, I want to thank my father, who always supports me greatly. And of course, I want to thank my two grandmothers and my grandfather, who are always here when I need help or advice.

And finally, I want to thank animated Nature for inspiring us all!

Glossary

Atomic Force Microscopy (AFM):

aspect ratio: the ratio of the width of an object to its height.

Bacteria are prokaryotic organism, which means that their DNA is not collected in a nucleus, but rather freely distributed in their bactericidal cytoplasm. Moreover, they possess small ring-like structure made of double-stranded DNA called plasmids. These can be transferred via horizontal gene transfer. In this study *Escherichia coli* (Gram-positive) and *Staphylococcus aureus* (Gram-positive) were investigated. They differ strongly from the structure of their bacterial cell wall.

- **Gram-positive** bacteria possess a cell membrane enclosed by a thick peptidoglycan layer, which is the reason why they get stained in the Gram staining method
- **Gram-negative** bacteria have an inner and an outer cell membrane. In-between these two membranes is a thin peptidoglycan layer.

Black Silicon is a surface modified Silicon, which shows very low reflectivity and high absorption of visible light. That is the reason for the name. The surface consists of particularly high aspect ratio structures. It is commonly used in the photovoltaic industry as it enables a higher efficiency.

Centroid is also called the geometric center. This means it is the arithmetic mean of all points in a geometric figure. In contrast to center of mass it does not take the density into account but only the shape.

Cicadas are insects which typically feed on the xylem fluids of plants. In this study three cicada species were investigated:

1. ***Amphipsalta cingulata*** (commonly known as clapping cicada) is endemic to New Zealand. Prefers sunny coastal scrubs as habitat.
2. ***Kikihia scutellaris*** (commonly known as lesser bronze cicada) is endemic to New Zealand. Prefers shady areas such as the understory of forests and is therefore called „shade singers".

3. ***Magicicada septendecim*** (commonly known as 17-year periodical cicada) emerges every 17 years synchronously in mass events, which are called Broods. Distributed in North America.

Commensalism describes the interaction of two organisms, where one has an advantage of this relationship, but the other side is unaffected. Compare to mutualism were both parties have an advantage.

Contact angle is the angle between a liquid-vapor interface, gets in contact with a solid phase. The angle is measured through the liquid.

Cytoplasm is the (semi-) fluid within a cell. Bacterial cytoplasm is often named as protoplasm as there is no nucleus within a prokaryotic cell.

Dorsal is the side of an animal, which is associated with the back. In case of cicadas the upper side.

Epicuticular waxes: thin wax coatings of the cuticle (the outermost layer of plant).

Fluorescence microscopy is an optical imaging method utilizes the fluorescence (Stokes shift) of the sample instead of the scattered, reflected or absorbed light. The sample gets excited with a certain wavelength and therefore emit light themselves in a shifted wavelength (Stokes shift). This light signal is then measured by the fluorescence microscope. Often it is used together with fluorescence stains or markers. In this study fluorescence microscopy was used for the bacterial tests.

Focused ion beam (FIB): has a similar setup to a SEM but uses focused beams of ions (mostly Gallium ions). It can be operated at low currencies for imaging or at high currents for removing material of the sample, which can be used to remove layer by layer. FIB-SEM utilizes electron beams for imaging as well as focused ion beams to manipulate the sample.

Hydrophobic surfaces show a modest to strong repellence of water. They are characterized by static contact angles above 90°. For contact angles above 150° see superhydrophobicity.

Imago (pl. imagines): final stage of the metamorphosis of an insect. Also called adult stage, in which the insect is fully mature and can sexually reproduce.

Live/dead tests: Tests which utilizes markers (such as fluorescence dyes) to distinguish between dead and living bacteria. In this study Propidium Iodide was used as stain for dead

bacteria as it can only enter cells through a damaged membrane. In contrast, Bisbenzimide Hoechst 33343 is permeable for intact membranes and therefore stains all cells.

Multidrug resistance means that microorganisms have built up chemical resistances against different antibiotics of different classes. As bacteria can horizontally transfer genes, resistance genes can spread quickly among populations.

Mutualism is the case if both parts of a relation profit from the partnership formed, it is a positive interaction for both parties.

are a fast and efficient possibilities to transfer nanostructures to various material. Often synonymously

Nanoimprinting/Nanoimprint Lithography (NIL) is a comparatively straightforward method to transfer structure on nanoscale, which is widely used in electronics. First of all, a master stamp is created, which then is further used to imprint the nanostructure onto another material. Nanoimprinting bears a large potential in biomimetics as it is a fast and low-cost method to transfer nanostructures of a biological template to another material.

Nanopillar is a certain type of a nanostructures, which are relatively high and narrow, which reminds of a pillar-like shape.

Nanoscale (or nanoscopic scale) describes a length scale in the range of 1 nm to 100 nm (10^{-9} m – 10^{-7}m).

Nanostructures are structures which show at least for one-dimension values at the nanoscale.

nymphal: a nymph is an immature stage of insects, which will undergo further metamorphosis to reach the adult stage (imago). In contrast to a larva a nymph already resembles the adult shape (except wings)

Poly-L-lysine coated microscope slide are microscope slides coated with the synthetic amino acid chain poly-L-lysine, which enhances the attachment and adhesion of cells.

Peptidoglycan (layer) is the main component of the bacterial cell wall and consists of glycan chains of repeating disaccharide units (consisting of N-acetyl glucosamine and N-acetyl muramic acid), which are cross linked by peptides. Gram-negative bacteria possess a thin

peptidoglycan layer in between both membranes, whereas Gram-positive bacteria show a thick peptidoglycan outside the cell membrane.

Polyvinyl siloxane is an addition-reaction silicone elastomer. It is stored in two separated components. When mixed together, the polyvinyl siloxane starts to cure and is able to capture the shape of structures at great detail. It is widely used in dentistry.

Reactive oxygen species (ROS) describe free radicals and reactive molecules derived from O_2

Scanning electron microscopy (SEM) is an imaging device, which uses electron beams to scan a surface. The electrons which are emitted by the atoms that are excited by the electron beam are called secondary electrons and get detected. The signal intensity is transferred into an image.

Self-cleaning surfaces which show properties, that allow the remove contaminants such as dust particles and bacteria. Often, they show low adhesion for foreign particles. One example for a self-cleaning surface is the Lotus leaf, which is superhydrophobic. When water drops on the leaf it is repelled and rolls off taking dirt particles with it. In this way the surface is cleaned.

Shade singer such as *Kikihia scutellaris* prefer to sing in shady places such as in deep bushes, which is rather unusual as most cicadas prefer to sing in sunny spots.

Superhydrophobicity: water repellent surfaces, drops jump or roll off. They are characterized by static contact angles of higher than 150° if in contact with water.

Velcro is a generic trademark for hook-and-loop fastener. George de Mestral named his invention as well as the company he founded Velcro®, as a combination of the French words „velour" (engl. velvet) and crochet (engl. hook).

Ventral describes the side of the belly of an animal, in case of cicadas it resembles the lower side.

Xylem is one of the main parts of the transport systems in vascular plants. It is mainly associated with the transport of water and mineral nutrients.

Literature

Alexander, R. D., & Moore, T. E. (1962). The evolutionary relationships of 17-year and 13-year cicadas, and three new species (Homoptera, Cicadidae, Magicicada). *Misc Publ Mus Zool Univ Michigan*, *121*(121), 5–59.

Arensburger, P., Simon, C., & Holsinger, K. (2004). Evolution and phylogeny of the New Zealand cicada genus Kikihia Dugdale (Homoptera: Auchenorrhyncha: Cicadidae) with reference to the origin of the Kermadec and Norfolk Islands' species. *Journal of Biogeography*, *31*(11), 1769–1783. https://doi.org/10.1111/j.1365-2699.2004.01098.x

Auer, G. K., & Weibel, D. B. (2017). Bacterial Cell Mechanics. *Biochemistry*, *56*(29), 3710–3724. https://doi.org/10.1021/acs.biochem.7b00346

Barthlott, W., & Neinhuis, C. (1997). Purity of the sacred lotus, or escape from contamination in biological surfaces. *Planta*, *202*(1), 1–8. https://doi.org/10.1007/s004250050096

Bertani, G. (1951). Studies on lysogenesis I. *Journal of Bacteriology*, *62*(3), 293–300. https://doi.org/10.1128/jb.62.3.293-300.1951

Brown, S., Santa Maria, J. P., & Walker, S. (2013). Wall teichoic acids of gram-positive bacteria. *Annual Review of Microbiology*, *67*, 313–336. https://doi.org/10.1146/annurev-micro-092412-155620

Budde, R. (1995). The story of Velcro. *Physics World*, *8*(1), 22–22. https://doi.org/10.1088/2058-7058/8/1/20

Callaham, M. A., Whiles, M. R., Meyer, C. K., Brock, B. L., & Charlton, R. E. (2000). Feeding ecology and emergence production of annual cicadas (Homoptera: Cicadidae) in tallgrass prairie. *Oecologia*, *123*(4), 535–542. https://doi.org/10.1007/s004420000335

Cerman, Z., Barthlott, W., & Nieder, J. (2005). *Erfindungen der Natur : Bionik - was wir von Pflanzen und Tieren lernen können*. Rowohlt Taschenbuch Verl. https://ubdata.univie.ac.at/AC04377867

Cheung, W. W. K., & Marshall, A. T. (1973). Water and ion regulation in cicadas in relation to xylem feeding. *Journal of Insect Physiology*, *19*(9), 1801–1816. https://doi.org/10.1016/0022-1910(73)90049-8

Ciancio, G., Pollack, A., Taupier, M. A., Block, N. L., & Irvin, G. L. (1988). Measurement of cell-cycle phase-specific cell death using Hoechst 33342 and propidium iodide: Preservation by ethanol fixation. *Journal of Histochemistry and Cytochemistry*, *36*(9), 1147–1152. https://doi.org/10.1177/36.9.2457047

Croxen, M. A., Law, R. J., Scholz, R., Keeney, K. M., Wlodarska, M., & Finlay, B. B. (2013). Recent advances in understanding enteric pathogenic Escherichia coli. In *Clinical*

Microbiology Reviews (Vol. 26, Issue 4, pp. 822–880). https://doi.org/10.1128/CMR.00022-13

Darwin, C. (2009). *The Origin of Species: By Means of Natural Selection, or the Preservation of Favoured Races in the Struggle for Life* (6th ed., Cambridge Library Collection - Darwin, Evolution and Genetics). Cambridge: Cambridge University Press. https://doi.org/10.1017/CBO9780511694295

Drelich, J. (1997). The effect of drop (bubble) size on contact angle at solid surfaces. *Journal of Adhesion*, *63*(1–3), 31–51. https://doi.org/10.1080/00218469708015212

Fritsche, O. (2016). Mikrobiologische Arbeitsmethoden. In O. Fritsche (Ed.), *Mikrobiologie* (pp. 311–333). Springer Berlin Heidelberg. https://doi.org/10.1007/978-3-662-49729-6_11

Gebeshuber, I. C., Gruber, P., & Drack, M. (2009). A gaze into the crystal ball: Biomimetics in the year 2059. *Proceedings of the Institution of Mechanical Engineers, Part C: Journal of Mechanical Engineering Science*, *223*(12), 2899–2918. https://doi.org/10.1243/09544062JMES1563

Gebeshuber, I. C., Rose, G., Pavlicek, A., & Gazsó, A. (2020). Bio-inspired and Biomimetic Nanomaterials. *Institute of Technology Assessment of the Austrian Academy of Sciences*, *July*, 6. https://doi.org/10.1553/ita-nt-054en

Gjertsen, D., & Daintith, J. (1999). *A Dictionary of scientists* (Abridged a). Oxford University Press.

Gordon, D. M. (2013). The ecology of Escherichia coli. In *Escherichia coli: Pathotypes and Principles of Pathogenesis: Second Edition* (pp. 3–20). Elsevier Inc. https://doi.org/10.1016/B978-0-12-397048-0.00001-2

Grant, P. R. (2005). The priming of periodical cicada life cycles. *Trends in Ecology and Evolution*, *20*(4), 169–174. https://doi.org/10.1016/j.tree.2005.01.016

Graw, J. (2010). *Genetik* (5., vollst). Springer-Verlag Berlin Heidelberg. http://dx.doi.org/10.1007/978-3-642-04999-6

Green, D. W., Watson, G. S., Watson, J., & Abraham, S. J. K. (2012). New biomimetic directions in regenerative ophthalmology. In *Advanced Healthcare Materials* (Vol. 1, Issue 2, pp. 140–148). https://doi.org/10.1002/adhm.201100039

Hasan, J., Webb, H. K., Truong, V. K., Pogodin, S., Baulin, V. A., Watson, G. S., Watson, J. A., Crawford, R. J., & Ivanova, E. P. (2013). Selective bactericidal activity of nanopatterned superhydrophobic cicada Psaltoda claripennis wing surfaces. *Applied Microbiology and Biotechnology*, *97*(20), 9257–9262. https://doi.org/10.1007/s00253-012-4628-5

Hosseinpour, S., Nanda, A., Walsh, L. J., & Xu, C. (2021). Microbial decontamination and antibacterial activity of nanostructured titanium dental implants: A narrative review. In *Nanomaterials* (Vol. 11, Issue 9). MDPI. https://doi.org/10.3390/nano11092336

Hu, H. M., Watson, J. A., Cribb, B. W., & Watson, G. S. (2011). Fouling of nanostructured insect cuticle: Adhesion of natural and artificial contaminants. *Biofouling*, *27*(10), 1125–1137. https://doi.org/10.1080/08927014.2011.637187

Huang, E., Skoufis, A., Denning, T., Qi, J., Dagastine, R., Tabor, R., & Berry, J. (2021). OpenDrop: Open-source software for pendant drop tensiometry contact angle measurements. *Journal of Open Source Software*, *6*(58), 2604. https://doi.org/10.21105/joss.02604

Ishak, M. I., Jenkins, J., Kulkarni, S., Keller, T. F., Briscoe, W. H., Nobbs, A. H., & Su, B. (2021). Insights into complex nanopillar-bacteria interactions: Roles of nanotopography and bacterial surface proteins. *Journal of Colloid and Interface Science*, *604*, 91–103. https://doi.org/10.1016/j.jcis.2021.06.173

Ivanova, E. P., Hasan, J., Webb, H. K., Gervinskas, G., Juodkazis, S., Truong, V. K., Wu, A. H. F., Lamb, R. N., Baulin, V. A., Watson, G. S., Watson, J. A., Mainwaring, D. E., & Crawford, R. J. (2013). Bactericidal activity of black silicon. *Nature Communications*, *4*. https://doi.org/10.1038/ncomms3838

Ivanova, E. P., Hasan, J., Webb, H. K., Truong, V. K., Watson, G. S., Watson, J. A., Baulin, V. A., Pogodin, S., Wang, J. Y., Tobin, M. J., Löbbe, C., & Crawford, R. J. (2012). Natural bactericidal surfaces: Mechanical rupture of pseudomonas aeruginosa cells by cicada wings. *Small*, *8*(16), 2489–2494. https://doi.org/10.1002/smll.201200528

Jaggessar, A., Shahali, H., Mathew, A., & Yarlagadda, P. K. D. V. (2017). Bio-mimicking nano and micro-structured surface fabrication for antibacterial properties in medical implants. In *Journal of Nanobiotechnology* (Vol. 15, Issue 1, pp. 1–20). BioMed Central. https://doi.org/10.1186/s12951-017-0306-1

Jenkins, J., Mantell, J., Neal, C., Gholinia, A., Verkade, P., Nobbs, A. H., & Su, B. (2020). Antibacterial effects of nanopillar surfaces are mediated by cell impedance, penetration and induction of oxidative stress. *Nature Communications*, *11*(1), 1–14. https://doi.org/10.1038/s41467-020-15471-x

Kaper, J. B., Nataro, J. P., & Mobley, H. L. T. (2004). Pathogenic Escherichia coli. In *Nature Reviews Microbiology* (Vol. 2, Issue 2, pp. 123–140). https://doi.org/10.1038/nrmicro818

Karban, R. (1986). Prolonged Development in Cicadas. In F. Taylor & R. Karban (Eds.), *The Evolution of Insect Life Cycles* (pp. 222–235). Springer US. https://doi.org/10.1007/978-1-4613-8666-7_14

Karban, R. (1997). Evolution of prolonged development: A life table analysis for periodical cicadas. *American Naturalist*, *150*(4), 446–461. https://doi.org/10.1086/286075

Kelleher, S. M., Habimana, O., Lawler, J., O'reilly, B., Daniels, S., Casey, E., & Cowley, A. (2016). Cicada Wing Surface Topography: An Investigation into the Bactericidal Properties of Nanostructural Features. *ACS Applied Materials and Interfaces*, *8*(24), 14966–14974. https://doi.org/10.1021/acsami.5b08309

Klapetek, P., Nečas, D., & Anderson, C. (2009). Gwyddion user guide. *User Guide*, 1–122. http://gwyddion.net/download/user-guide/gwyddion-user-guide-en.pdf

Knippers, J., & Speck, T. (2012). Design and construction principles in nature and architecture. *Bioinspiration and Biomimetics*, *7*(1). https://doi.org/10.1088/1748-3182/7/1/015002

Koch, K., Schulte, A. J., Fischer, A., Gorb, S. N., & Barthlott, W. (2008). A fast, precise and low-cost replication technique for nano- and high-aspect-ratio structures of biological and artificial surfaces. *Bioinspiration and Biomimetics*, *3*(4). https://doi.org/10.1088/1748-3182/3/4/046002

Köller, M., Ziegler, N., Sengstock, C., Schildhauer, T. A., & Ludwig, A. (2018). Bacterial cell division is involved in the damage of gram-negative bacteria on a nano-pillar titanium surface. *Biomedical Physics and Engineering Express*, *4*(5). https://doi.org/10.1088/2057-1976/aad2c1

Kuehnert, M. J., Hill, H. A., Kupronis, B. A., Tokars, J. I., Solomon, S. L., & Jernigan, D. B. (2005). Methicillin-resistant-Staphylococcus aureus hospitalizations, United States. *Emerging Infectious Diseases*, *11*(6), 868–872. https://doi.org/10.3201/eid1106.040831

Lienhard, J., Schleicher, S., Poppinga, S., Masselter, T., Milwich, M., Speck, T., & Knippers, J. (2011). Flectofin: A hingeless flapping mechanism inspired by nature. *Bioinspiration and Biomimetics*, *6*(4), 045001. https://doi.org/10.1088/1748-3182/6/4/045001

Lowy, F. D. (2003). Antimicrobial resistance: the example of Staphylococcus aureus. *Journal of Clinical Investigation*, *111*(9), 1265–1273. https://doi.org/10.1172/jci200318535

Marshall, D. C., & Cooley, J. R. (2000). Reproductive character displacement and speciation in periodical cicadas, with description of a new species, 13-year Magicicada neotredecim. *Evolution*, *54*(4), 1313–1325. https://doi.org/10.1111/j.0014-3820.2000.tb00564.x

Marshall, D. C., Hill, K. B. R., Marske, K. A., Chambers, C., Buckley, T. R., & Simon, C. (2012). Limited, episodic diversification and contrasting phylogeography in a New Zealand cicada radiation. *BMC Evolutionary Biology*, *12*(1). https://doi.org/10.1186/1471-2148-12-177

Marshall, D. C., Moulds, M., Hill, K. B. R., Price, B. W., Wade, E. J., Owen, C. L., Goemans, G., Marathe, K., Sarkar, V., Cooley, J. R., Sanborn, A. F., Kunte, K., Villet, M. H., & Simon, C. (2018). A molecular phylogeny of the cicadas (Hemiptera: Cicadidae) with a review of tribe and subfamily classification. In *Zootaxa* (Vol. 4424, Issue 1, pp. 1–64). Magnolia Press. https://doi.org/10.11646/zootaxa.4424.1.1

Marshall, D. C., Slon, K., Cooley, J. R., Hill, K. B. R., & Simon, C. (2008). Steady Plio-Pleistocene diversification and a 2-million-year sympatry threshold in a New

Zealand cicada radiation. *Molecular Phylogenetics and Evolution*, *48*(3), 1054–1066. https://doi.org/10.1016/j.ympev.2008.05.007

Mestral, G. de. (1955). Velvet type fabric and method of producing same. In *United States Patent and Trademark Office*. https://patentimages.storage.googleapis.com/dd/e5/a7/d781d1d7a5dbdf/US2717437.pdf

Nachtigall, W. (1992). Technische Biologie und Bionik - was ist das? In W. Nachtigall (Ed.), *BIONA-report 8 - Technische Biologie und Bionik 1. 1. Bionik-Kongress, Wiesbaden 1992* (pp. 1–12). Akademie der Wissenschaften und Literatur, Mainz: G. Fischer, Stuttgart, New York.

Nachtigall, W., & Wisser, A. (2013). Bionik in Beispielen. In A. Wisser (Ed.), *Bionik in Beispielen* (Issue ISBN 9783642347672). Berlin, Heidelberg : Springer Berlin Heidelberg. https://doi.org/10.1007/978-3-642-34767-2

Nečas, D., & Klapetek, P. (2012). Gwyddion: An open-source software for SPM data analysis. In *Central European Journal of Physics* (Vol. 10, Issue 1, pp. 181–188). https://doi.org/10.2478/s11534-011-0096-2

Nguyen, D. H. K., Loebbe, C., Linklater, D. P., Xu, X., Vrancken, N., Katkus, T., Juodkazis, S., Maclaughlin, S., Baulin, V., Crawford, R. J., & Ivanova, E. P. (2019a). The idiosyncratic self-cleaning cycle of bacteria on regularly arrayed mechano-bactericidal nanostructures †. *Nanoscale*, *11*, 48–61. https://doi.org/10.1039/c9nr05923g

Nguyen, D. H. K., Loebbe, C., Linklater, D. P., Xu, X., Vrancken, N., Katkus, T., Juodkazis, S., Maclaughlin, S., Baulin, V., Crawford, R. J., & Ivanova, E. P. (2019b). The idiosyncratic self-cleaning cycle of bacteria on regularly arrayed mechano-bactericidal nanostructures. *Nanoscale*, *11*(35), 16455–16462. https://doi.org/10.1039/c9nr05923g

Nowlin, K., Boseman, A., Covell, A., & LaJeunesse, D. (2014). Adhesion-dependent rupturing of Saccharomyces cerevisiae on biological antimicrobial nanostructured surfaces. *Journal of the Royal Society Interface*, *12*(102). https://doi.org/10.1098/rsif.2014.0999

Ogston, A. (1882). Micrococcus Poisoning. *Journal of Anatomy and Physiology*, *17*(Pt 1), 24–58. https://pubmed.ncbi.nlm.nih.gov/17231450/

Oh, J., Dana, C. E., Hong, S., Román, J. K., Jo, K. D., Hong, J. W., Nguyen, J., Cropek, D. M., Alleyne, M., & Miljkovic, N. (2017). Exploring the Role of Habitat on the Wettability of Cicada Wings. *ACS Applied Materials and Interfaces*, *9*(32), 27173–27184. https://doi.org/10.1021/acsami.7b07060

Oh, J., Hoffman, J. B., Hong, S., Jo, K. D., Román-Kustas, J., Reed, J. H., Dana, C. E., Cropek, D. M., Alleyne, M., & Miljkovic, N. (2020). Dissolvable Template Nanoimprint Lithography: A Facile and Versatile Nanoscale Replication Technique. *Nano Letters*, *20*(10), 6989–6997. https://doi.org/10.1021/acs.nanolett.0c01547

Pham, V. T. H., Truong, V. K., Orlowska, A., Ghanaati, S., Barbeck, M., Booms, P., Fulcher, A. J., Bhadra, C. M., Buividas, R., Baulin, V., James Kirkpatrick, C., Doran, P., Mainwaring, D. E., Juodkazis, S., Crawford, R. J., & Ivanova, E. P. (2016a). Race for the Surface: Eukaryotic Cells Can Win. *ACS Applied Materials and Interfaces*, *8*(34), 22025–22031. https://doi.org/10.1021/acsami.6b06415

Pham, V. T. H., Truong, V. K., Orlowska, A., Ghanaati, S., Barbeck, M., Booms, P., Fulcher, A. J., Bhadra, C. M., Buividas, R., Baulin, V., James Kirkpatrick, C., Doran, P., Mainwaring, D. E., Juodkazis, S., Crawford, R. J., & Ivanova, E. P. (2016b). Race for the Surface: Eukaryotic Cells Can Win. *ACS Applied Materials and Interfaces*, *8*(34), 22025–22031. https://doi.org/10.1021/acsami.6b06415

Pogodin, S., Hasan, J., Baulin, V. A., Webb, H. K., Khanh Truong, V., Hong Phong Nguyen, T., Boshkovikj, V., Fluke, C. J., Watson, G. S., Watson, J. A., Crawford, R. J., & Ivanova, E. P. (2013). Biophysical Model of Bacterial Cell Interactions with Nanopatterned Cicada Wing Surfaces. *Biophysj*, *104*(4), 835–840. https://doi.org/10.1016/j.bpj.2012.12.046

Pogodin, S., Hasan, J., Baulin, V. A., Webb, H. K., Truong, V. K., Phong Nguyen, T. H., Boshkovikj, V., Fluke, C. J., Watson, G. S., Watson, J. A., Crawford, R. J., & Ivanova, E. P. (2013). Biophysical model of bacterial cell interactions with nanopatterned cicada wing surfaces. *Biophysical Journal*, *104*(4), 835–840. https://doi.org/10.1016/j.bpj.2012.12.046

Raetz, C. R. H., & Whitfield, C. (2002). Lipopolysaccharide endotoxins. In *Annual Review of Biochemistry* (Vol. 71, pp. 635–700). Annual Reviews 4139 El Camino Way, P.O. Box 10139, Palo Alto, CA 94303-0139, USA. https://doi.org/10.1146/annurev.biochem.71.110601.135414

Robertson, J., McGoverin, C., Vanholsbeeck, F., & Swift, S. (2019). Optimisation of the protocol for the liVE/DEAD®BacLightTM bacterial viability kit for rapid determination of bacterial load. *Frontiers in Microbiology*, *10*(APR). https://doi.org/10.3389/fmicb.2019.00801

Román-Kustas, J., Hoffman, J. B., Reed, J. H., Gonsalves, A. E., Oh, J., Li, L., Hong, S., Jo, K. D., Dana, C. E., Miljkovic, N., Cropek, D. M., & Alleyne, M. (2020). Molecular and Topographical Organization: Influence on Cicada Wing Wettability and Bactericidal Properties. *Advanced Materials Interfaces*, *7*(10). https://doi.org/10.1002/admi.202000112

Rosenbach, F. J. (1884). Mikroorganismen bei den Wundinfectionskrankheiten des Menschen. *Deutsche Medizinische Wochenschrift*, *10*(39), 631–632. https://doi.org/10.1055/s-0029-1209600

Roy, J. C., Salaün, F., Giraud, S., Ferri, A., Chen, G., & Guan, J. (2017). Solubility of Chitin: Solvents, Solution Behaviors and Their Related Mechanisms. In *Solubility of Polysaccharides*. InTech. https://doi.org/10.5772/intechopen.71385

RStudio Team(2015). (2015). RStudio: Integrated Development for R. In *RStudio, Inc., Boston, MA* (1.4.1106; p. http://www.rstudio.com/.). RStudio. http://www.rstudio.com/

Sandle, T. (2016). 9 - Microbial identification. In T. Sandle (Ed.), *Pharmaceutical Microbiology* (pp. 103–113). Woodhead Publishing. https://doi.org/https://doi.org/10.1016/B978-0-08-100022-9.00009-8

Schindelin, J., Arganda-Carreras, I., Frise, E., Kaynig, V., Longair, M., Pietzsch, T., Preibisch, S., Rueden, C., Saalfeld, S., Schmid, B., Tinevez, J. Y., White, D. J., Hartenstein, V., Eliceiri, K., Tomancak, P., & Cardona, A. (2012). Fiji: An open-source platform for biological-image analysis. In *Nature Methods* (Vol. 9, Issue 7, pp. 676–682). Nature Publishing Group. https://doi.org/10.1038/nmeth.2019

Schneider, C. A., Rasband, W. S., & Eliceiri, K. W. (2012). NIH Image to ImageJ: 25 years of image analysis. In *Nature Methods* (Vol. 9, Issue 7, pp. 671–675). https://doi.org/10.1038/nmeth.2089

Schulte, A. J., Koch, K., Spaeth, M., & Barthlott, W. (2009). Biomimetic replicas: Transfer of complex architectures with different optical properties from plant surfaces onto technical materials. *Acta Biomaterialia*, *5*(6), 1848–1854. https://doi.org/10.1016/j.actbio.2009.01.028

Senevirathne, S. W. M. A. I., Hasan, J., Mathew, A., Woodruff, M., & Yarlagadda, P. K. D. V. (2021). Bactericidal efficiency of micro- And nanostructured surfaces: A critical perspective. In *RSC Advances* (Vol. 11, Issue 3, pp. 1883–1900). Royal Society of Chemistry. https://doi.org/10.1039/d0ra08878a

Shahali, H., Hasan, J., Mathews, A., Wang, H., Yan, C., Tesfamichael, T., & Yarlagadda, P. K. D. V. (2019). Multi-biofunctional properties of three species of cicada wings and biomimetic fabrication of nanopatterned titanium pillars. *Journal of Materials Chemistry B*, *7*(8), 1300–1310. https://doi.org/10.1039/C8TB03295E

Shapiro, S. S., & Wilk, M. B. (1965). An Analysis of Variance Test for Normality (Complete Samples). *Biometrika*, *52*(3/4), 591. https://doi.org/10.2307/2333709

Shulman, S. T., Friedmann, H. C., & Sims, R. H. (2007). Theodor Escherich: the first pediatric infectious diseases physician? *Clinical Infectious Diseases : An Official Publication of the Infectious Diseases Society of America*, *45*(8), 1025–1029. https://doi.org/10.1086/521946

Silhavy, T. J., Kahne, D., & Walker, S. (2010). The bacterial cell envelope. In *Cold Spring Harbor perspectives in biology* (Vol. 2, Issue 5). https://doi.org/10.1101/cshperspect.a000414

Simon, C. (2009). Using NZ examples to teach Darwin'sOrigin of Speices. Print version. *New Zealand Science Review*, *66*(3).

Simon, C., Cooley, J. R., Karban, R., & Sota, T. (2022). Advances in the Evolution and Ecology of 13- and 17-Year Periodical Cicadas. In *Annual Review of Entomology*

(Vol. 67, pp. 457–482). Annual Reviews Inc. https://doi.org/10.1146/annurev-ento-072121-061108

Smith, J. L., Fratamico, P. M., & Gunther, N. W. (2007). Extraintestinal pathogenic Escherichia coli. In *Foodborne Pathogens and Disease* (Vol. 4, Issue 2, pp. 134–163). Foodborne Pathog Dis. https://doi.org/10.1089/fpd.2007.0087

Speck, O., Speck, D., Horn, R., Gantner, J., & Sedlbauer, K. P. (2017). Biomimetic bio-inspired biomorph sustainable? An attempt to classify and clarify biology-derived technical developments. *Bioinspiration and Biomimetics*, *12*(1), 011004. https://doi.org/10.1088/1748-3190/12/1/011004

Stachelberger, H., Gruber, P., & Gebeshuber, I. C. (2011). Biomimetics: Its Technological and Societal Potential. In P. Gruber, D. Bruckner, C. Hellmich, H.-B. Schmiedmayer, H. Stachelberger, & I. C. Gebeshuber (Eds.), *Biomimetics - Materials, Structures and Processes : Examples, Ideas and Case Studies* (pp. 1–6). Springer. https://doi.org/10.1007/978-3-642-11934-7_1

Sun, J., Rutherford, S. T., Silhavy, T. J., & Huang, K. C. (2022). Physical properties of the bacterial outer membrane. In *Nature Reviews Microbiology* (Vol. 20, Issue 4, pp. 236–248). Nature Publishing Group. https://doi.org/10.1038/s41579-021-00638-0

Sun, M., Liang, A., Zheng, Y., Watson, G. S., & Watson, J. A. (2011). A study of the anti-reflection efficiency of natural nano-arrays of varying sizes. *Bioinspiration and Biomimetics*, *6*(2), 026003. https://doi.org/10.1088/1748-3182/6/2/026003

Sun, M., Watson, G. S., Zheng, Y., Watson, J. A., & Liang, A. (2009). Wetting properties on nanostructured surfaces of cicada wings. *Journal of Experimental Biology*, *212*(19), 3148–3155. https://doi.org/10.1242/jeb.033373

Sun, M., Zhang, J., Watson, G. S., Watson, J. A., Han, D., & Liang, A. (2018). Differences in nanostructure and hydrophobicity of cicada (Cryptotympana atrata) forewing surface with the distribution of precipitation. *Applied Bionics and Biomechanics*, *2018*. https://doi.org/10.1155/2018/5305847

Tenaillon, O., Skurnik, D., Picard, B., & Denamur, E. (2010). The population genetics of commensal Escherichia coli. In *Nature Reviews Microbiology* (Vol. 8, Issue 3, pp. 207–217). https://doi.org/10.1038/nrmicro2298

Thomer, L., Schneewind, O., & Missiakas, D. (2016). Pathogenesis of Staphylococcus aureus Bloodstream Infections. *Annual Review of Pathology: Mechanisms of Disease*, *11*, 343–364. https://doi.org/10.1146/annurev-pathol-012615-044351

Timischl, W. (2013). Angewandte Statistik [Book]. In *Angewandte Statistik* (3. Aufl. 2). Springer Vienna. https://doi.org/10.1007/978-3-7091-1349-3

Tong, S. Y. C., Davis, J. S., Eichenberger, E., Holland, T. L., & Fowler, V. G. (2015). Staphylococcus aureus infections: Epidemiology, pathophysiology, clinical manifestations, and management. *Clinical Microbiology Reviews*, *28*(3), 603–661. https://doi.org/10.1128/CMR.00134-14

Wang, S., & Jiang, L. (2007). Definition of superhydrophobic states. In *Advanced Materials* (Vol. 19, Issue 21, pp. 3423–3424). https://doi.org/10.1002/adma.200700934

Wang, X., Bhadra, C. M., Yen Dang, T. H., Buividas, R., Wang, J., Crawford, R. J., Ivanova, E. P., & Juodkazis, S. (2016). A bactericidal microfluidic device constructed using nano-textured black silicon. *RSC Advances*, *6*(31), 26300–26306. https://doi.org/10.1039/c6ra03864f

Watson, G. S., Gellender, M., & Watson, J. A. (2014). Self-propulsion of dew drops on lotus leaves: A potential mechanism for self cleaning. *Biofouling*, *30*(4), 427–434. https://doi.org/10.1080/08927014.2014.880885

Watson, G. S., Green, D. W., Schwarzkopf, L., Li, X., Cribb, B. W., Myhra, S., & Watson, J. A. (2015). A gecko skin micro/nano structure - A low adhesion, superhydrophobic, anti-wetting, self-cleaning, biocompatible, antibacterial surface. *Acta Biomaterialia*, *21*, 109–122. https://doi.org/10.1016/j.actbio.2015.03.007

Watson, G. S., Green, D. W., Sun, M., Liang, A., Li, X., Cribb, B. W., & Watson, J. A. (2015). The Insect (cicada) Wing Membrane Micro/Nano Structure – Nature's Templates for Control of Optics, Wetting, Adhesion, Contamination, Bacteria and Eukaryotic Cells. *Journal of Nanoscience with Advanced Technology*, *1*(2), 6–16. https://doi.org/10.24218/jnat.2015.07

Wertheim, H. F. L., Melles, D. C., Vos, M. C., van Leeuwen, W., van Belkum, A., Verbrugh, H. A., & Nouwen, J. L. (2005). The role of nasal carriage in Staphylococcus aureus infections. In *Lancet Infectious Diseases* (Vol. 5, Issue 12, pp. 751–762). https://doi.org/10.1016/S1473-3099(05)70295-4

Williams, K. S., & Simon, C. (1995). The ecology, behavior, and evolution of periodical cicadas. *Annual Review of Entomology*, *40*(1), 269–295. https://doi.org/10.1146/annurev.en.40.010195.001413

Wisdom, K. M., Watson, J. A., Qu, X., Liu, F., Watson, G. S., & Chen, C. H. (2013). Self-cleaning of superhydrophobic surfaces by self-propelled jumping condensate. *Proceedings of the National Academy of Sciences of the United States of America*, *110*(20), 7992–7997. https://doi.org/10.1073/pnas.1210770110

Xie, G., Zhang, G., Lin, F., Zhang, J., Liu, Z., & Mu, S. (2008). The fabrication of subwavelength anti-reflective nanostructures using a bio-template. *Nanotechnology*, *19*(9). https://doi.org/10.1088/0957-4484/19/9/095605

Young, R. J., & Moore, M. v. (2005). Dual-beam (FIB-SEM) systems techniques and automated applications. In *Introduction to Focused Ion Beams: Instrumentation, Theory, Techniques and Practice* (pp. 247–268). Springer, Boston, MA. https://doi.org/10.1007/0-387-23313-X_12

Zan, G., & Wu, Q. (2016). Biomimetic and Bioinspired Synthesis of Nanomaterials/Nanostructures. In *Advanced Materials* (Vol. 28, Issue 11, pp. 2099–2147). https://doi.org/10.1002/adma.201503215

Zobl, S. (2017). *Strukturfarben im Brennpunkt der Bionik. Zwischen Kunst und Naturwissenschaften*. Springer Spektrum.

Zobl, S., Salvenmoser, W., Schwerte, T., Gebeshuber, I. C., & Schreiner, M. (2016). Morpho peleides butterfly wing imprints as structural colour stamp. *Bioinspiration and Biomimetics*, *11*(1). https://doi.org/10.1088/1748-3190/11/1/016006